INTEGRATION OF PRECLINICAL AND CLINICAL DATA WITH PHARMACOKINETIC MODELING AND SIMULATIONS TO CHARACTERIZE THE DISPOSITION OF ORALLY-ACTIVE ANTIPARASITIC PRODRUGS AND METABOLITES: PREDICTION OF THE DOSE-EXPOSURE RELATIONSHIP IN HUMANS

Zhixia Yan

A dissertation submitted to the faculty of the University of North Carolina at Chapel Hill in partial fulfillment of the requirements for the degree of Doctor of Philosophy in UNC Eshelman School of Pharmacy.

Chapel Hill
2011

Approved by,

Co-advisor: Mary F. Paine, Ph.D.

Co-advisor: Kim L.R. Brouwer, Ph.D.

Chairperson: Gary M. Pollack, Ph.D.

Reader: James E. Hall, Ph.D.

Reader: Michael Zhuo Wang, Ph.D.

ABSTRACT

Zhixia Yan

Integration of Preclinical and Clinical Data with Pharmacokinetic Modeling and Simulations to Characterize the Disposition of Orally-Active Antiparasitic Prodrugs and Metabolites: Prediction of the Dose-Exposure Relationship in Humans

(Under the direction of Mary F. Paine, R.Ph., Ph.D. and Kim L.R. Brouwer, Pharm.D., Ph.D.)

Prediction of the disposition and selection of the appropriate dosage regimen of drug candidates prior to clinical studies presents a major challenge in drug development. In this dissertation project, a multiexperimental approach, including Caco-2 cells, rat isolated perfused livers (IPLs), rat and human sandwich-cultured hepatocytes (SCH), a plasma/tissue binding assay, and pharmacokinetic modeling was employed to 1) examine mechanisms underlying differences in systemic exposure of two active metabolites (furamidine and CPD-0801) of respective antiparasitic prodrugs (pafuramidine and CPD-0868), and 2) quantitatively integrate preclinical and clinical data to elucidate the dose-plasma/exposure relationship in humans using pafuramidine/furamidine as a model prodrug/active metabolite pair.

Pafuramidine and CPD-0868 exhibited similar permeability properties in Caco-2 monolayers when the basolateral compartment was supplemented with 4% bovine serum albumin, suggesting that the difference in systemic exposure of active metabolites was not due to the difference in intestinal permeabilities between the prodrugs. Hepatic accumulation of both active metabolites was extensive (>95% of total formed) in rat IPLs and SCH. Compared to furamidine, the extent of formation and perfusate/medium exposure of CPD-0801 was greater, by ≤2.5- and ≥7-fold, respectively. The unbound fraction of both

active metabolites in rat liver ($f_{u,L}$) was lower than that in plasma and perfusate by ≥24-fold; $f_{u,L}$ of CPD-0801 was 5-fold higher than that of furamidine (1.6 versus 0.3%). These observations suggested that intrahepatic binding influences the disposition of these active metabolites. A higher $f_{u,L}$ mostly explained the enhanced perfusate exposure of CPD-0801 compared to furamidine in rat IPLs. A strong concordance between rat IPL and SCH data substantiated SCH as a useful tool to study the hepatobiliary disposition of these compounds.

Pafuramidine/furamidine preclinical and clinical data were used as a training set to develop whole-body semi-physiologically-based pharmacokinetic (PBPK) models for rats and humans. The PBPK models suggested that the intestine may contribute to pre-systemic furamidine formation. Based on the prodrug dose-plasma/exposure relationship predicted by the human model, a dosage regimen of pafuramidine, 40 mg/day, was proposed. This dissertation project, through integration of preclinical and clinical data with pharmacokinetic modeling and simulations, provided a framework to guide dose-ranging studies in humans for next-in-class antiparasitic compounds.

ACKNOWLEDGEMENTS

I am truly thankful to many people who have contributed to where I am today. First, I would like to express my sincere gratitude to my coadvisors, Drs. Kim Brouwer and Mary Paine, for their guidance and support over these years. I benefited tremendously from their broad knowledge, dedication to science, qualities being excellent scientists, and invaluable feedback on my dissertation research. These qualities helped me grow to be a contributing scientist with a wide range of skill sets. I would like to especially thank Dr. J. Ed. Hall for providing me the opportunity to work in his laboratory during my first semester. It was this opportunity that helped me to develop a very inspiring and fulfilling project, which can impact the lives of others. I have been deeply touched by Dr. Hall's personality and kindness over these years. His belief in me, compassion, and encouragement had a substantial impact on both my graduate studies and personal life. I would also like to thank my committee members, Drs. Gary Pollack and Michael Zhuo Wang for their support, time, and insightful discussions. "Pharmacokinetics" taught by Dr. Pollack was my favorite class during my graduate training. His knowledge and insight have been the motivating factors that push me to excel in my scientific career. To all members and staff of the Brouwer, Paine, and Hall Laboratories, I would like to express my thanks for your support and helpful suggestions throughout the years.

Finally, I would like to thank my family for their understanding, support, and encouragement during my near 8-year study abroad. For that, I dedicate this work to them.

My dissertation research was supported by grants from the National Institutes of Health [R01 GM41935 and R25 GM74088] and the Consortium for Parasitic Drug

Development. I was supported by an Eli Lilly Predoctoral Fellowship in Pharmacokinetics and Drug Disposition from 2009 to 2010.

TABLE OF CONTENTS

Page

LIST OF TABLES……x

LIST OF FIGURES……xi

LIST OF ABBREVIATIONS……xiii

CHAPTER

1. INTRODUCTION……1

A. HUMAN AFRICAN TRYPANOSOMIASIS ……2

A.1. Overview……2

A.2. Current Chemotherapy……3

A.2.1. Chemotherapy for First Stage HAT……3

A.2.2. Chemotherapy for Second Stage HAT……4

B. ORALLY-ACTIVE PENTAMIDINE ANALOGUES……6

B.1. Pafuramidine ……7

B.2. 2, 5-Bis [5-(*N*-methoxyamidino)-2-pyridyl] furan (CPD-0868)……8

C. INTEGRATION OF PRECLINICAL AND MATHEMATICAL MODELS TO OPTIMIZE PRODRUG DOSE-SELECTION STRATEGY……9

C.1. Preclinical Models……11

C.1.1. Intestinal Absorption Models……12

C.1.2. Hepatobiliary Models……14

C.2. PBPK Modeling-Based Dose-Selection Strategy ……17

D. OVERVIEW OF PROJECT……22

E. FIGURES……26

F. REFERENCES……30

2. COMPARISON OF THE INTESTINAL DISPOSITION OF TWO ANTIPARASITIC PRODRUGS PAFURAMIDINE AND CPD-0868 USING THE HUMAN INTESTINAL CELL LINE CACO-2……...38

A. ABSTRACT.....39

B. INTRODUCTION.....40

C. METHODS.....43

D. RESULTS.....47

E. DISCUSSION.....49

F. TABLES.....53

G. FIGURES.....54

H. REFERENCES.....59

3. MECHANISMS UNDERLYING DIFFERENCES IN SYSTEMIC EXPOSURE OF STRUCTURALLY SIMILAR ACTIVE METABOLITES: COMPARISON OF TWO PRECLINICAL HEPATIC MODELS……..…61

A. ABSTRACT.....62

B. INTRODUCTION.....63

C. METHODS.....66

D. RESULTS.....72

E. DISCUSSION.....75

F. TABLES.....80

G. FIGURES.....85

H. REFERENCES 92

4. A SEMI-PHYSIOLOGICALLY-BASED PHARMACOKINETIC MODELING APPROACH TO PREDICT THE DOSE-EXPOSURE RELATIONSHIP FOR AN ANTIPARASITIC PRODRUG/ACTIVE METABOLITE PAIR……..95

A. ABSTRACT.....96

B. INTRODUCTION 97

C. METHODS 100

D. RESULTS.....110

E. DISCUSSION.....115

F. APPENDIX.....120

G. TABLES.....125

H. FIGURES.....129

I. REFERENCES.....135

5. CONCLUSIONS.....138

A. SUMMARY AND DISCUSSION.....139

A.1. Characterization and Comparison of the Intestinal and Hepatobiliary Disposition of Pafuramidine and DPD-0868 and Derived Metabolites in Preclinical Models.....141

A.2. Prediction of the Dose-Exposure Relationship via Semi-PBPK Modeling.....144

B. FUTURE DIRECTIONS.....151

B.1. Characterize the Intracellular localization of Active Metabolites in the Liver.....151

B.2. Identify Transport Protein(s) Involved in the Hepatobiliary Disposition of Furamidine.....153

B.3. Characterize First-Pass Metabolism of Prodrugs in the Gut.....154

B.4. Determine the Therapeutic-Safety Index of the Active Metabolite Furamidine.....156

B.5. Apply the PBPK Modeling-based Strategy to Future Drug Development.....157

C. FIGURES.....159

D. REFERENCES.....160

LIST OF TABLES

Table 2.1 Comparison of Transport of pafuramidine and CPD-0868 across Caco-2 Cell Monolayers……..……..53

Table 3.1 Hepatic clearances and extraction ratio of prodrugs in rat isolated perfused livers……80

Table 3.2 Kinetic parameters, generated from Model 1, associated with the disposition of prodrugs (pafuramidine and CPD-0868) and derived metabolites in rat isolated perfused livers……..…81

Table 3.3 Comparison of hepatic disposition of active metabolites in isolated perfused livers (IPLs) and day-4 sandwich-cultured hepatocytes (SCH) from rats……82

Table 3.4 Kinetic parameters, generated from Model 2, associated with the hepatic excretion of unbound active metabolites in rat isolated perfused livers……83

Table 3.5 Kinetic parameters, generated from Model 1, associated with disposition of prodrugs (pafuramidine and CPD-0868) and derived metabolites in Day-4 sandwich-cultured rat hepatocytes……...84

Table 4.1 Physiologically-based pharmacokinetic model parameters associated with the disposition of pafuramidine and furamidine in rats and humans……..…125

Table 4.2 Kinetic parameters associated with disposition of pafuramidine and furamidine in rat and human sandwich-cultured hepatocytes (SCH)…..…127

Table 4.3 PBPK Model prediction of furamidine formation and excretion in rats and humans after administration of a single oral dose of pafuramidine (7.5 μmol/kg and 100mg, respectively)……....128

LIST OF FIGURES

Figure 1.1 Chemical structures of drugs for treatment of first stage (left) and second stage (right) human African trypanosomiasis……26

Figure 1.2 Chemical structures of orally-active pentamidine analogues, pafuramidine/CPD-0868 and respective active metabolites, furamidine/CPD-0801……..……27

Figure 1.3 Biocoversion of the prodrug pafuramidine to the active metabolite furamidine in human liver microsomes……..……...28

Figure 1.4 Schemes for a generic physiologically-based pharmacokinetic (PBPK) model……..…….29

Figure 2.1 Chemical structures of pentamidine, pafuramidine/furamidine and CPD-0868/CPD-0801…….……...…….54

Figure 2.2 Schematic representation of Caco-2 permeability assay for intestinal absorption…….…….55

Figure 2.3 Translocation of pafuramidine and CPD-0868 (1 μM) across Caco-2 cell monolayers in the absence of BSA in the incubation medium……..……56

Figure 2.4 Apical-to-Basolateral (A→B) translocation of pafuramidine and CPD-0868 (1 μM) across Caco-2 cell monolayers in the presence of 4% BSA in the B compartment…….57

Figure 2.5 Cellular accumulation of pafuramidine or CPD-0868 in the Caco-2 cells at the end of transport experiment (60 min)……..…..58

Figure 3.1 Biotransformation of prodrug to active metabolite and corresponding chemical structures……..….85

Figure 3.2 Model schemes depicting disposition of prodrugs/metabolites in rat IPLs and SCH (Model 1) and hepatic excretion of unbound active metabolite in rat IPLs (Model 2)…….86

Figure 3.3 Disposition of prodrugs, pafuramidine (A) and CPD-0868 (B), and corresponding metabolites over 120 min in rat isolated perfused livers……....87

Figure 3.4 Extent of formation of active metabolites in isolated perfused livers (A) and sandwich-cultured hepatocytes (B) from rats……...88

Figure 3.5 Disposition of prodrugs, pafuramidine (A) and CPD-0868 (B) and corresponding metabolites over 24 h in day-4 sandwich-cultured rat hepatocytes……..…...89

Figure 3.S1 Plot of the weighted residual versus time data from the computer-generated best fit of Model 1 to the rat isolated perfused liver data depicted in Fig. 3.3……90

Figure 3.S2 Plot of the weighted residual *vs.* time data from the computer-generated best fit of Model 1 to the rat sandwich-cultured hepatocyte data depicted in Fig. 3.5……..…91

Figure 4.1 Semi-PBPK model schemes depicting disposition of pafuramidine and furamidine in rat IPLs (A) and in vivo in rats and humans (B)…….129

Figure 4.2 Disposition of pafuramidine (diamonds) and furamidine (triangles) over 24 h in sandwich-cultured hepatocytes (SCH) from (A) rats and (B) humans……..….131

Figure 4.3 Disposition of pafuramidine (diamonds) and furamidine (triangles) in rats administered a single oral dose of pafuramidine (7.5 μmol/kg). ……..……..….132

Figure 4.4 Disposition of pafuramidine (diamonds) and furamidine (triangles) in healthy male subjects administered a single oral dose of ^{14}C-pafuramidine (100 mg, equivalent to 274 μmol) in capsule form……...133

Figure 4.5 Semi-PBPK model-predicted (scheme depicted in Fig. 4.1B) plasma and liver concentration-time profiles of furamidine in humans following oral administration of 100 mg pafuramidine twice daily and 40 mg pfuramidine once daily ……..134

Figure 5.1 Subcellular localization of generated active metabolites, furamidine and CPD-0801, in rat isolated perfused livers……135

LIST OF ABBREVIATIONS

A	Apical
ACN	Acetonitrile
ADME	Absorption, distribution, metabolism, and excretion
AUC	Area under the curve
B	Basolateral
BCRP	Breast cancer resistance protein
BCS	Biopharmaceutical Classification System
BLQ	Below limit of quantification
BSA	Bovine serum albumin
Caco-2	Human Colon Adenocarcinoma cell line
Cl_H	Hepatic clearance
CNS	Central nervous system
CNT	Concentrative nucleoside transporter
CPD-0801	2, 5-Bis (5-amidino)-2-pyridyl) furan
CPD-0868	2, 5-Bis [5-(N-methoxyamidino)-2-pyridyl] furan
C_{ss}	Steady-state concentration
CYP	Cytochrome P450
DAPI	4',6-Diamidino-2-phenylindole
DEX	Dexamethasone
DILI	Drug-induced liver injury
DMEM	Dulbecco's modified Eagle's medium
DMSO	Dimethylsulfoxide
EGTA	Ethylenebis(oxyethylenenitrilo)tetraacetic acid
ENT	Equilibrative nucleoside transporter
f_a	Fraction absorbed

f_u	Unbound fraction
Furamidine	2,5-Bis(4-amidinophenyl) furan
FBS	Fetal bovine serum
GFR	Glomerular filtration rate
GI	Gastrointestinal
HAT	Human African trypanosomiasis
HBSS	Hanks' balanced salt solution
IC_{50}	50% inhibitory concentration
IPLs	Isolated perfused livers
ITS^{+TM}	Insulin/transferrin/selenium
K_p	Tissue-to-plasma partition coefficient
LC-MS/MS	Liquid chromatography tandem mass spectrometry
LDH	Lactate dehydrogenase
MATE	Multidrug and toxin extrusion transporter
MRP	Multidrug reistance protein
NEAA	Nonessential amino acids
NECT	Nifurtimox-Eflornithine Combination Therapy
NOAEL	No observable adverse effect level
NTCP	Sodium/taurocholate co-peptide transporter
OATP	Organic anion transporting polypeptide
OCT	Organic cation transporter
Pafuramidine	2,5-Bis(4-amidinophenyl)furan-bis-O-methylamidoxime
P_{app}	Apparent permeability
PBPK	Physiologically-based pharmacokinetic
PBS	Phosphate buffered saline
P-gp	P-glycoprotein

PK	Pharmacokinetics
RNAi	RNA interference
SCH	Sandwich-cultured hepatocytes
T. b.	*Trypanosoma brucei*
TEER	Transepithelial electrical resistance
TFA	Trifluoroacetic acid
WHO	World Health Organization

CHAPTER 1

INTRODUCTION

A. HUMAN AFRICAN TRYPANOSOMIASIS

A.1. Overview

Human African trypanosomiasis (HAT), one of four neglected tropical diseases identified by the World Health Organization (WHO) (WHO, 2010a), is transmitted through infected tsetse flies. HAT in west and central Africa is primarily a chronic disease caused by the protozoan parasite *Trypanosoma brucei* (*T. b.*) *gambiense*; HAT in east and southern Africa is primarily an acute and virulent disease caused by *T. b. rhodesiense* (Barrett et al., 2007). HAT has afflicted hundreds of thousands of people in rural areas of sub-Saharan Africa. Because of improved HAT control over the past decade, the number of new cases reported to WHO in 2009 has decreased to historically low level (<10,000) in 50 years (WHO, 2010b). However, political unrest, declining contributions by nongovernmental organizations, demographic evolution, climate changes, and reduced funding for HAT control all can lead to resurgence of HAT cases, as occurred in the 1980s (Simarro et al., 2011). As such, close surveillance and continued research of the disease and treatment options must be maintained.

HAT consists of two stages. The first stage of infection begins when parasites are restricted in the hemolymphatic system, accompanied with generalized symptoms, including fever, headache, and joint pain. If untreated, the symptoms progress to endocrine, cardiac, renal, and/or anemic disorders. Second stage infection occurs when the parasites extend their distribution to the central nervous system (CNS), leading to severe neurological dysfunction, with the characteristic symptom of breakdown in the sleep-wake patterns, hence the more common term for this disease: “sleeping sickness”. Without treatment, the disease is 100% fatal, progressing from neurological and psychiatric disorders to coma, and ultimately to death (Barrett, 2010).

HAT treatment is crucial for reducing the trypanosome reservoir in humans and, consequently, for controlling the disease. However, infected individuals often live in resource-deficient and insecure areas of Africa with limited access to health care. Disease control and management, therefore, are extremely challenged by logistical issues, lack of optimal control tools and insufficient financial support for research and development.

A.2. Current Chemotherapy

An effective vaccine has not yet been developed for this deadly disease. In addition, only four licensed compounds are used currently to treat HAT, the choice of which depends on the causative subspecies and disease progression stages (Barrett, 2010). There have been no therapeutic advances in more than 40 years. Chemotherapy for both stages of HAT has been limited to pentamidine and suramin for first stage infection and melarsoprol, eflornithine, and a combination of eflornithine and nifurtimox for second stage infection.

A.2.1. Chemotherapy for First Stage HAT

Pentamidine, an aromatic diamidine (Fig. 1.1), was introduced in the early 1940s and remains the primary therapy for prophylaxis and treatment of *Pneumocystis jirovecii* pneumonia, several forms of American cutaneous leishmaniasis, and first stage of *T. b. gambiense* HAT (Dorlo and Kager, 2008). The diamidine structure of pentamidine has been shown to be essential for antimicrobial activity (Dorlo and Kager, 2008). Despite efficacy against the aforementioned infections, pentamidine has a number of untoward effects, including severe hypo- or hyper-glycemia, severe hypotension, and nephrotoxicity.

Suramin, a sulfonated naphthylamine (Fig. 1.1), was introduced in the early 1920s and, to date, remains the drug of choice for treatment of the first stage of *T. b. rhodesiense* HAT. Suramin is associated with severe side effects, including collapse, nausea, nephrotoxicity and anemia (Bouteille et al., 2003). However, no significant resistance has

been observed in preclinical and clinical isolates, which could be due to its ability to inhibit multiple pharmacological targets (Fairlamb, 2003)

Due to the highly hydrophilic nature of both pentamidine and suramin, they have poor oral absorption and must be given parenterally; neither drug crosses the blood brain barrier in sufficient concentrations to act against the organisms that invade the CNS. Therefore, both drugs are only effective against first stage HAT.

A.2.2. Chemotherapy for Second Stage HAT

Invasion of parasites into the CNS poses a major challenge in drug development for second stage HAT due to the limited ability of many compounds to cross the blood brain barrier. To date, the only antitrypanosomal compounds that can reach therapeutic concentrations in the central nervous system are melarsoprol and eflornithine, both of which have been used for treatment of second stage HAT for many decades (Fairlamb, 2003).

Melarsoprol, an old organic arsenical compound (Fig. 1.1), has been the drug of choice for second stage HAT caused by either *T. b. gambiense* or *T. b. rhodesiense* since 1949 (Fairlamb, 2003). Melarsoprol is a highly lipophilic compound that crosses the blood brain barrier by passive diffusion (Nok, 2003). However, because of poor water solubility, melarsoprol must be administered intravenously after being dissolved in propylene glycol, which is highly irritating to tissues (Nok, 2003). Administration of melarsoprol, therefore, is very painful. The standard melarsoprol treatment regimen, which consists of 26-day consecutive injections, is protracted and associated with severe adverse effects; up to 10% of patients die during treatment from drug-induced reactive encephalopathy (Pepin and Milord, 1994). A newer short-course (10-day) alternative regimen demonstrated comparable efficacy, but a similar incidence of reactive encephalopathy (Burri et al., 2000).

Eflornithine (DFMO), an irreversible inhibitor of ornithine decarboxylase (Fig. 1.1), was introduced in the 1970s (Fairlamb, 2003). Eflornithine exhibits excellent penetration into

the CNS in humans and is effective against both stages of HAT caused by *T. b. gambiense*. Eflornithine is not recommended for *T. b. rhodesiense* infection due to innate tolerance of this strain to the drug (Iten et al. 1995). Compared to melarsoprol, eflornithine is relatively nontoxic with tolerable side effects such as gastrointestinal disturbances and anemia. However, the dosage regimen, which consists of 400 mg/kg per day in four daily infusions over 2 h for at least ten days, is burdensome and costly because it requires in-patient hospitalization. All of these factors limit the widespread use of eflornithine in rural areas of Africa with limited resources (Bouteille et al., 2003).

Nifurtimox, a nitroheterocyclic compound (Fig. 1.1), originally was developed for treatment of American trypanosomiasis (Chaga's disease). The major advantage of nifurtimox is that it is orally active. Common side effects include neurological dysfunction and gastrointestinal tract disorders (Bouteille et al., 2003). Nifurtimox has been used as a companion drug to treat second stage HAT when other treatments (melarsoprol or eflornithine) have failed.

Nifurtimox-Eflornithine Combination Therapy (NECT) was included in the WHO Essential List of Medicines as a new treatment option for second stage *T. b. gambiense* HAT in 2009 (WHO, 2009). Eflornithine combined with nifurtimox offers a more feasible treatment regimen, by significantly reducing the frequency and number of eflornithine infusions from four times daily for 2 weeks to twice daily for one week combined with nifurtimox administered orally three times daily for 10 days; this combination has shown equivalent effectiveness without increased side effects compared with eflornithine alone (Barrett, 2010). Furthermore, this combination may decrease the emergence of resistance to monotherapy and avoid the risk of severe adverse events associated with melarsoprol (encephalopathy). Despite these advantages, NECT has a number of limitations: it is less effective against *T. b. rhodesiense* HAT and requires administration of two drugs (IV and oral) for 7-10 days, which is a relatively complicated regimen.

In conclusion, although all of the current treatments for both stages of HAT have been used for decades, none of them are satisfactory. Increasing rates of treatment failures due to parasite resistance, inconvenient regimens, painful formulations, significant adverse events, costly regimens, and involvement of specialized health personnel are all limitations of current therapies. Parenteral administration due to poor oral bioavailability poses significant challenges in remote regions of Africa where this disease is prevalent. Limitations of current chemotherapies highlight the desirable features of new drugs for HAT treatment (DNDi, 2009), which include: 1) low toxicity; 2) oral activity; 3) efficacy towards both stages of HAT; 4) a broad spectrum against both *T. b. gambiense and rhodesiense*; 5) short treatment duration; 6) product stability over long-term storage; and 7) affordability. Without question, an orally-active drug with a convenient treatment regimen and a low potential for toxicity would have great clinical benefit in the treatment of both stages of HAT.

B. ORALLY-ACTIVE PENTAMIDINE ANALOGUES

Pentamidine (Fig. 1.1) has been used clinically since 1939 and remains an important agent to treat first stage HAT despite a loss of activity when administered orally and toxicity when administered intravenously. The diamidine structure of pentamidine has been shown to be essential for antimicrobial activity, which is assumed to result from binding to the minor groove of DNA at AT-rich regions (Barrett et al., 2007). The exact mechanism of action of pentamidine is currently unknown. Of the many structurally related compounds that have been synthesized and tested to date, the dicationic agent, 2,5-bis(4-amidinophenyl)furan (furamidine; Fig. 1.2) has emerged as the most promising agent in terms of efficacy and toxicity when administered intravenously. However, like pentamidine, furamidine has the diamidine moiety ($pK_a \approx 10$), which carries positive charges at physiological pH and limits the ability of furamidine to cross the intestinal epithelia when administered orally. As such, a

prodrug strategy that focuses on attempting to mask these positive charges with *O*-alkyl moieties was devised to improve the oral bioavailability of diamidine.

B.1. Pafuramidine

Pafuramidine (Fig. 1.2) (Boykin et al., 1996), a methylamidoxime prodrug of furamidine, exhibits enhanced intestinal permeability and oral activity in mouse and monkey models (Zhou et al., 2002). To date, pafuramidine is the only orally available agent that has shown promise in clinical trials for the treatment of first stage HAT (Paine et al., 2010). In a multi-center phase III trial conducted from 2005 to 2007, 273 patients were enrolled and randomized to treatment with pafuramidine (100 mg oral, twice daily for 10 days) or pentamidine (4 mg/kg intramuscular, once daily for 7 days). Pafuramidine demonstrated promising efficacy, comparable to pentamidine; the 24-month post-treatment efficacy was 84% and 89%, respectively (Paine et al., 2010). As requested by the U.S. Food and Drug Administration, an expanded phase I safety study was initiated in late 2007 involving healthy indigenous African volunteers, and the treatment regimen was extended from 10 to 14 days. During this study, approximately 25% of subjects developed transiently elevated liver transaminases five days after completion of the 14-day dosage regimen. This adverse event placed pafuramdine development program on clinical hold (www.immtechpharma.com/documents/news_022208.pdf) (Paine et al., 2010). Mechanisms responsible for pafuramidine-induced elevated hepatic signals currently are being investigated in preclinical models.

Bioactivation of pafuramidine to the active metabolite, furamidine, is believed to occur primarily in the liver. The metabolic pathway involves sequential oxidative *O*-demethylation reactions catalyzed by multiple cytochrome P450 enzymes (notably, CYP4F2/3B) and reductive *N*-dehydroxylation reactions catalyzed by cytochrome b_5/NADH cytochrome b_5 reductases (Fig. 1.3) (Saulter et al., 2005; Wang et al., 2006). In rats

administered a single oral dose (10 mg/kg) of ^{14}C-pafuramidine, total radioactivity, largely as furamidine, accumulated in the liver at substantially higher concentrations (~1300 fold) than those measured in plasma 24 hr post-administration; radioactivity was still measurable in the liver after seven days (Midgley et al., 2007). Validation of a rat toxicity model currently is being undertaken by our collaborators at the Hamner Institute for Health Sciences (RTP, NC). Preliminary results showed that pafuramidine demonstrated dose-dependent elevation of liver transaminases in rats (unpublished observations). Furamidine is generated primarily in the liver, where accumulation of furamidine increases with increment of pafuramidine dose. Whether furamidine accumulates in livers of humans in vivo is not known.

B.2. 2, 5-Bis [5-(*N*-methoxyamidino)-2-pyridyl] furan (CPD-0868)

Drug treatment for second stage infection still relies on the old monotherapy (melarsoprol or eflornithine) and newly approved combination therapy (NECT), all of which require complicated/protracted treatment and inconvenient parenteral administration. Both pafuramidine and furamidine were unsuccessful for treatment of second stage infection because of limited access of furamidine to the brain (Mdachi et al., 2009). Structural analogs currently are being tested in various in vitro and in vivo systems, one of which is 2, 5-bis (5-amidino)-2-pyridyl) furan (CPD-0801; Fig. 1.2).

In vitro IC_{50} studies indicated that CPD-0801 was highly potent against both *T. b. gambiense and rhodesiense,* similar to furamidine and pentamidine. In vivo studies with a second stage mouse model administered CPD-0801 (20 mg/kg intraperitoneal, once daily for 10 days) demonstrated 100% cure; infected mice survived for more than 180 days after infection without showing a parasitemia relapse (Wenzler et al., 2009). Under the same experimental conditions, neither furamidine nor pentamidine showed efficacy against second stage infection in mice (Wenzler et al., 2009). An acetate salt of CPD-0801 (CPD-0802) is currently under consideration for clinical testing in the treatment of second stage

HAT (Paine et al., 2010). Despite promising efficacy, CPD-0801 is an aromatic diamidine and exhibits poor oral activity due to inherent hydrophilic properties. Therefore, its methoxy prodrug, 2, 5-bis [5-(*N*-methoxyamidino)-2-pyridyl] furan (CPD-0868; Fig. 1.2), was synthesized.

CPD-0868, a structural analog of pafuramidine, differs from pafuramidine by a single nitrogen incorporated into both phenyl rings. CPD-0868 was shown to be effective against both first and second stage infection in mice (Wenzler et al., 2009). Despite the remarkable structural similarity, CPD-0868 demonstrated a much higher cure rate compared to pafuramidine (4/5 versus 1/5) when administered at a oral dose of 50 mg/kg once daily for 10 days in a second stage mouse model (Wenzler et al., 2009). Systemic exposure of the corresponding active metabolite (CPD-0801) was higher than that of furamidine, the active metabolite of pafuramidine (Wu et al., 2007). Higher systemic concentrations of CPD-0801 could lead to enhanced brain exposure of this active metabolite, and hence, adequate therapeutic concentrations to kill the parasites in the brain. These results supported the hypothesis that CPD-868 may be a promising prodrug for treatment of second stage HAT.

C. INTEGRATION OF PRECLINICAL AND MATHEMATICAL MODELS TO OPTIMIZE PRODRUG DOSE-SELECTION STRATEGY

Successful completion of proof-of-concept phase II and multi-center phase III trials of pafuramidine were promising milestones in the development of this orally-active agent for patients who are suffering from this devastating disease without proper treatment. However, the transiently elevated liver transaminases observed in the subsequent safety study involving indigenous African healthy volunteers suspended the development of this promising agent (www.immtechpharma.com/documents/news_022208.pdf) (Paine et al., 2010). Although pafuramidine is no longer under development, there are many promising

compounds currently under preclinical evaluation, including CPD-0868, a lead candidate for both first and second stages of HAT (Wenzler et al., 2009).

Drug-induced toxicity is the primary cause of attrition of compounds during drug development and post-marketing withdrawals in recent years. Approximately 6.7% of hospitalized patients suffer serious adverse drug reactions, defined as those resulting in hospitalization or causing disability or death; adverse drug reactions are the sixth leading cause of death in the United States (Lazarou et al., 1998). It is important to realize that absolute toxicity is rare. Relative toxicity is more common and may be influenced by many factors such as disease processes, dose/frequency/duration of treatment regimens, ADME properties, and drug/diet-drug interactions. In the case of orally-active antiparasitic agents, suspension of the pafuramidine program during late stage clinical studies was not attributed to a lack of efficacy, but to an overt drug-induced adverse event. Based on tissue distribution studies in rats administered a single oral dose of pafuramidine (10 mg/kg), furamidine was sequestered significantly in the liver (Midgley et al., 2007). Whether or not extensive accumulation of furamidine in the liver triggered pafuramidine-induced elevation of liver transaminases in human subjects remains unclear. As mentioned previously, CPD-0868 demonstrated a higher efficacy and an enhanced systemic exposure of derived active metabolite, CPD-0801, compared to pafuramidine/furamidine in a second stage mouse model (Wu et al., 2007; Wenzler et al., 2009). In rats administered a single oral dose of CPD-0868 or pafuramidine (30 μmol/kg), CPD-0801 exhibited 7- and 40-fold less kidney retention compared to furamidine, six hours and eight days post administration of respective prodrug, respectively (Goldsmith, 2011). These observations emphasized the need to gain an improved understanding of the relationship between dose and systemic or tissue exposure, as well as their interrelation to efficacy and safety profiles of these antiparasitic prodrugs and active metabolites.

Drug efficacy results from the complex interplay of several pharmacokinetic processes, including intestinal absorption, distribution into blood and tissues, phase I and/or II metabolism, and renal and/or fecal drug excretion, which act in concert to provide pharmacologically active concentrations at the site of the respective target, e.g., the parasite in the brain during second stage HAT. After oral administration, the prodrugs pafuramidine and CPD-0868 must first traverse the intestinal epithelium and reach the bioactivation site (gut and/or liver) where they are metabolized to the respective active compounds, furamidine and CPD-0801, through complicated metabolic pathways (Fig. 1.3) (Zhou et al., 2004; Generaux, 2010). The fact that insertion of a single nitrogen into each phenyl ring of pafuramidine led to improved efficacy of CPD-0868 towards second stage infection and enhanced systemic exposure of the corresponding active metabolite (CPD-0801) may be reflected by the differences in the intestinal and hepatobiliary disposition between the two prodrug/active metabolite pairs.

To address these important issues, careful selection of relevant and predictive model systems is critical to quantify the impact of both intestinal/hepatic transport and metabolism on the overall disposition of these prodrugs/metabolites. Coupled with mathematical modeling, this integrated approach can provide valuable insight into the intestinal and hepatobiliary disposition of these compounds by assigning significance to each process and identifying the key step(s) that governs the systemic/tissue exposure of these active metabolites.

C.1. Preclinical Models

A compound will not be an effective drug, regardless of the extent of pharmacological activity, unless it is well absorbed, distributed to the target site, metabolized and eliminated in a suitable manner. The ideal antiparasitic prodrug should be rapidly and almost completely absorbed from the gut, and reach the primary bioactivation site in the liver,

where it is efficiently converted to the active metabolite. Once formed, the active metabolite should be efficiently excreted from the liver and reach sufficient concentrations in the systemic circulation to kill the parasites in the hemolymphatic system (first stage), or in the brain to elicit antitrypanosomal effects in the central nervous system (second stage). It is also important that prodrugs and derived active metabolites do not accumulate to a toxic level in the target organs. In order to identify compounds that possess the aforementioned desirable ADME features, proper selection of in vitro and in vivo model systems with descriptive and predictive capabilities is imperative.

C.1.1. Intestinal Absorption Models

Transport of compounds across the intestinal membrane is a complex and dynamic process, and dictated by various influx and efflux mechanisms via transcellular (passive diffusion or carrier/transporter-mediated process) and paracellular (via the tight junctions between the enterocytes) routes (Artursson et al., 2001). Many techniques have been developed and utilized to evaluate the intestinal permeability of drug candidates during early drug discovery (Miret et al., 2004; Penzotti et al., 2004). The commonly used methodologies include: in vitro systems, such as animal tissue-based Ussing chamber and membrane vesicles, human colon adenocarcinoma cell line (Caco-2) and Mardin-Darby canine kidney (MDCK), parallel artificial membrane permeability assay (PAMPA) and immobilized artificial membranes (IAM); in situ intestine perfusion; in vivo animal studies; and in silico methods (Balimane et al., 2000; Lennernas, 2007). Artificial membrane-based systems and computer-based models are high-throughput screening tools, but the lack of mechanistic basis of these methods often causes less predictive results; although more predictive, in situ and in vivo studies are animal- and labor-intensive. As such, in vitro models, which are balanced between predictability and throughput, are the method of choice for permeability assessment in both academic and industrial settings.

Among all the in vitro models, the Caco-2 cell monolayer permeability assay is the most popular and well-recognized model in drug permeability studies (Artursson and Karlsson, 1991). Upon culture, Caco-2 cells differentiate and become confluent to form monolayers with tight junctions and polarized apical (A; gut lumen) and basolateral (B; blood) membranes that are structurally and functionally similar to those of enterocytes in vivo (Sun et al., 2008). Multiple uptake and efflux transporters, such as breast cancer resistance protein (BCRP), P-glycoprotein (P-gp), multidrug resistance protein (MRP), organic anion-transporting polypeptide (OATP), and organic cation transporter (OCT) also are expressed and functional in Caco-2 cells (Hirohashi et al., 2000; Kobayashi et al., 2003; Muller et al., 2005; Sun et al., 2008). In addition, phase II drug metabolizing enzymes, such as sulfotransferases and glutathione S-transferases reside in the Caco-2 cells (Peters and Roelofs, 1989; Sun et al., 2008). Although some phase I enzymes, particularly CYP3A4, are lacking in Caco-2 cells, medium supplemented with 1α,25-dihydroxy-vitamin-D_3 (1α,25-$(OH)_2$-D_3) can induce the CYP3A4 enzyme levels in a dose-dependent manner (Schmiedlin-Ren et al., 1997). In addition to CYP3A4 enzyme, expression and activity of various transporters including P-gp, MRP1, and MRP2 also are significantly increased (p<0.05) in 1α,25-$(OH)_2$-D_3-treated Caco-2 cells (Fan et al., 2009). These characteristics of Caco-2 cells allow for studying both intestinal metabolism and transport in a single cell-based system.

Previous studies showed that absorptive permeability coefficient ($P_{app,A\rightarrow B}$) of drugs derived in Caco-2 cell monolayers correlates well with the fraction of compound absorbed (f_a) measured in humans in a sigmoidal shape (Artursson and Karlsson, 1991; Keldenich, 2009). According to Artursson and Karlsson, compounds that have $P_{app,A\rightarrow B}$ greater than 1×10^{-6} cm/s in Caco-2 cells may be absorbed completely from the small intestine in humans. Another report showed that only drugs that have $P_{app,A\rightarrow B}$ greater than 7×10^{-6} cm/s are considered to be highly permeable ($f_a \approx 100\%$) (Keldenich, 2009). It is well known that the main limitation of Caco-2 is the inter-laboratory variability (Stewart et al., 1995; Dressman et

al., 2008); the thresholds for permeability classification are, therefore, assay-specific and may differ from lab to lab. $P_{app,A\rightarrow B}$ value may not accurately predict f_a when drugs are absorbed primarily via a paracellular route or transporters due to the narrower tight junctions and over- or under-expression of transporters in Caco-2 cells, respectively (Chong et al., 1996; Collett et al., 1996; Yee, 1997).

In addition to the permeability across the intestinal membrane, formulations and physicochemical properties including molecular weight, solubility, lipophilicity, pK_a also are important determinants in the prediction of f_a in humans (Keldenich, 2009). Following oral administration, the compound must be released from the dosage form, dissolved in the gastrointestinal (GI) fluids to be available in solution form at the sites of absorption (i.e., intestine). The Biopharmaceutical Classification System (BCS), provided by U.S. Food and Drug Administration, categorizes compounds into one of the four biopharmaceutical classes based on their water solubility and membrane permeability and allows the prediction of the rate-limiting step in the intestinal absorption process following oral administration (Polli et al., 2008). In addition, food components also can play a role in the oral absorption of drugs, especially for poorly water-soluble but highly permeable compounds, absorption of which is usually bolstered when drugs are administered with food (Welling, 1996). Therefore, results with Caco-2 cells need to be considered within the context of other factors in the estimation of f_a in humans.

C.1.2. Hepatobiliary Models

After oral administration and absorption through the GI tract, drugs reach the primary clearing organ, the liver, where compounds can be metabolized by phase I or II enzymes, sequestered in the liver, excreted into bile, and/or effluxed back to the systemic circulation. Hepatobiliary disposition may play an important role in the overall therapeutic and/or toxicologic profile of a drug. For this reason, preclinical hepatic models that can accurately

resemble in vivo disposition of drug candidates in the liver can provide a mechanistic understanding of the hepatic disposition of a compound at an early developmental stage. Several in vitro or ex vivo hepatic models have been developed in the past few decades, including microsomes, cytosol, S9 fraction, cell lines, primary hepatocytes, liver slices, and perfused liver (Brandon et al., 2003). Model selection depends on the purpose of the study (e.g. phenotyping, biotransformation pathways, drug-drug interactions, hepatic uptake, and/or biliary excretion). In order to accurately investigate the overall hepatobiliary disposition of compounds, polarized whole-cell model systems must be utilized.

Isolated perfused livers (IPLs) are the most physiologically-relevant ex vivo hepatic model because this model most closely approximates the whole liver in vivo (Brouwer and Thurman, 1996). Depending on the study objectives, IPLs can be performed in a either single-pass or recirculating manner; corresponding surgical procedures and experimental conditions have been described (Xiong et al., 2000; Ward et al., 2001; Zamek-Gliszczynski et al., 2006). In contrast to in vitro models including microsomes, isolated/cultured hepatocytes, and liver slices, IPLs preserve hepatic architecture, cell polarity, and bile flow in the absence of the influences from in vivo non-hepatic and neural-hormonal effects (Gores et al., 1986). Besides, IPLs allow repeated sampling of perfusate, permit easy exposure of the liver to different concentrations of “victim” (test substrate) and “perpetrators” (inhibitors or inducers of metabolism and transport), and are amenable to alterations in physiology (blood flow and/or disease state) that would not be tolerated or feasible in vivo (Brouwer and Thurman, 1996). These advantages make IPLs a valuable model to elucidate the impact of the physiologic, pathologic, and pharmacologic factors on the hepatobiliary disposition of xenobiotics. Despite all these advantages, there are a number of reasons why IPLs are not used routinely, especially in the industry setting. The availability of viable human livers is limited due to ethical reasons, and livers from preclinical species may not be a useful predictor of drug disposition in humans. Furthermore, IPLs are labor intensive,

require delicate surgical procedures, and the functional integrity of metabolic systems and biliary excretion typically is limited to 2 h (Brouwer and Thurman, 1996).

Sandwich-cultured hepatocytes (SCH) represent an alternative in vitro model to study the hepatobiliary disposition of xenobiotics (Dunn et al., 1989). Primary hepatocytes from animals or humans cultured between two layers of gelled collagen form extensive bile canalicular networks (LeCluyse et al., 1994). When hepatocytes are cultured in a collagen-sandwich configuration, the cells differentiate, allowing for sinusoidal and canalicular transport protein localization to the proper domain. SCH may represent a useful tool for investigating the hepatobiliary disposition of compounds. However, a major limitation of SCH is the decrease in cytochrome P450 enzyme activities observed over days in culture (Hoen et al., 2000; Boess et al., 2003). Medium supplemented with inducers such as phenobarbital and dexamethasone (DEX) can reverse the decline in enzyme expression and maintain the enzyme levels comparable to in vivo conditions, as determined by gene expression and enzyme activity analysis (Kienhuis et al., 2007).

Because of the presence of complete phase I/II metabolizing enzymes and cofactors, SCH are an appropriate system for metabolite identification and metabolic stability evaluation. These applications are supported by numerous reports on the similarity in metabolite profiles between SCH and in vivo models (Ansede and Brouwer, 2008; Wolf et al., 2008; Yan et al., 2011). A handful of literature reports demonstrated that SCH also are capable of studying drug-drug interactions at the levels of both hepatic uptake/efflux and metabolic processes (Annaert and Brouwer, 2005; Hewitt et al., 2007a; Lengyel et al., 2008; Jackson et al., 2009). Another advantage of SCH is its ability to differentiate the contribution of transporters via RNA interference (RNAi) of single or multiple transport proteins, particularly when probe substrates or inhibitors are not available. This technique showed success in specifically knocking down Bcrp/BCRP and Oatp/OATP in rat and human SCH (Yue et al., 2009; Liao et al., 2010).

Drug-induced liver injury (DILI) is the most common reason for safety-related drug marketing withdrawals and is a primary toxicological cause of attrition during drug development. Many hepatotoxic compounds are not recognized in preclinical species until later clinical studies, indicating that tolerability to toxic substances varies between animals and humans. Therefore, a human-derived in vitro model that can accurately predict DILI at early preclinical stage is highly needed. Bosentan, an endothelin receptor antagonist for the treatment of pulmonary arterial hypertension, demonstrated hepatotoxicity in humans, but not in rats (Fattinger et al., 2001; Cohen et al., 2004). Using rat and human SCH, the mechanism of bosentan-induced preferential hepatotoxic effect in humans was explained by a differential inhibition of Na^+-dependent taurocholate cotransporting polypeptide (Ntcp/NTCP) between the two species, resulting a greater extent of intrahepatic accumulation of bile acid in humans (Leslie et al., 2007). Studies on hepato-protective effect of DEX against trabectedin-mediated cytotoxicity further substantiated SCH as a useful in vitro model to assess and predict the hepatotoxicity of xenobiotics (Lee et al., 2008).

SCH, cultured in different formats (6- to 96-well plates), are widely utilized in both industrial and academic research settings because of the versatility of this in vitro system to address a variety of scientific questions and applications. Compared to ex vivo (e.g. IPLs) and in vivo models, SCH represent a higher-throughput and more cost-effective system by significantly reducing the number of animals and amount of compounds required for experimentation. In addition, SCH from humans offer significant advantages over existing methodologies (e.g. liver microsomes and suspended/conventionally-cultured hepatocytes) to characterize and predict human biotransformation and transport processes.

C.2. PBPK Modeling-Based Dose-Selection Strategy

Once the differential influence of ADME factors on the overall disposition of prodrugs and active metabolites is elucidated, translation of these results together with previously

generated preclinical data to make them therapeutically meaningful is warranted. This translational step is crucial to fill the gap between scientific research at the preclinical stage and the application of this information to the clinical setting.

Selection of an appropriate dosage regimen is essential in clinical drug development of drug candidates that have shown therapeutic promise in preclinical evaluations. If too high of a dose is selected, immediate toxicity and early termination of the drug candidate may occur. If too low of a dose is selected, it will add unnecessary testing and expense to the dose-ranging studies (Peck and Cross, 2007). Estimating the starting dose is a complicated and important task, and yet there is little uniformity or standardization of approaches. Dose calculations are performed in many different ways, often using empirical methods (Poulin and Theil, 2002). The approach used often depends on the training and experience of the scientists involved, and/or clinically used dosing regimens of structurally similar analogs. A mechanism-based approach is needed to select the right dose on a less empirical, more rational basis. Integration of the pharmacokinetic and pharmacodynamic properties of drug candidates utilizing mathematical model-based drug-development techniques would provide a sound scientific strategy for efficient dose optimization (Zhang et al., 2006; Lalonde et al., 2007; Wetherington et al., 2010).

Empirical allometric scaling, based on body weight, is a commonly used method for extrapolating doses from animals to humans (Ito and Houston, 2005). Although many drugs are well predicted in humans from animal data using this method, some fail in the scaling exercise. For compounds that are distributed by passive distribution and that are mainly eliminated through hepatic metabolism or glomerular filtration, allometric scaling can provide relatively good predictions in pharmacokinetics for humans. In contrast, such method have proven to be of limited value for compounds that show large interspecies differences in the distribution and excretion processes (Mahmood, 2000).

Physiologically-based pharmacokinetic (PBPK) modeling, initially used in the areas of environmental toxicology and human health risk assessment, has been increasingly accepted and utilized in drug development over the years, primarily as a means to extrapolate pharmacokinetic behaviors from animals to humans (Andersen and Krishnan, 1994; Bjorkman et al., 2001; Germani et al., 2005; Chiu et al., 2007; Germani et al., 2007). Unlike empirical allometric scaling, PBPK modeling includes specific tissue compartments involved in exposure, toxicity, metabolism, and biliary/renal excretory processes associated with blood flow (Fig. 1.4). Because compartments and blood flows are described using physiologically-relevant parameters, extrapolation between species can be performed by altering these physiological parameters (Rowland et al., 2004).

In most cases, tissues are considered as “well-stirred” compartments, where the distribution of compounds between organs and blood is determined only by the flow rate of blood perfusing the organ (flow-limited kinetics); on the subtissue level, tissue blood and intracellular space can be further separated when diffusion across physiological membrane barriers becomes the rate-limiting step in the distribution of compounds within tissues (diffusion-limited kinetics) (von Kleist and Huisinga, 2007; Evans et al., 2008). Tissue-to-plasma partition coefficient (K_p) is a key parameter to describe the rate and extent of distribution of a compound between the two compartments. K_p is often measured by either in vivo animal studies under the steady-state conditions or in vitro equilibrium dialysis (Kousba and Sultatos, 2002). However, this measurement process is elaborate, limiting the widespread use of PBPK modeling. It has become increasingly popular and accepted to estimate K_p based on physicochemical properties of compounds such as lipophilicity and pK_a (Poulin and Theil, 2000; Rodgers and Rowland, 2006). However, when active transport processes are involved, K_p of compounds needs to be determined experimentally.

Hepatic clearance (Cl_H) also is a very important parameter that dictates the overall disposition of compounds. Methods for predicting human in vivo Cl_H from in vitro systems

(e.g., hepatocytes and microsomes) and in vivo animal models have been described in detail (Obach, 1999; Luttringer et al., 2003; Ito and Houston, 2005; Lipscomb and Poet, 2008). Through the incorporation of these drug-specific ADME properties derived from in silico, in vitro, ex vivo, and in vivo systems into the model, PBPK modeling is capable of extrapolating between routes of exposure (intravenous versus oral), species (rat versus human), and dosage regimens (single versus multiple dose). For this reason, dosage regimens can be selected based upon model simulations on plasma/tissue concentration-time profiles and anticipated therapeutic and safety margins of compounds (Parrott et al., 2005).

Dose selection for antiparasitic drugs traditionally has relied on correlations between plasma concentrations in animal models and humans. Clinically-used dosage regimen of pafuramidine also was selected based on this method. However, the relationship between pafuramidine dose and furamidine plasma/tissue exposure is not known. This prodrug/active metabolite pair has been studied in multiple preclinical species (mice, rats, and monkeys) and humans by different collaborative labs and institutes involved in the Consortium for Parasitic Drug Development (CPDD). A large body of pafuramidine/furamidine pharmacokinetic and efficacy/safety data exists in various in vitro and in vivo model systems. The mechanistic and physiologic nature of PBPK modeling served as an ideal platform to combine all the preclinical/clinical results in an integrated manner to predict the dose-plasma/tissue exposure relationship. In this dissertation project, additional preclinical models (in vitro and ex vivo) were selected and implemented in the mechanistic investigations of the intestinal and hepatobiliary disposition of pafuramidine and CPD-0868 and respective active metabolites, furamidine and CPD-0801. With the aid of PBPK models developed in this project, concentration-time profiles of furamidine in plasma and tissue (liver and kidney) were simulated under various dosing scenarios in humans. The dose-plasma/exposure relationship was predicted for the model antiparasitic prodrug/active metabolite pair,

pafuramidine and furamidine. This PBPK modeling-based strategy could be applied to next-in-class compounds to guide dose-ranging studies in humans.

D. OVERVIEW OF PROJECT

Human dose projection is a key component of preclinical development before initiation of the first-in-human study. Selection of a first-in-human dose plays an important role in the anticipation of therapeutic-safety index, allowing for early discrimination of selection of potential drug candidates for later phase II/III trials. An appropriate dosage regimen should allow the drug candidate to achieve therapeutic concentrations at the site of action for a suitable duration of time, while maintaining these concentrations associated with a desirable safety profile. Therefore, preclinical studies should not only focus on the evaluation of efficacy, safety, and PK profiles in various preclinical models, but also the prediction of clinical outcomes via quantitative integration of preclinical data.

In this dissertation project, pafuramidine, a prodrug of furamidine, and CPD-0868, a prodrug of CPD-0801, were selected as model prodrug/active metabolite pairs for investigation of these aforementioned issues. Pafuramidine was the only orally-active agent that entered clinical trials for treatment of first stage HAT (Paine et al., 2010). However, clinical development of pafuramidine was suspended due to transiently elevated liver transaminases observed in an expanded phase I safety study (http://www.immtechpharma.com/documents/news_022208.pdf) (Paine et al., 2010). Furamidine exhibited extensive hepatic retention in rats following a single oral dose of pafuramidine (Midgley et al., 2007). CPD-0868, a lead candidate for oral treatment of second stage HAT, currently is under preclinical development. The active metabolite, CPD-0801 exhibited a greater systemic exposure than furamidine, despite remarkable structural similarity between these two active metabolites (Wu et al., 2007). An improved mechanistic understanding of the disposition and the dose-exposure relationship of these prodrugs and metabolites is needed. These unaddressed important issues serve as the foundation for the central hypothesis and aims of this dissertation.

Central Hypothesis: Integration of preclinical data and mechanism-based pharmacokinetic modeling can elucidate mechanisms underlying the difference in systemic/tissue exposure between the two antiparasitic active metabolites, and provide a framework for prediction of the disposition and the dose-plasma/tissue exposure relationship of prodrugs/metabolites in humans.

To test this hypothesis, a multiexperimental approach, which included the human intestinal cell line Caco-2, rat isolated perfused livers (IPLs), rat and human sandwich-cultured hepatocytes (SCH), a plasma/tissue binding assay, and pharmacokinetic (compartmental/noncompartmental and PBPK) modeling, was employed as outlined in the following specific aims:

AIM #1. CHARACTERIZE AND COMPARE THE INTESTINAL DISPOSITION OF THE PRODRUGS PAFURAMIDINE AND CPD-0868 USING THE HUMAN INTESTINAL CELL LINE CACO-2.

Hypothesis: *The improved efficacy of the prodrug CPD-0868 compared to pafuramidine is due to superior permeability through the intestinal epithelium, which results in increased hepatic exposure to CPD-0868.*

1.a. Determine the permeability coefficient (P_{app}) of pafuramidine and CPD-0868 across Caco-2 cell monolayers (A→B and B→A) under serum-free conditions.

1.b. Determine the permeability coefficient (P_{app}) of pafuramidine and CPD-0868 across Caco-2 cell monolayers (A→B) under "sink" conditions (addition of 4% BSA into the B compartment)

1 c. Evaluate the accumulation of pafuramidine and CPD-0868 in Caco-2 cells.

AIM #2. ELUCIDATE MECHANISMS UNDERLYING THE DIFFERENCE IN SYSTEMIC EXPOSURE OF ACTIVE METABOLITES, FURAMIDINE AND CPD-0801, BY COMPARING THE HEPATOBILIARY DISPOSITION OF RESPECTIVE PRODRUGS AND DERIVED METABOLITES IN TWO PRECLINICAL HEPATIC MODELS.

Hypothesis: *The enhanced systemic exposure of CPD-0801 compared to furamidine reflects superior hepatobiliary disposition characteristics, including a greater extent of conversion, less intrahepatic sequestration, and/or more efficient excretion of CPD-0801 from hepatocytes into the systemic circulation.*

2.a. Quantify in recirculating isolated perfused livers (IPLs) from rats the extent of conversion of each prodrug to the corresponding active metabolite and the hepatocellular accumulation, biliary excretion and basolateral efflux of each prodrug and derived metabolites.

2.b. Quantify in sandwich-cultured hepatocytes (SCH) from rats the extent of conversion of each prodrug to the corresponding active metabolite and the hepatocellular accumulation, biliary excretion and basolateral efflux of each prodrug and derived metabolites.

2.c. Utilize the data generated from AIMS 2a and 2b and compartmental pharmacokinetic modeling to compare the hepatobiliary disposition of pafuramidine and CPD-0868 and derived metabolites, and elucidate the predominant process(es) that govern the hepatic disposition of respective active metabolites.

2.d. Compare the data generated in rat SCH with rat IPL data.

AIM #3. DESIGN A SYSTEMATIC STRATEGY FOR DOSE SELECTION VIA PBPK MODELING AND SIMULATION USING PAFURAMIDINE/FURAMIDINE AS A MODEL PRODRUG/ACTIVE METABOLITE PAIR.

Hypothesis: Incorporation of preclinical data into a PBPK model can be used to predict the disposition and the dose-plasma/tissue exposure relationship of pafuramidine/furamidine in humans.

3.a. Develop a whole-liver rat semi-PBPK model for pafuramidine/furamidine using rat IPL data generated from Aim 2a.

3.b. Develop a whole-body rat semi-PBPK model for pafuramidine/furamidine with integration of the IPL model and data from in vivo studies, tissue partitioning and renal excretion; examine the accuracy of the prediction by comparing with in vivo plasma data.

3.c. Develop a whole-body human semi-PBPK model for pafuramidine/furamidine to 1) predict the plasma/tissue and excretion profiles, and 2) predict the dose-exposure relationship in humans.

E. FIGURES

First Stage

Pentamidine

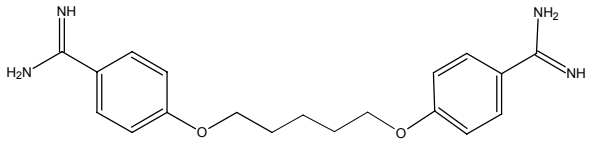

Suramin

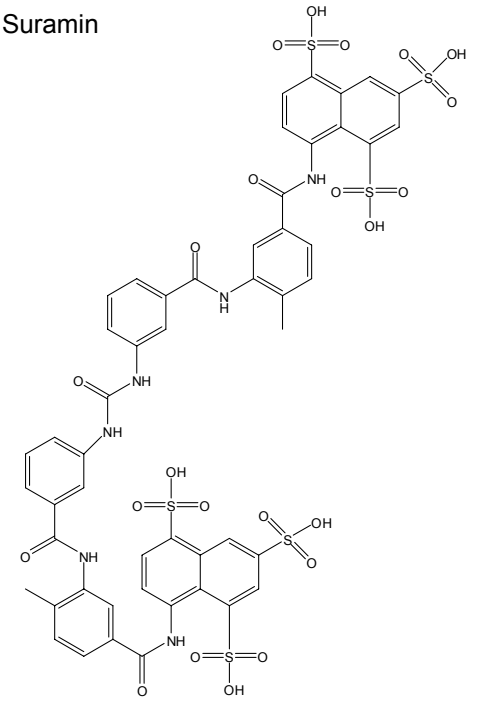

Second Stage

Melarsoprol

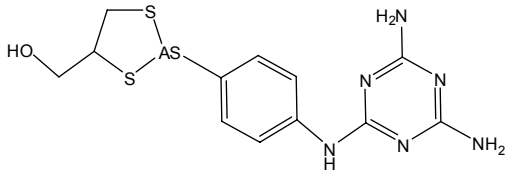

Eflornithine

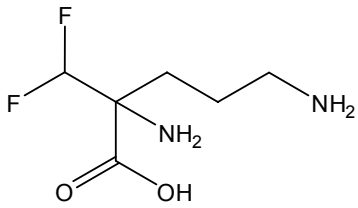

Nifurtimox

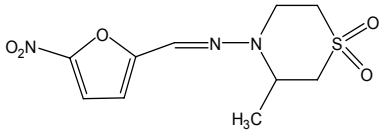

Figure 1.1. Chemical structures of drugs for treatment of first stage (left) and second stage (right) human African trypanosomiasis.

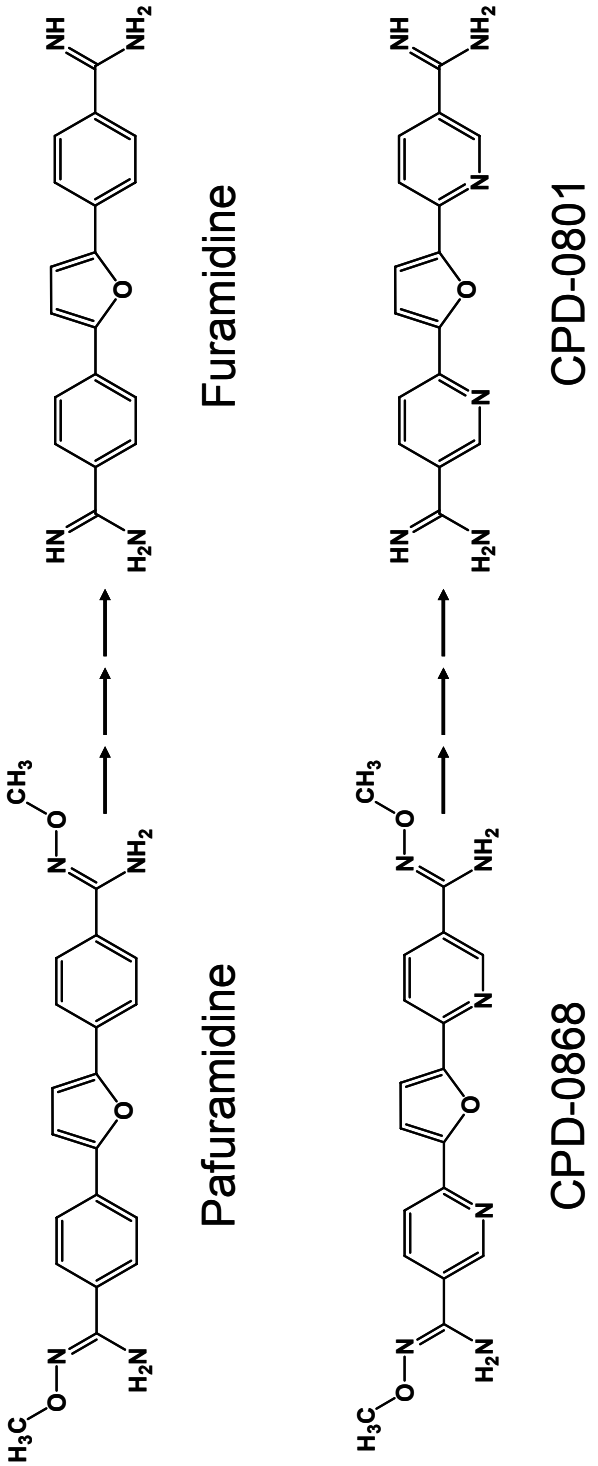

Figure 1.2. Chemical structures of orally-active pentamidine analogues, pafuramidine and 2, 5-bis [5-(*N*-methoxyamidino)-2-pyridyl] furan (CPD-0868), and corresponding active metabolites, furamidine and 2, 5-bis (5-amidino)-2-pyridyl) furan (CPD-0801). Arrows denote sequential metabolic pathways involved in the conversion of prodrugs to respective active metabolites.

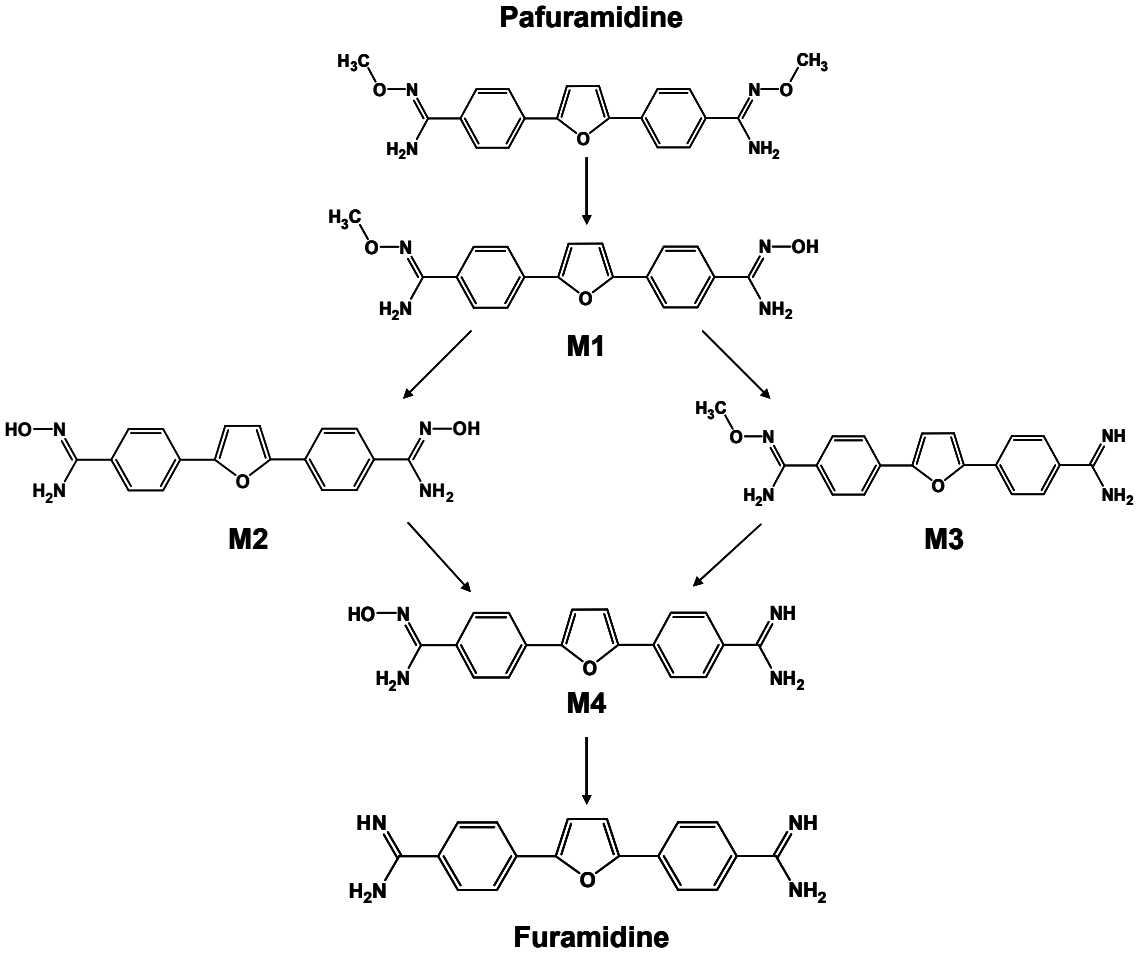

Figure 1.3. Biocoversion of the prodrug pafuramidine to the active metabolite furamidine in human liver microsomes. M1-M4 represent four intermediate phase I metabolites.

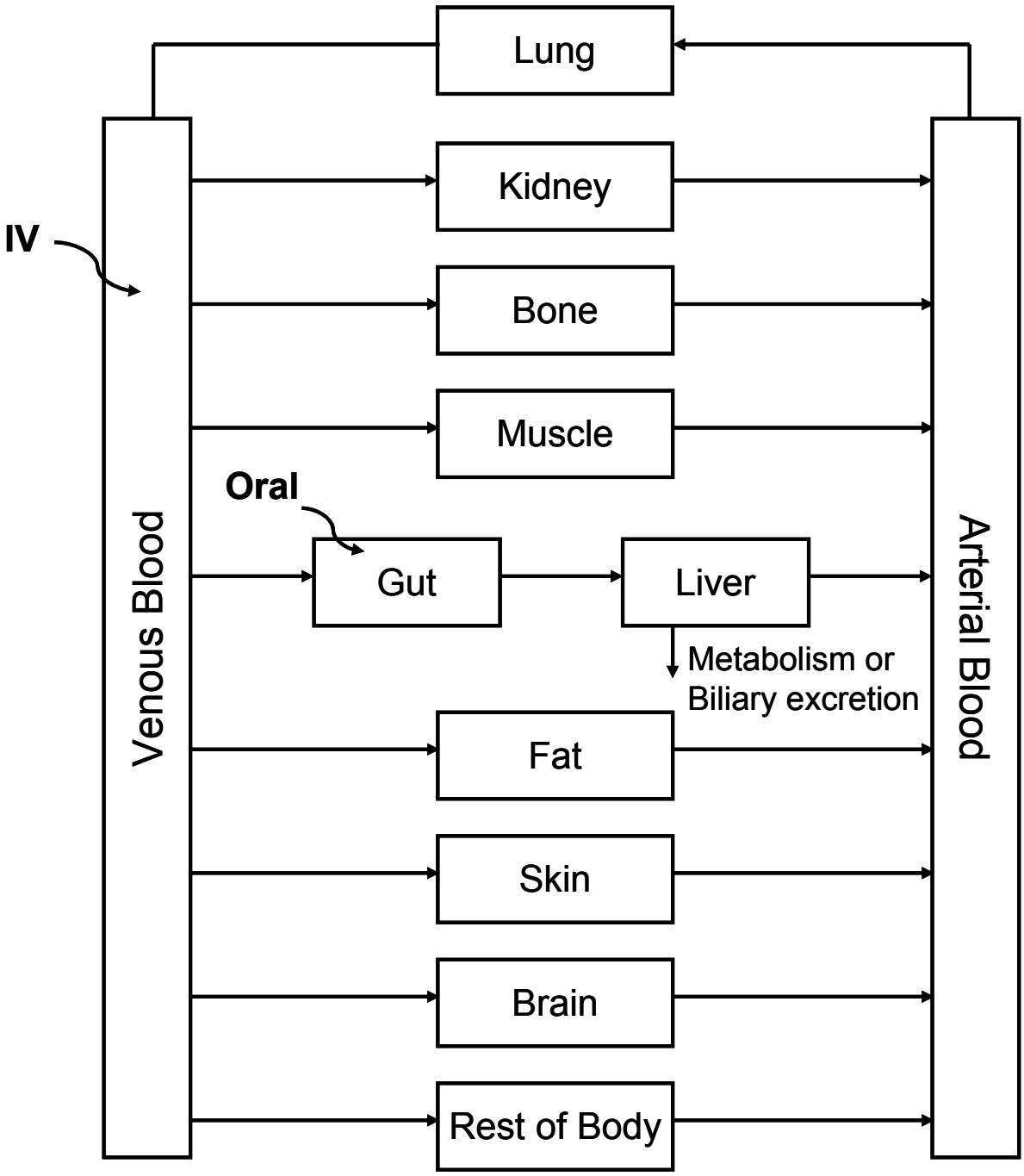

Figure 1.4. Scheme for a generic physiologically-based pharmacokinetic (PBPK) model.

F. REFERENCES

Andersen ME and Krishnan K (1994) Physiologically based pharmacokinetics and cancer risk assessment. *Environ Health Perspect* **102 Suppl 1**:103-108.

Annaert PP and Brouwer KL (2005) Assessment of drug interactions in hepatobiliary transport using rhodamine 123 in sandwich-cultured rat hepatocytes. *Drug Metab Dispos* **33**:388-394.

Ansede JH and Brouwer KR (2008) Transport of Naloxone Glucuronide in B-Clear (Sandwich-Cultured Rat Hepatocytes) and its Application as an In Vitro Model for Determining the Directional Transport of Metabolites, in *10th European ISSX Meeting*, Vienna, Austria.

Artursson P and Karlsson J (1991) Correlation between oral drug absorption in humans and apparent drug permeability coefficients in human intestinal epithelial (Caco-2) cells. *Biochem Biophys Res Commun* **175**:880-885.

Artursson P, Palm K and Luthman K (2001) Caco-2 monolayers in experimental and theoretical predictions of drug transport. *Adv Drug Deliv Rev* **46**:27-43.

Balimane PV, Chong S and Morrison RA (2000) Current methodologies used for evaluation of intestinal permeability and absorption. *J Pharmacol Toxicol Methods* **44**:301-312.

Barrett MP (2010) Potential new drugs for human African trypanosomiasis: some progress at last. *Curr Opin Infect Dis* **23**:603-608.

Barrett MP, Boykin DW, Brun R and Tidwell RR (2007) Human African trypanosomiasis: pharmacological re-engagement with a neglected disease. *Br J Pharmacol* **152**:1155-1171.

Bjorkman S, Wada DR, Berling BM and Benoni G (2001) Prediction of the disposition of midazolam in surgical patients by a physiologically based pharmacokinetic model. *J Pharm Sci* **90**:1226-1241.

Boess F, Kamber M, Romer S, Gasser R, Muller D, Albertini S and Suter L (2003) Gene expression in two hepatic cell lines, cultured primary hepatocytes, and liver slices compared to the in vivo liver gene expression in rats: possible implications for toxicogenomics use of in vitro systems. *Toxicol Sci* **73**:386-402.

Bouteille B, Oukem O, Bisser S and Dumas M (2003) Treatment perspectives for human African trypanosomiasis. *Fundam Clin Pharmacol* **17**:171-181.

Boykin DW, Kumar A, Hall JE, Bender BC and Tidwell RR (1996) Anti-*Pneumocystis carinii* activity of bis-amidoximes and bis-*O*-alkylamidoxime prodrugs. *Bioorg Med Chem* **6**:3017-3020.

Brandon EF, Raap CD, Meijerman I, Beijnen JH and Schellens JH (2003) An update on in vitro test methods in human hepatic drug biotransformation research: pros and cons. *Toxicol Appl Pharmacol* **189**:233-246.

Brouwer KL and Thurman RG (1996) Isolated perfused liver. *Pharm Biotechnol* **8**:161-192.

Burri C, Nkunku S, Merolle A, Smith T, Blum J and Brun R (2000) Efficacy of new, concise schedule for melarsoprol in treatment of sleeping sickness caused by Trypanosoma brucei gambiense: a randomised trial. *Lancet* **355**:1419-1425.

Chiu WA, Barton HA, DeWoskin RS, Schlosser P, Thompson CM, Sonawane B, Lipscomb JC and Krishnan K (2007) Evaluation of physiologically based pharmacokinetic models for use in risk assessment. *J Appl Toxicol* **27**:218-237.

Chong S, Dando SA, Soucek KM and Morrison RA (1996) In vitro permeability through caco-2 cells is not quantitatively predictive of in vivo absorption for peptide-like drugs absorbed via the dipeptide transporter system. *Pharm Res* **13**:120-123.

Cohen H, Chahine C, Hui A and Mukherji R (2004) Bosentan therapy for pulmonary arterial hypertension. *Am J Health Syst Pharm* **61**:1107-1119.

Collett A, Sims E, Walker D, He YL, Ayrton J, Rowland M and Warhurst G (1996) Comparison of HT29-18-C1 and Caco-2 cell lines as models for studying intestinal paracellular drug absorption. *Pharm Res* **13**:216-221.

DNDi (2009) Human African trypanosomiasis: Target Product Profile (TPP).

Dorlo TP and Kager PA (2008) Pentamidine dosage: a base/salt confusion. *PLoS Negl Trop Dis* **2**:e225.

Dressman JB, Thelen K and Jantratid E (2008) Towards quantitative prediction of oral drug absorption. *Clin Pharmacokinet* **47**:655-667.

Dunn JC, Yarmush ML, Koebe HG and Tompkins RG (1989) Hepatocyte function and extracellular matrix geometry: long-term culture in a sandwich configuration. *Faseb J* **3**:174-177.

Evans MV, Dowd SM, Kenyon EM, Hughes MF and El-Masri HA (2008) A physiologically based pharmacokinetic model for intravenous and ingested dimethylarsinic acid in mice. *Toxicol Sci* **104**:250-260.

Fairlamb AH (2003) Chemotherapy of human African trypanosomiasis: current and future prospects. *Trends Parasitol* **19**:488-494.

Fan J, Liu S, Du Y, Morrison J, Shipman R and Pang KS (2009) Up-regulation of transporters and enzymes by the vitamin D receptor ligands, 1alpha,25-dihydroxyvitamin D3 and vitamin D analogs, in the Caco-2 cell monolayer. *J Pharmacol Exp Ther* **330**:389-402.

Fattinger K, Funk C, Pantze M, Weber C, Reichen J, Stieger B and Meier PJ (2001) The endothelin antagonist bosentan inhibits the canalicular bile salt export pump: a potential mechanism for hepatic adverse reactions. *Clin Pharmacol Ther* **69**:223-231.

Generaux CN (2010) Effects of Parasitic Infection on the Pharmacokinetics and Disposition of Pentamidine Ananalogs. PhD thesis, in *Eshelman School of Pharmacy*, University of North Carolina, Chapel Hill.

Germani M, Crivori P, Rocchetti M, Burton PS, Wilson AG, Smith ME and Poggesi I (2005) Evaluation of a physiologically-based pharmacokinetic approach for simulating the first-time-in-animal study. *Basic Clin Pharmacol Toxicol* **96**:254-256.

Germani M, Crivori P, Rocchetti M, Burton PS, Wilson AG, Smith ME and Poggesi I (2007) Evaluation of a basic physiologically based pharmacokinetic model for simulating the first-time-in-animal study. *Eur J Pharm Sci* **31**:190-201.

Goldsmith RB (2011) Detection and mechanistic comparison of two anti-trypanosomal diamidines in a rat renal model. PhD thesis, in *School of Medicine* University of North Carolina, Chapel Hill.

Gores GJ, Kost LJ and LaRusso NF (1986) The isolated perfused rat liver: conceptual and practical considerations. *Hepatology* **6**:511-517.

Hirohashi T, Suzuki H, Chu XY, Tamai I, Tsuji A and Sugiyama Y (2000) Function and expression of multidrug resistance-associated protein family in human colon adenocarcinoma cells (Caco-2). *J Pharmacol Exp Ther* **292**:265-270.

Hoen PA, Commandeur JN, Vermeulen NP, Van Berkel TJ and Bijsterbosch MK (2000) Selective induction of cytochrome P450 3A1 by dexamethasone in cultured rat hepatocytes: analysis with a novel reverse transcriptase-polymerase chain reaction assay section sign. *Biochem Pharmacol* **60**:1509-1518.

Ito K and Houston JB (2005) Prediction of human drug clearance from in vitro and preclinical data using physiologically based and empirical approaches. *Pharm Res* **22**:103-112.

Jackson JP, Kabirov KK, Kapetanovic IM and Lyubimov A (2009) In vitro assessment of P450 induction potential of novel chemopreventive agents SR13668, 9-cis-UAB30, and pentamethychromanol in primary cultures of human hepatocytes. *Chem Biol Interact* **179**:263-272.

Keldenich J (2009) Measurement and prediction of oral absorption. *Chem Biodivers* **6**:2000-2013.

Kienhuis AS, Wortelboer HM, Maas WJ, van Herwijnen M, Kleinjans JC, van Delft JH and Stierum RH (2007) A sandwich-cultured rat hepatocyte system with increased metabolic competence evaluated by gene expression profiling. *Toxicol* In vitro **21**:892-901.

Kobayashi D, Nozawa T, Imai K, Nezu J, Tsuji A and Tamai I (2003) Involvement of human organic anion transporting polypeptide OATP-B (SLC21A9) in pH-dependent transport across intestinal apical membrane. *J Pharmacol Exp Ther* **306**:703-708.

Kousba A and Sultatos LG (2002) Continuous system modeling of equilibrium dialysis for determinations of tissue partitioning of parathion and paraoxon. *Toxicol Lett* **133**:153-159.

Lalonde RL, Kowalski KG, Hutmacher MM, Ewy W, Nichols DJ, Milligan PA, Corrigan BW, Lockwood PA, Marshall SA, Benincosa LJ, Tensfeldt TG, Parivar K, Amantea M, Glue P, Koide H and Miller R (2007) Model-based drug development. *Clin Pharmacol Ther* **82**:21-32.

Lazarou J, Pomeranz BH and Corey PN (1998) Incidence of adverse drug reactions in hospitalized patients: a meta-analysis of prospective studies. *Jama* **279**:1200-1205.

LeCluyse EL, Audus KL and Hochman JH (1994) Formation of extensive canalicular networks by rat hepatocytes cultured in collagen-sandwich configuration. *Am J Physiol* **266**:C1764-1774.

Lee JK, Leslie EM, Zamek-Gliszczynski MJ and Brouwer KL (2008) Modulation of trabectedin (ET-743) hepatobiliary disposition by multidrug resistance-associated proteins (Mrps) may prevent hepatotoxicity. *Toxicol Appl Pharmacol* **228**:17-23.

Lengyel G, Veres Z, Tugyi R, Vereczkey L, Molnar T, Glavinas H, Krajcsi P and Jemnitz K (2008) Modulation of sinusoidal and canalicular elimination of bilirubin-glucuronides by rifampicin and other cholestatic drugs in a sandwich culture of rat hepatocytes. *Hepatol Res* **38**:300-309.

Lennernas H (2007) Animal data: the contributions of the Ussing Chamber and perfusion systems to predicting human oral drug delivery in vivo. *Adv Drug Deliv Rev* **59**:1103-1120.

Leslie EM, Watkins PB, Kim RB and Brouwer KL (2007) Differential inhibition of rat and human Na+-dependent taurocholate cotransporting polypeptide (NTCP/SLC10A1)by bosentan: a mechanism for species differences in hepatotoxicity. *J Pharmacol Exp Ther* **321**:1170-1178.

Liao M, Raczynski AR, Chen M, Chuang BC, Zhu Q, Shipman R, Morrison J, Lee D, Lee FW, Balani SK and Xia CQ (2010) Inhibition of hepatic organic anion-transporting polypeptide by RNA interference in sandwich-cultured human hepatocytes: an in vitro model to assess transporter-mediated drug-drug interactions. *Drug Metab Dispos* **38**:1612-1622.

Lipscomb JC and Poet TS (2008) In vitro measurements of metabolism for application in pharmacokinetic modeling. *Pharmacol Ther* **118**:82-103.

Luttringer O, Theil FP, Poulin P, Schmitt-Hoffmann AH, Guentert TW and Lave T (2003) Physiologically based pharmacokinetic (PBPK) modeling of disposition of epiroprim in humans. *J Pharm Sci* **92**:1990-2007.

Mahmood I (2000) Critique of prospective allometric scaling: does the emperor have clothes? *J Clin Pharmacol* **40**:341-344; discussion 345-346.

Mdachi RE, Thuita JK, Kagira JM, Ngotho JM, Murilla GA, Ndung'u JM, Tidwell RR, Hall JE and Brun R (2009) Efficacy of the novel diamidine compound 2,5-Bis(4-amidinophenyl)- furan-bis-O-Methlylamidoxime (Pafuramidine, DB289) against Trypanosoma brucei rhodesiense infection in vervet monkeys after oral administration. *Antimicrob Agents Chemother* **53**:953-957.

Midgley I, Fitzpatrick K, Taylor LM, Houchen TL, Henderson SJ, Wright SJ, Cybulski ZR, John BA, McBurney A, Boykin DW and Trendler KL (2007) Pharmacokinetics and metabolism of the prodrug DB289 (2,5-bis[4-(N-methoxyamidino)phenyl]furan monomaleate) in rat and monkey and its conversion to the antiprotozoal/antifungal drug DB75 (2,5-bis(4-guanylphenyl)furan dihydrochloride). *Drug Metab Dispos* **35**:955-967.

Miret S, Abrahamse L and de Groene EM (2004) Comparison of in vitro models for the prediction of compound absorption across the human intestinal mucosa. *J Biomol Screen* **9**:598-606.

Muller J, Lips KS, Metzner L, Neubert RH, Koepsell H and Brandsch M (2005) Drug specificity and intestinal membrane localization of human organic cation transporters (OCT). *Biochem Pharmacol* **70**:1851-1860.

Nok AJ (2003) Arsenicals (melarsoprol), pentamidine and suramin in the treatment of human African trypanosomiasis. *Parasitol Res* **90**:71-79.

Obach RS (1999) Prediction of human clearance of twenty-nine drugs from hepatic microsomal intrinsic clearance data: An examination of in vitro half-life approach and nonspecific binding to microsomes. *Drug Metab Dispos* **27**:1350-1359.

Paine MF, Wang MZ, Generaux CN, Boykin DW, Wilson WD, De Koning HP, Olson CA, Pohlig G, Burri C, Brun R, Murilla GA, Thuita JK, Barrett MP and Tidwell RR (2010) Diamidines for human African trypanosomiasis. *Curr Opin Investig Drugs* **11**:in press.

Parrott N, Jones H, Paquereau N and Lave T (2005) Application of full physiological models for pharmaceutical drug candidate selection and extrapolation of pharmacokinetics to man. *Basic Clin Pharmacol Toxicol* **96**:193-199.

Peck CC and Cross JT (2007) "Getting the dose right": facts, a blueprint, and encouragements. *Clin Pharmacol Ther* **82**:12-14.

Penzotti JE, Landrum GA and Putta S (2004) Building predictive ADMET models for early decisions in drug discovery. *Curr Opin Drug Discov Devel* **7**:49-61.

Pepin J and Milord F (1994) The treatment of human African trypanosomiasis. *Adv Parasitol* **33**:1-47.

Peters WH and Roelofs HM (1989) Time-dependent activity and expression of glutathione S-transferases in the human colon adenocarcinoma cell line Caco-2. *Biochem J* **264**:613-616.

Polli JE, Abrahamsson BS, Yu LX, Amidon GL, Baldoni JM, Cook JA, Fackler P, Hartauer K, Johnston G, Krill SL, Lipper RA, Malick WA, Shah VP, Sun D, Winkle HN, Wu Y and

Zhang H (2008) Summary workshop report: bioequivalence, biopharmaceutics classification system, and beyond. *Aaps J* **10**:373-379.

Poulin P and Theil FP (2000) A priori prediction of tissue:plasma partition coefficients of drugs to facilitate the use of physiologically-based pharmacokinetic models in drug discovery. *J Pharm Sci* **89**:16-35.

Poulin P and Theil FP (2002) Prediction of pharmacokinetics prior to in vivo studies. II. Generic physiologically based pharmacokinetic models of drug disposition. *J Pharm Sci* **91**:1358-1370.

Rodgers T and Rowland M (2006) Physiologically based pharmacokinetic modelling 2: predicting the tissue distribution of acids, very weak bases, neutrals and zwitterions. *J Pharm Sci* **95**:1238-1257.

Rowland M, Balant L and Peck C (2004) Physiologically based pharmacokinetics in drug development and regulatory science: a workshop report (Georgetown University, Washington, DC, May 29-30, 2002). *AAPS PharmSci* **6**:E6.

Saulter JY, Kurian JR, Trepanier LA, Tidwell RR, Bridges AS, Boykin DW, Stephens CE, Anbazhagan M and Hall JE (2005) Unusual dehydroxylation of antimicrobial amidoxime prodrugs by cytochrome b5 and NADH cytochrome b5 reductase. *Drug Metab Dispos* **33**:1886-1893.

Schmiedlin-Ren P, Thummel KE, Fisher JM, Paine MF, Lown KS and Watkins PB (1997) Expression of enzymatically active CYP3A4 by Caco-2 cells grown on extracellular matrix-coated permeable supports in the presence of 1alpha,25-dihydroxyvitamin D3. *Mol Pharmacol* **51**:741-754.

Simarro PP, Diarra A, Ruiz Postigo JA, Franco JR, Jannin JG (2011) The Human African Trypanosomiasis Control and Surveillance Programme of the World Health Organization 2000–2009: The Way Forward. PLoS Negl Trop Dis 5(2): e1007. doi:10.1371/journal.pntd.0001007

Stewart BH, Chan OH, Lu RH, Reyner EL, Schmid HL, Hamilton HW, Steinbaugh BA and Taylor MD (1995) Comparison of intestinal permeabilities determined in multiple in vitro and in situ models: relationship to absorption in humans. *Pharm Res* **12**:693-699.

Sun H, Chow EC, Liu S, Du Y and Pang KS (2008) The Caco-2 cell monolayer: usefulness and limitations. *Expert Opin Drug Metab Toxicol* **4**:395-411.

Tuschl G, Hrach J, Walter Y, Hewitt PG and Mueller SO (2009) Serum-free collagen sandwich cultures of adult rat hepatocytes maintain liver-like properties long term: a valuable model for in vitro toxicity and drug-drug interaction studies. *Chem Biol Interact* **181**:124-137.

von Kleist M and Huisinga W (2007) Physiologically based pharmacokinetic modelling: a sub-compartmentalized model of tissue distribution. *J Pharmacokinet Pharmacodyn* **34**:789-806.

Wang MZ, Saulter JY, Usuki E, Cheung YL, Hall M, Bridges AS, Loewen G, Parkinson OT, Stephens CE, Allen JL, Zeldin DC, Boykin DW, Tidwell RR, Parkinson A, Paine MF and Hall JE (2006) CYP4F enzymes are the major enzymes in human liver microsomes that catalyze the O-demethylation of the antiparasitic prodrug DB289 [2,5-bis(4-amidinophenyl)furan-bis-O-methylamidoxime]. *Drug Metab Dispos* **34**:1985-1994.

Ward ES, Pollack GM and Brouwer KL (2001) Probenecid-associated alterations in valproate glucuronide hepatobiliary disposition: mechanistic assessment using mathematical modeling. *J Pharmacol Exp Ther* **297**:141-147.

Welling PG (1996) Effects of food on drug absorption. *Annu Rev Nutr* **16**:383-415.

Wenzler T, Boykin DW, Ismail MA, Hall JE, Tidwell RR and Brun R (2009) New treatment option for second-stage African sleeping sickness: in vitro and in vivo efficacy of aza analogs of DB289. *Antimicrob Agents Chemother* **53**:4185-4192.

Wetherington JD, Pfister M, Banfield C, Stone JA, Krishna R, Allerheiligen S and Grasela DM (2010) Model-based drug development: strengths, weaknesses, opportunities, and threats for broad application of pharmacometrics in drug development. *J Clin Pharmacol* **50**:31S-46S.

WHO (2006) Human African trypanosomiasis (sleeping sickness): epidemiological update. *Wkly Epidemiol Rec* **81**:71-80.

WHO (2009) WHO includes combination of eflornithine and nifurtimox in its Essential List of Medicines for the treatment of human African trypanosomiasis.

WHO (2010a) Neglected tropical diseases. Innovative and Intensified Disease Management (IDM).

WHO (2010b) Human African trypanosomiasis: number of new cases drops to historically low levels in 50 years.

Wolf KK, Bridges AS, Lee JK, Polli JW, Brouwer KR and Pollack GM (2008) Hepatobiliary Disposition of Morphine and Generated Morphine 3-Glucuronide in Sandwich-Cultured Rat Hepatocytes, in *15th Annual ISSX North American Regional Meeting*, San Diego, CA.

Wu H, Ming X, Wang MZ, Tidwell R and Hall JE (2007) Comparative Pharmacokinetics of the Antitrypanosomal Diamidines DB75, DB820 and DB829 Following Oral Administration of Their Dimethamidoximes Prodrugs in Mice. *The AAPS Journal. 2007; 9(S2).*

Xiong H, Turner KC, Ward ES, Jansen PL and Brouwer KL (2000) Altered hepatobiliary disposition of acetaminophen glucuronide in isolated perfused livers from multidrug resistance-associated protein 2-deficient TR(-) rats. *J Pharmacol Exp Ther* **295**:512-518.

Yan GZ, Brouwer KLR, Pollack GM, Wang MZ, Tidwell RR, Hall JE and Paine MF (2011) Mechanisms Underlying Differences in Systemic Exposure of Structurally Similar Active Metabolites: Comparison of Two Preclinical Hepatic Models
J Pharmacol Exp Ther **In press**.

Yee S (1997) In vitro permeability across Caco-2 cells (colonic) can predict in vivo (small intestinal) absorption in man--fact or myth. *Pharm Res* **14**:763-766.

Yue W, Abe K and Brouwer KL (2009) Knocking down breast cancer resistance protein (Bcrp) by adenoviral vector-mediated RNA interference (RNAi) in sandwich-cultured rat hepatocytes: a novel tool to assess the contribution of Bcrp to drug biliary excretion. *Mol Pharm* **6**:134-143.

Zamek-Gliszczynski MJ, Hoffmaster KA, Humphreys JE, Tian X, Nezasa K and Brouwer KL (2006) Differential involvement of Mrp2 (Abcc2) and Bcrp (Abcg2) in biliary excretion of 4-methylumbelliferyl glucuronide and sulfate in the rat. *J Pharmacol Exp Ther* **319**:459-467.

Zhang L, Sinha V, Forgue ST, Callies S, Ni L, Peck R and Allerheiligen SR (2006) Model-based drug development: the road to quantitative pharmacology. *J Pharmacokinet Pharmacodyn* **33**:369-393.

Zhou L, Lee K, Thakker DR, Boykin DW, Tidwell RR and Hall JE (2002) Enhanced permeability of the antimicrobial agent 2,5-bis(4-amidinophenyl)furan across Caco-2 cell monolayers via its methylamidoidme prodrug. *Pharm Res* **19**:1689-1695.

CHAPTER 2

COMPARISON OF THE INTESTINAL ABSORPTION OF TWO ANTIPARASITIC PRODRUGS USING CACO-2 CELL MONOLAYERS

A. ABSTRACT

A successful oral prodrug should have sufficient permeability to traverse the gut wall and reach major site(s) of bioactivation to the active metabolite. Pafuramidine, a prodrug of furamidine, exhibited potent trypanocidal activity against first stage human African trypanosomiasis (HAT). 2, 5-Bis [5-(*N*-methoxyamidino)-2-pyridyl] furan (CPD-0868), a prodrug of 2, 5-bis (5-amidino)-2-pyridyl) furan (CPD-0801), showed improved efficacy and enhanced systemic exposure to the active metabolite (CPD-0801) compared to pafuramidine/furamidine in a second stage mouse model of HAT. To test the hypothesis that the superiority of CPD-0868 in terms of efficacy and systemic exposure is due in part to a greater extent of absorption, the human intestinal cell line Caco-2 was utilized to elucidate and compare the intestinal absorption properties of pafuramidine and CPD-0868. The similar absorptive and exsorptive permeability, in the absence of basolateral serum protein, suggested that both prodrugs are absorbed across the intestinal epithelium by passive diffusion. Application of 4% bovine serum albumin (BSA) to the basolateral compartment increased absorptive permeability of pafuramidine (by ~5-fold), but not CPD-0868, suggesting that portal plasma protein binding has a more significant impact on pafuramidine absorption. Comparable permeability coefficients of both prodrugs under this more physiologic condition suggested that the extent of absorption between pafuramidine and CPD-0868 may be similar in vivo.

B. INTRODUCTION

Human African trypanosomiasis (HAT), also known as “sleeping sickness”, is a life-threatening disease if untreated (Barrett et al., 2003). First stage infection is characterized by restriction of parasites to the hemolymphatic system; second stage infection occurs once parasites enter the central nervous system (CNS) (Checchi and Barrett, 2008). Current treatments for HAT are limited to four drugs as monotherapy: pentamidine or suramin for first stage infection, and melarsoprol or eflornithine for second stage infection. All of these agents are associated with toxicities and increasing clinical failure and require parenteral administration (intravenous or intramuscular), posing challenges in rural areas of Africa where HAT is most prevalent (Checchi and Barrett, 2008). Orally-active drugs are, therefore, preferred as an alternative route to parenteral administration in resource-constrained settings.

Pentamidine (Fig 2.1), was discovered in 1941 and still remains the drug of choice for the treatment of first stage HAT, regardless of adverse effects (Dorlo and Kager, 2008). Of many structural analogs of pentamidine, furamidine (Fig. 2.1), synthesized in the early 1970s, showed promise, comparable to pentamidine, in animal models of first stage infection (Boykin et al., 1996). However, like pentamidine, furamidine carries positive charges at physiologic pH due to the diamidine moiety ($pK_a \approx 10$), which contributes to poor oral absorption (Zhou et al., 2002). Consequently, furamidine must be administered parenterally to achieve sufficient systemic trypanocidal concentrations at the target site. An approach to improve oral bioavailability of furamidine focused on masking the cationic groups. Accordingly, pafuramidine (Fig. 2.1), an *O*-methylamidoxime prodrug of furamidine, was synthesized (Boykin et al., 1996). Pafuramidine exhibited improved oral activity in mouse and monkey infection models and was the only orally-active agent that had shown efficacy in the treatment of first stage HAT (Paine et al., 2010). However, pafuramidine was

not successful for the treatment of second stage (CNS) infection in a monkey model (Wenzler et al., 2009).

Structural modifications to pafuramidine currently are being evaluated. To date, the most potent analogue is 2, 5-bis [5-(*N*-methoxyamidino)-2-pyridyl] CPD-0868 (Fig. 2.1), a prodrug of 2, 5-bis (5-amidino)-2-pyridyl) furan CPD-0801 (Fig. 2.1), which differs from pafuramidine by substitution of the phenyl rings with pyridines. CPD-0868 demonstrated a higher cure rate (4/5 vs. 1/5 at 50 mg/kg p.o. for 10 days) compared to pafuramidine in a second stage mouse model of infection (Wenzler et al., 2009); systemic exposure to CPD-0801 was >2-fold higher than that to furamidine in mice given the same dose of respective prodrugs (Wu et al., 2007).

These observations led to the hypothesis that the improved efficacy of the prodrug CPD-0868 and enhanced systemic exposure to the active metabolite CPD-0801, compared to pafuramidine/furamidine, is due to superior permeability of CPD-0868 through the intestinal epithelium. Following oral administration, pafuramidine or CPD-0868 must traverse the intestinal epithelium before reaching the portal circulation. Accurate prediction of human intestinal absorption can facilitate selection of candidates with optimal absorption properties for further development as oral drugs. The aims of this study were to 1) ascertain the means of absorption of pafuramidine and CPD-0868; and 2) compare the intestinal permeability between these two prodrugs using the well-characterized human intestine-derived cell line Caco-2.

Caco-2 cells resemble morphologically and functionally the enterocytes of the human small intestine (Artursson, 1999). Caco-2 cells have been used widely as an in vitro tool to predict human drug absorption and elucidate transport mechanisms of drug molecules. The spontaneous differentiation process in cell culture leads to formation of tight junctions and development of cell polarity. Various phase I and phase II drug metabolizing enzymes as well as uptake and efflux transporters including the breast cancer resistance

protein (BCRP), P-glycoprotein (P-gp), multidrug resistance protein (MRP), organic anion-transporting polypeptide (OATP), and organic cation transporter (OCT) also are expressed and functional in Caco-2 cells (Muller et al., 2005; Sun et al., 2008). In many respects, Caco-2 cells mimic the human intestinal epithelium. One functional difference between enterocytes and Caco-2 cells is the relative lack of expression of cytochrome P450 (CYP) enzymes, particularly CYP3A4, which is expressed normally at high levels in the intestine (Sun et al., 2008). However, addition of 1α,25-dihydroxy-vitamin-D_3 (1α,25-$(OH)_2$-D_3) to the culture medium can induce CYP3A4 expression and activity in a dose-dependent manner (Schmiedlin-Ren et al., 1997).

Caco-2 monolayers were employed (Fig. 2.2) to evaluate both absorption and exsorption of pafuramidine and CPD-0868 by adding the test compound to either the apical (A) compartment (luminal side) or the basolateral (B) compartment (blood side); the A→B and B→A permeability coefficients (P_{app}s) were calculated and compared to elucidate means of absorption (passive diffusion versus transporter-mediated pathways). In addition, the A→B translocation of prodrugs was evaluated further under “sink” conditions, when the B compartment was supplemented with 4% bovine serum albumin (BSA) to mimic the physiologic situation.

C. METHODS

Materials and chemicals. BioCoat™ control cell culture inserts (4.2 cm^2, 1 μm pore size) and murine laminin were purchased from BD Biosciences Labware (Bedford, MA). Dulbecco's modified Eagle's medium (DMEM) (containing 25 mM D-glucose and L-glutamine) and nonessential amino acids (NEAA) were purchased from Invitrogen (Carlsbad, CA). Fetal bovine serum (FBS) was purchased from Thermo Scientific HyClone (Logan, UT). Vitamin E, zinc sulfate, sodium selenite, gentamicin, and BSA were purchased from Sigma-Aldrich (St. Louis, MO). Pafuramidine, CPD-0868, and internal standards (deuterium-labeled prodrugs, d_8-pafuramidine and d_6-CPD-0868) were synthesized in the laboratory of Dr. David W. Boykin (Georgia State University, Atlanta, GA) (Boykin et al., 1996; Ismail et al., 2003). All other chemicals and reagents were of analytical grade and were used without further purification.

Caco-2 Cell Culture Conditions. Cell culture inserts were coated with murine laminin (5 μg/cm^2) prior to seeding with the Caco-2 cell clone P27.7 (Schmiedlin-Ren et al.,1997) (passage 24) at a density of ~5 x 10^5 cells/cm^2. The cell cultures were maintained in growth medium (consisting of DMEM, 20% FBS, 0.1 % (v/v) NEAA, 50 μg/ml gentamicin, and 45 nM vitamin E) until reaching confluence, as determined by transepithelial electrical resistance (TEER) values of ≥250 Ω-cm^2. Cell monolayers were then treated with differentiation medium (consisting of DMEM, 5% heat-inactivated FBS, 0.1 % (v/v) NEAA, 50 μg/ml gentamicin, 45 nM vitamin E, 0.1 μM sodium selenite, and 3 μM zinc sulfate) for 21 days as described previously (Paine et al., 2005).

Disposition of Pafuramidine and CPD-0868 in Caco-2 cells. *Serum-Free Conditions.* To evaluate the absorptive (A→B) and exsorptive (B→A) translocation (Fig. 2.2), 1.5 ml of incubation medium (differentiation medium devoid of FBS) containing pafuramidine or CPD-0868 (1 μM; 0.01% DMSO) was added to the donor compartment, followed by 1.5 ml of drug-free incubation medium to the receiver compartment. Aliquots (25 μl) were

collected from the A and B compartments at 0, 10, 20, 30, 40, and 60 min. Cells were collected at the end of the experiment by scraping into 200 µl of cold incubation medium, after which acetonitrile (600 µl) was added. Cellular supernatants were collected followed by vortex-mixing and centrifugation at 1800 g for 10 min. TEER values were measured before and after the experiment to assess effects of test compounds on cell monolayer integrity. *Sink Conditions*. The experimental procedure for evaluation of A→B translocation of prodrugs under sink conditions was similar as described above, only the incubation medium in the B compartment was supplemented with 4% BSA. Samples from the donor and receiver compartments and cellular supernatants were stored at -80°C pending analysis for prodrugs by LC-MS/MS. The dosing concentration (1 µM) was based on prodrug solubility in the incubation medium and assay sensitivity to quantify prodrug in the receiver compartment.

Sample Preparation and LC-MS/MS Analysis. Donor samples were diluted 10-fold by adding 12.5 µl to 112.5 µl of acetonitrile (ACN). Receiver samples were diluted 5-fold by adding 25 µl to 100 µl of ACN. The internal standards (d_8-pafuramidine and d_6-CPD-0868) were prepared by diluting the stock solution (100 µM in 100% DMSO) to generate a working solution (600 nM in 99.4% ACN and 0.6% DMSO), 25 µl of which was added to 125 µl of donor, receiver, and cell samples. After vortex-mixing and centrifugation at 1800 g for 10 min, the supernatant (100 µl) was transferred to HPLC vials and quantified for pafuramidine and CPD-0868 on an API 4000 triple quadrupole mass spectrometer (Applied Biosystems, Foster City, CA) equipped with a Turbo IonSpray interface (MDS Sciex, San Francisco, CA). Analytes were separated with an Aquasil C18 HPLC column (2.1 mm × 50 mm, 5 µm) (Thermo Electron, Waltham, MA) and a high-pressure linear gradient program consisting of 0.1% formic acid in HPLC-grade water (A) and 0.1% formic acid in HPLC-grade methanol (B) delivered by a Shimadzu pumping system (Shimadzu, Kyoto, Japan) at a flow rate of 0.75 ml/min as follows: after a 0.5-min initial hold at 10% B, mobile phase composition was increased from 10% to 90% B over 3.5 min, and held at 90% B for 0.5 min; the column was

re-equilibrated for 0.5 min before the next injection. The mass spectrometer was operated in positive ion mode using multiple reaction monitoring: pafuramidine, 365.1→334.1 m/z; d_8-pafuramidine, 373.1→342.2 m/z; CPD-0868, 367.1→336.1 m/z; d_6- CPD-0868, 373.1→342.1 m/z; furamidine, 305.3→288.1 m/z; CPD-0801, 307.3→290.1 m/z. Although not quantified, the active metabolites (furamidine and CPD-0801) were monitored for peaks of the respective m/z ratios. Calibration curves were prepared in appropriate matrices (medium and cell supernatant) and were linear over 5-2000 nM ($R^2 > 0.99$).

LogP Calculation. The log octanol-to-water partition coefficients (logP) for pafuramidine and CPD-0868 were calculated using ACD/ChemSketch (Advanced Chemistry Development Inc., Toronto, Canada).

Data Analysis. The apparent permeability coefficients (P_{app}) of both absorptive (A→B) and exsorptive (B→A) transport were calculated according to the following equation (Artursson, 1990):

$$P_{app} = (dQ/dt)/(A \bullet C_0) \quad \text{(Eqn 1)}$$

where dQ/dt is the appearance rate of prodrug in the receiver compartment, calculated by regression of the linear portion of concentration-time profiles; A is the surface area of the culture insert (4.2 cm^2); and C_0 is the initial concentration of the test compound added to the donor compartment (1 μM).

The ratio of the exsorptive to absorptive permeability coefficient was calculated to obtain information regarding any asymmetry in the translocation of the test compound. Thus, efflux ratios were calculated as the ratio of $P_{app, B\rightarrow A}$ to $P_{app, A\rightarrow B}$. Recoveries following apical and basolateral dosing were determined as the sum of amounts recovered in the apical, basolateral, and cellular compartments at 60 min as a percentage of the initial amount added. Cellular accumulation was calculated based on the amount recovered in cell scrapings as a percentage of the initial amount added.

Statistical Analysis. Data are expressed as mean ± SD of triplicate culture inserts. Statistical significant differences between P_{app} values and between cellular accumulation at 60 min, were determined by the unpaired Student's *t*-test ($p < 0.05$).

D. RESULTS

Effects of Prodrugs on Monolayer Integrity. Under all conditions, the TEER measurements exceeded 250 Ω-cm^2 and varied <15% over the 60-min experiment, indicating that membrane integrity remained intact as a function of prodrug/BSA treatments and time.

Disposition of Pafuramidine and CPD-0868 in Caco-2 cells under Serum-Free Conditions. *Translocation.* For both pafuramidine and CPD-0868, translocation through Caco-2 cell monolayers in the A→B direction was nearly superimposable with that in the B→A direction (Fig. 2.3), resulting in similar apparent permeability coefficients (P_{app}) measured in both directions and efflux ratios near unity (Table 2.1). Corresponding P_{app} (A→B and B→A) of CPD-0868 were significantly higher than those of pafuramidine, differing by approximately 3- to 4-fold (Table 2.1). At the end of the experiment, almost 100% of both prodrugs were recovered except that pafuramidine recovery was <80% when added into the B compartment (Table 2.1). *Cellular Accumulation.* The cellular accumulation of pafuramidine at 60 min averaged 33% following apical administration; there was a significant decrease (2-fold) in cellular accumulation of pafuramidine under the same conditions following basolateral dosing (Fig. 2.4). In comparison to pafuramidine, the cellular accumulation of CPD-0868 at 60 min was significantly lower following the same administration route (33 versus 6% for apical dose and 17 versus 4% for basolateral dose) (Fig. 2.4). *Metabolism.* Neither of the active metabolites (furamidine or CPD-0801) was detected throughout the experiment regardless of whether the prodrug was dosed into the A or B compartment.

Disposition of Pafuramidine and CPD-0868 in Caco-2 Cells under Sink Conditions. *Translocation.* When the B compartment was supplemented with 4% BSA, the A→B translocation of both prodrugs became nearly superimposable (Fig. 2.5). In addition, the $P_{app,\ A\rightarrow B}$ value of pafuramidine increased by ~5-fold in the presence relative to the

absence of BSA (Table 2.1); no significant difference in $P_{app, A \rightarrow B}$ associated with BSA was observed for CPD-0868 (Table 2.1). As a consequence, A→B permeability of pafuramidine and CPD-0868 became comparable (Table 2.1). *Cellular Accumulation.* In the presence of BSA, cellular accumulation of pafuramidine following apical dosing was significantly reduced, by approximately 2-fold, compared to the absence of BSA (33 versus 16%). Nevertheless, cellular accumulation of pafuramidine was still much higher than that of CPD-0868 (16 versus 4%) (Fig. 2.4). *Metabolism.* Neither of the active metabolites (furamidine or CPD-0801) was detected throughout the experiment.

E. DISCUSSION

Current treatments for both the first and second stage of HAT require inconvenient parenteral administration, which limits widespread use of these drugs in areas affected by HAT. Prodrugs are one approach to enhance drug absorption of low permeability compounds. Pafuramidine, a lipophilic prodrug of furamidine, has greatly improved oral potency, compared to the hydrophilic active metabolite (furamidine), towards first stage HAT (Boykin et al., 1996). Despite its improved intestinal permeability, pafuramidine was not effective against second stage HAT. The structural analog, CPD-0868, may represent an alternative for second stage infection, as evidenced by a higher cure rate and improved systemic exposure of derived active metabolite (CPD-0801) in a second stage (CNS) mouse model (Wu et al., 2007; Wenzler et al., 2009). To investigate whether intestinal absorption plays a role in the observed difference in efficacy and pharmacokinetics between pafuramidine and CPD-0868, a well-characterized in vitro model of the intestinal epithelium, Caco-2 cells, was utilized to assess permeability and transport characteristics of both prodrugs.

A previous study showed that the prodrug pafuramidine crossed the intestinal epithelium predominantly via a transcellular route (Zhou et al., 2002). Masking the cationic functionalities of furamidine by *O*-methylamidoxime moieties greatly enhanced the lipophilicity of the prodrug, pafuramidine, by increasing the LogD value from -3 to 4.3 (Zhou et al., 2002). At physiologic pH, passive diffusion would be expected to represent the major pathway for the uncharged (pKa ≈ 4) and lipophilic prodrug, pafuramidine, to traverse the intestinal epithelium. The nearly superimposable translocation profiles (Fig. 2.3) and similar P_{app} values (Table 2.1) for both pafuramidine and CPD-0868 after apical and basolateral dosing in Caco-2 cells (without serum in the medium) support the aforementioned postulation. Although both prodrugs crossed cell monolayers by passive diffusion, in the absence of serum in the medium, both absorptive and exsorptive permeability coefficients of

CPD-0868 were more than 3-fold higher than those of pafuramidine (Table 2.1), which could be attributed to the much lower cellular accumulation compared to pafuramidine (Fig. 2.4).

As reported previously, the presence of BSA significantly increased absorptive P_{app} values of only the most lipophilic (logP > 3.0) and highly protein bound (f_u < 5%) compounds (chlorpromazine and nelfinavir) by reducing cellular drug accumulation and non-specific binding to plastic wells (Aungst et al., 2000). Another study also demonstrated that addition of 4% BSA into the receiver compartment increased the absorptive permeability of a highly lipophilic compound, Sch-Y (logP = 4.0), by 5-fold, but the P_{app} values of a relatively less lipophilic compound, Sch 56592 (logP = 2.4), remained unchanged (Saha and Kou, 2002). Consistent with these previous results, when 4% BSA was added into the basolateral compartment to mimic plasma protein binding in the portal circulation, the cellular accumulation of the highly lipophilic prodrug, pafuramidine (LogP = 4.0; Table 2.1), decreased significantly (Fig. 2.4). As a consequence, the permeability of pafuramidine increased by 5-fold, comparable to CPD-0868 (Table 2.1). This observation indicated that BSA served as a “sink” for pafuramidine to reduce backward flux and cellular accumulation of this prodrug. In contrast, little difference in permeability and cellular accumulation of the relatively less lipophilic prodrug, CPD-0868 (LogP = 2.2; Table 2.1), was observed in the absence and presence of BSA (Table. 2.1 and Fig. 2.4). Consistent with the relative lipophilicity between these two prodrugs, the unbound fraction (f_u) of pafuramidine in human plasma was 35-fold less than that of CPD-0868 (Table 2.1). If BSA is the major protein that both prodrugs are bound to in the human plasma, the f_u of CPD-0868 in 4% BSA would be expected to be much higher than that of pafuramidine, which could explain the fact that binding to BSA in the B compartment has a much lower impact on the permeability of CPD-0868 across Caco-2 cell monolayers compared to pafuramidine.

Both pafuramidine and CPD-0868 are poorly water-soluble compounds, thus, the dosing solutions of both prodrugs need to be prepared in a hydrophobic solvent, such as

DMSO. According to the Biopharmaceutical Classification System (BCS), pafuramidine and CPD-0868 can be classified as low solubility–high permeability class II compounds (Polli et al., 2008). Therefore, the extent of absorption of these prodrugs, expressed as the fraction of absorbed (f_a), would be expected to be limited by the solubility rather than the permeability. In addition to the inherent physicochemical properties, local solubility of compounds in the gastrointestinal tract also can be influenced by a variety of factors, such as, surfactants, pH, buffer capacity, and food components (Dressman and Reppas, 2000). Numerous reports showed that the presence of food, particularly consisting of fat components, can greatly increase the extent of absorption of class II compounds (Welling, 1996; Dressman and Reppas, 2000; Dressman et al., 2008). In the case of these antiparasitic prodrugs, administration accompanied by plenty of water and a high fat meal would be expected to enhance the f_a, and in turn, the portal exposure for biotransformation to the active metabolites in the liver.

In the current study, both prodrugs exhibited near complete recoveries in the Caco-2 model, except for pafuramidine when dosed in the basolateral compartment. Considering the higher lipophilicity and more extensive binding of pafuramidine, the incomplete recovery of this prodrug when dosed into the B compartment may have reflected a greater extent of non-specific binding to the larger surface area of culture well/insert. In addition, no active metabolite formation was observed for either prodrug over the 60-min transport study. A previous study using human intestinal microsomes showed that human enteric CYP4F may play a role in the pre-systemic biotransformation of pafuramidine (Wang et al., 2007). Studies using human liver microsomes showed that CYP3A4 may be also involved in the sequential metabolism of pafuramidine to form furamidine (Wang et al., 2006). The activity/expression levels of some phase I metabolizing enzymes, particularly CYP3A4, in Caco-2 cells are considerably lower than those detected in human intestinal epithelium (Sun et al., 2008). The expression/activity levels of enzymes involved in biotransformation of

these prodrugs (e.g., CYP4F/CYP3A4) may not be adequate in Caco-2 cells to predict and study the metabolism of these compounds in the small intestine.

In conclusion, no apparent difference in the $P_{app,\ A\rightarrow B}$ of these two prodrugs was observed under more physiologically-relevant conditions in the Caco-2 model, suggesting that the permeability of pafuramidine and CPD-0868 through the intestinal epithelium may be similar in vivo, hence, the intestinal permeability of prodrugs may have little impact on the difference in the systemic exposure of respective active metabolites observed *in vivo*. This study further demonstrated the utility of Caco-2 model to characterize the translocation of compounds in the gut and highlighted the importance of BSA in accurate assessment of $P_{app,A\rightarrow B}$ and permeability ranking of highly lipophilic compounds. The method used in this study can facilitate selection of lead candidates with desirable intestinal permeability properties for oral treatment of HAT.

F. TABLES

Table 2.1 Comparison of pafuramidine and CPD-0868 translocation across Caco-2 cell monolayers.

Prodrug	Translocation Direction	P_{app} (10^{-6} cm/s)[a]	Efflux Ratio[b]	Recovery at 60 min (%)[c]	LogP[d]	f_u (%) in Human Plasma[e]
Pafuramidine	A → B	8.0 ± 0.3	0.9 ± 0.1	98 ± 8	4.0 ± 0.7	0.2 ± 0.02
	B → A	7.0 ± 0.2		73 ± 1		
	A → B (w/ BSA)[f]	44 ± 3[#]	N.A.[g]	100 ± 4		
CPD-0868	A → B	27 ± 2*	1.0 ± 0.1	100 ± 5	2.2 ± 0.7	7 ± 0.6
	B → A	27 ± 3*		96 ± 2		
	A → B (w/ BSA)	33 ± 1	N.A.	100 ± 1		

[a]*Calculated based on equation (1); comparisons between pafuramidine and CPD-0868 P_{app} values were made using the two-tailed Student's t-test.* [#]*$p<0.05$* versus *the absence of BSA in the basolateral compartment.* **$p<0.05$* versus *pafuramidine in the same translocation direction. Values denote mean ± SD of 3 culture inserts.*

[b]*Determined as the ratio of the P_{app} value in the B → A direction to that in the A → B direction.*

[c]*Calculated as the sum of amount of prodrug recovered in the A and B compartments and cells as a percentage of initial amount of prodrug added to the donor compartment.*

[d]*Calculated as described in Materials and Methods.*

[e]*f_u denotes unbound fraction of pafuramidine or CPD-0868 in human plasma, which was determined using a method described in a previous study (Yan et al., 2011).*

[f]*Incubation medium in the B compartment was supplemented with 4% BSA.*

[g]*Not applicable.*

G. FIGURES

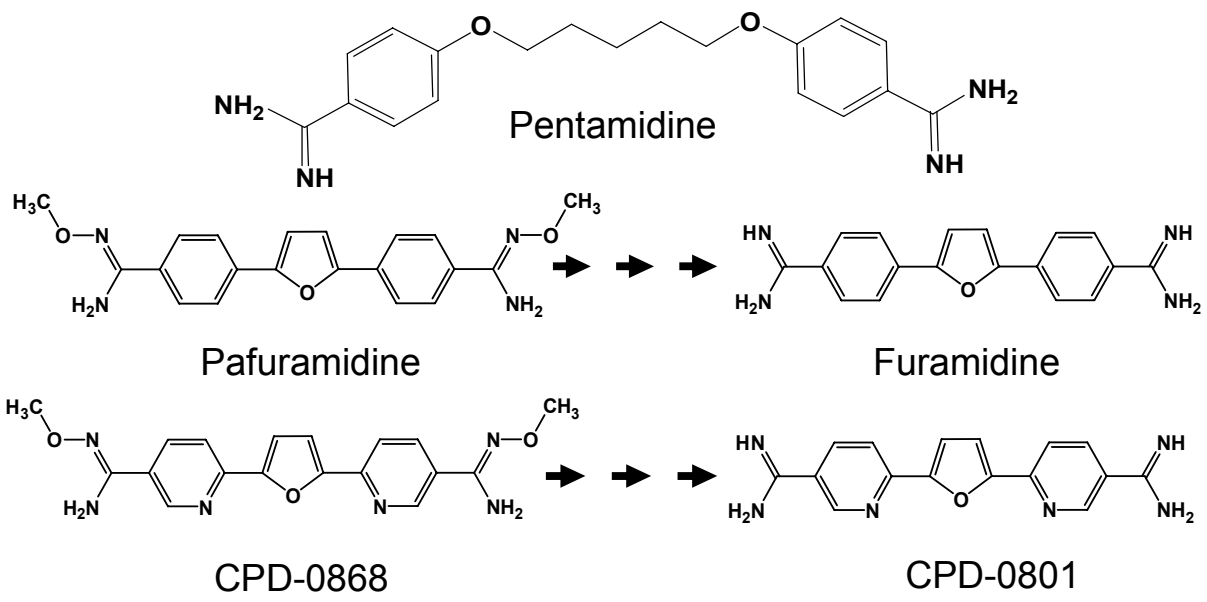

Figure 2.1 Chemical structures of pentamidine, pafuramidine, furamidine, CPD-0868, and CPD-0801. Arrows denote sequential metabolic pathways involved in the conversion of prodrugs to respective active metabolites.

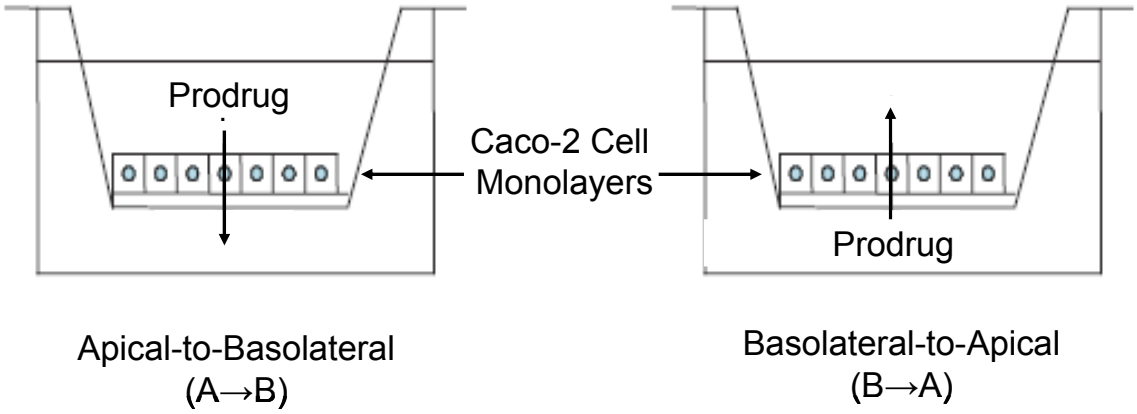

Figure 2.2 Schematic representation of the Caco-2 permeability assay.

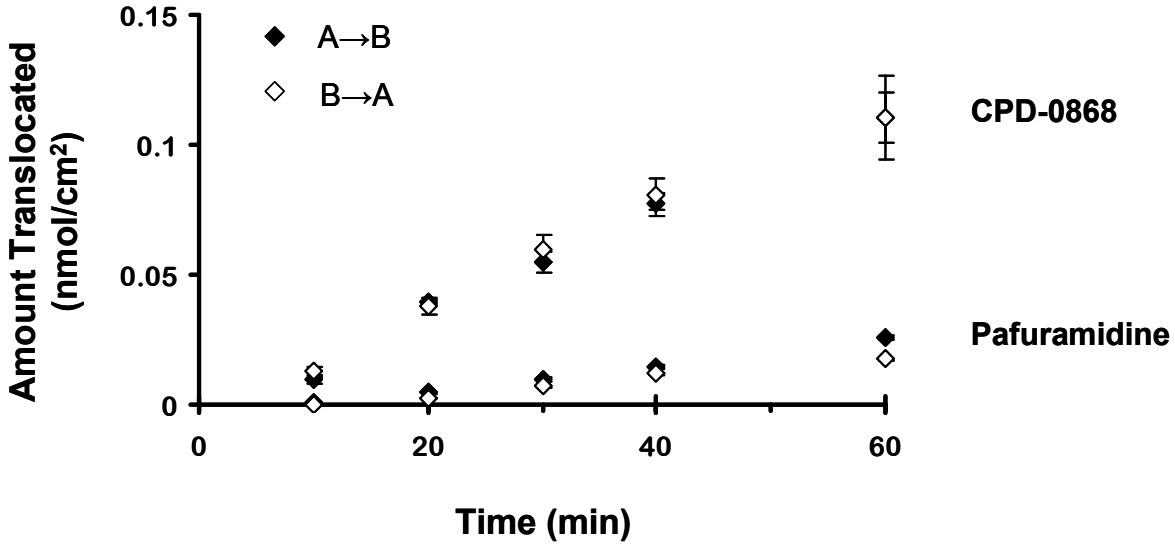

Figure 2.3 Translocation of pafuramidine and CPD-0868 (1 μM) across Caco-2 cell monolayers. Symbols and error bars denote means and SDs, respectively, of triplicate culture inserts.

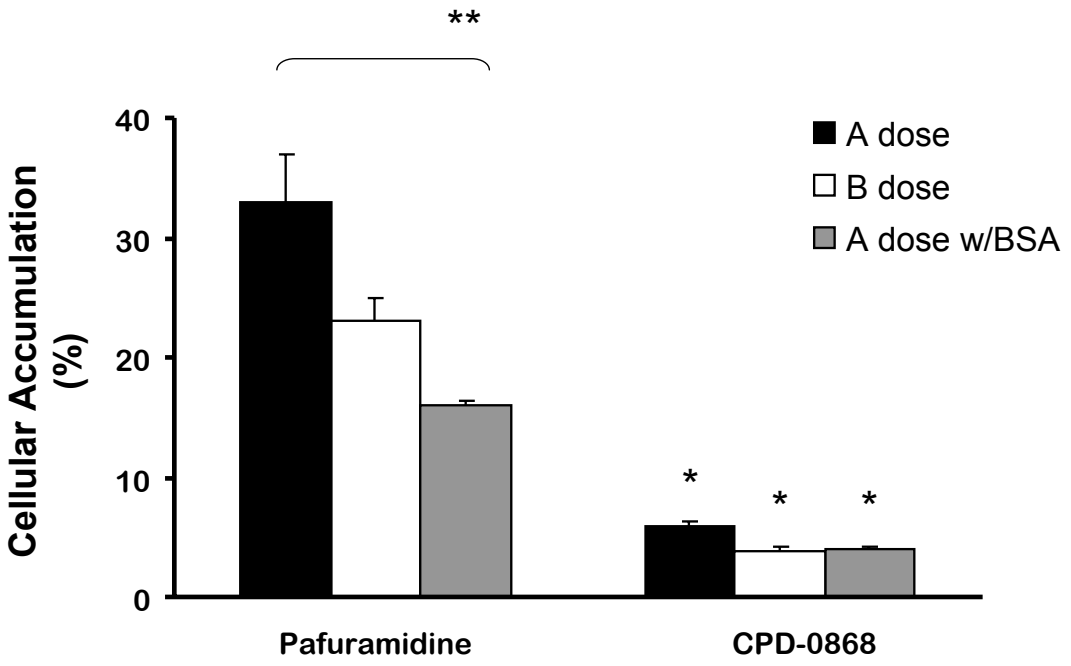

Figure 2.4 Cellular accumulation of pafuramidine or CPD-0868 in Caco-2 cells at the end of the 60-min experiment. Black, white, and gray bars represent the amount of each prodrug recovered in the cell scrapings as a percentage of initial amount added to the apical (A) or basolateral (B) compartment or apical compartment with 4% BSA in the B compartment containing 4% BSA. *p <0.05 versus CPD-0868 under the same dosing condition; **p <0.*05* versus A dose w/BSA (Student's t-test).

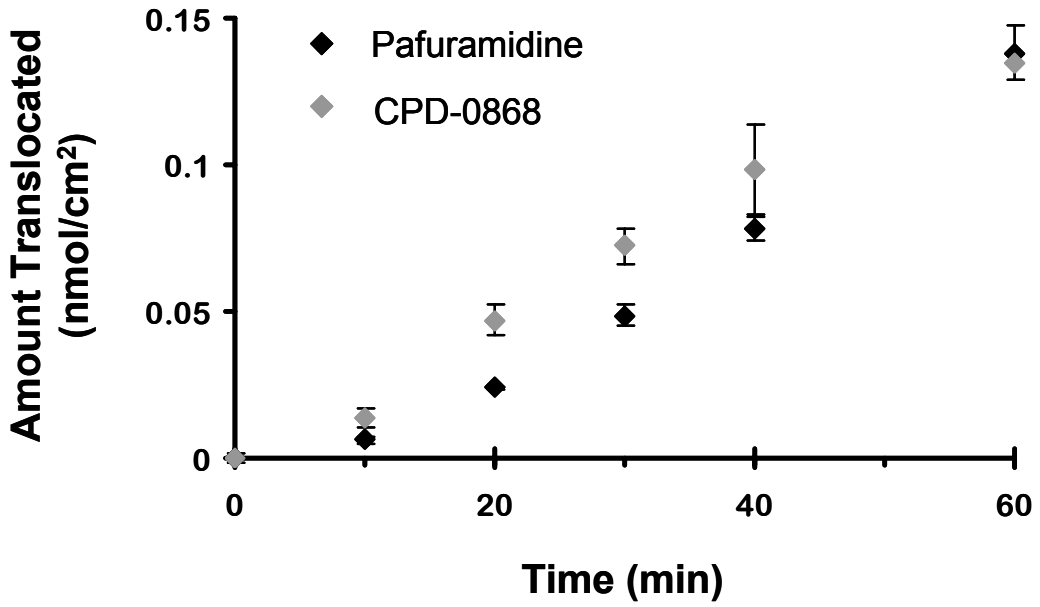

Figure 2.5 Apical-to-basolateral translocation of pafuramidine and CPD-0868 (1 μM) across Caco-2 cell monolayers in the presence of 4% BSA in the basolateral compartment. Symbols and error bars denote means and SDs, respectively, of triplicate culture inserts.

H. REFERENCES

Artursson P (1990) Epithelial transport of drugs in cell culture. I: A model for studying the passive diffusion of drugs over intestinal absorptive (Caco-2) cells. *J Pharm Sci* **79**:476-482.

Artursson P (1999) Cell cultures as models for drug absorption across the intestinal mucosa. *Crit Rev Ther Drug Carrier Syst.* **8**:305-330.

Aungst BJ, Nguyen NH, Bulgarelli JP and Oates-Lenz K (2000) The influence of donor and reservoir additives on Caco-2 permeability and secretory transport of HIV protease inhibitors and other lipophilic compounds. *Pharm Res* **17**:1175-1180.

Barrett MP, Burchmore RJ, Stich A, Lazzari JO, Frasch AC, Cazzulo JJ and Krishna S (2003) The trypanosomiases. *Lancet* **362**:1469-1480.

Boykin DW, Kumar A, Hall JE, Bender BC and Tidwell RR (1996) Anti-*Pneumocystis carinii* activity of bis-amidoximes and bis-*O*-alkylamidoxime prodrugs. *Bioorg Med Chem* **6**:3017-3020.

Checchi F and Barrett MP (2008) African sleeping sickness. *Bmj* **336**:679-680.

Dorlo TP and Kager PA (2008) Pentamidine dosage: a base/salt confusion. *PLoS Negl Trop Dis* **2**:e225.

Dressman JB and Reppas C (2000) In vitro-in vivo correlations for lipophilic, poorly water-soluble drugs. *Eur J Pharm Sci* **11 Suppl 2**:S73-80.

Dressman JB, Thelen K and Jantratid E (2008) Towards quantitative prediction of oral drug absorption. *Clin Pharmacokinet* **47**:655-667.

Ismail MA, Brun R, Easterbrook JD, Tanious FA, Wilson WD and Boykin DW (2003) Synthesis and antiprotozoal activity of aza-analogues of furamidine. *J Med Chem* **46**:4761-4769.

Muller J, Lips KS, Metzner L, Neubert RH, Koepsell H and Brandsch M (2005) Drug specificity and intestinal membrane localization of human organic cation transporters (OCT). *Biochem Pharmacol* **70**:1851-1860.

Paine MF, Criss AB and Watkins PB (2005) Two major grapefruit juice components differ in time to onset of intestinal CYP3A4 inhibition. *J Pharmacol Exp Ther* **312**:1151-1160.

Paine MF, Wang MZ, Generaux CN, Boykin DW, Wilson WD, De Koning HP, Olson CA, Pohlig G, Burri C, Brun R, Murilla GA, Thuita JK, Barrett MP and Tidwell RR (2010) Diamidines for human African trypanosomiasis. *Curr Opin Investig Drugs* **11**:in press.

Polli JE, Abrahamsson BS, Yu LX, Amidon GL, Baldoni JM, Cook JA, Fackler P, Hartauer K, Johnston G, Krill SL, Lipper RA, Malick WA, Shah VP, Sun D, Winkle HN, Wu Y and Zhang H (2008) Summary workshop report: bioequivalence, biopharmaceutics classification system, and beyond. *Aaps J* **10**:373-379.

Saha P and Kou JH (2002) Effect of bovine serum albumin on drug permeability estimation across Caco-2 monolayers. *Eur J Pharm Biopharm* **54**:319-324.

Schmiedlin-Ren P, Thummel KE, Fisher JM, Paine MF, Lown KS and Watkins PB (1997) Expression of enzymatically active CYP3A4 by Caco-2 cells grown on extracellular matrix-coated permeable supports in the presence of 1alpha,25-dihydroxyvitamin D3. *Mol Pharmacol* **51**:741-754.

Sun H, Chow EC, Liu S, Du Y and Pang KS (2008) The Caco-2 cell monolayer: usefulness and limitations. *Expert Opin Drug Metab Toxicol* **4**:395-411.

Wang MZ, Saulter JY, Usuki E, Cheung YL, Hall M, Bridges AS, Loewen G, Parkinson OT, Stephens CE, Allen JL, Zeldin DC, Boykin DW, Tidwell RR, Parkinson A, Paine MF and Hall JE (2006) CYP4F enzymes are the major enzymes in human liver microsomes that catalyze the O-demethylation of the antiparasitic prodrug DB289 [2,5-bis(4-amidinophenyl)furan-bis-O-methylamidoxime]. *Drug Metab Dispos* **34**:1985-1994.

Wang MZ, Wu JQ, Bridges AS, Zeldin DC, Kornbluth S, Tidwell RR, Hall JE and Paine MF (2007) Human enteric microsomal CYP4F enzymes O-demethylate the antiparasitic prodrug pafuramidine. *Drug Metab Dispos* **35**:2067-2075.

Welling PG (1996) Effects of food on drug absorption. *Annu Rev Nutr* **16**:383-415.

Wenzler T, Boykin DW, Ismail MA, Hall JE, Tidwell RR and Brun R (2009) New treatment option for second-stage African sleeping sickness: in vitro and in vivo efficacy of aza analogs of DB289. *Antimicrob Agents Chemother* **53**:4185-4192.

Wu H, Ming X, Wang MZ, Tidwell R and Hall JE (2007) Comparative Pharmacokinetics of the Antitrypanosomal Diamidines DB75, DB820 and DB829 Following Oral Administration of Their Dimethamidoximes Prodrugs in Mice. *The AAPS Journal. 2007; 9(S2).*

Yan GZ, Brouwer KLR, Pollack GM, Wang MZ, Tidwell RR, Hall JE and Paine MF (2011) Mechanisms Underlying Differences in Systemic Exposure of Structurally Similar Active Metabolites: Comparison of Two Preclinical Hepatic Models
J Pharmacol Exp Ther **In press**.

Zhou L, Lee K, Thakker DR, Boykin DW, Tidwell RR and Hall JE (2002) Enhanced permeability of the antimicrobial agent 2,5-bis(4-amidinophenyl)furan across Caco-2 cell monolayers via its methylamidoidme prodrug. *Pharm Res* **19**:1689-1695.

CHAPTER 3

MECHANISMS UNDERLYING DIFFERENCES IN SYSTEMIC EXPOSURE OF STRUCTURALLY SIMILAR ACTIVE METABOLITES: COMPARISON OF TWO PRECLINICAL HEPATIC MODELS

This chapter was accepted by the *Journal of Pharmacology and Experimental Therapeutics*, in press.

A. ABSTRACT

Selection of in vitro models that accurately characterize metabolite systemic and hepatobiliary exposure remains a challenge in drug development. In the present study, mechanisms underlying differences in systemic exposure of two active metabolites, furamidine and 2, 5-bis (5-amidino)-2-pyridyl) furan (CPD-0801), were examined using two hepatic models from rats: isolated perfused livers (IPLs) and sandwich-cultured hepatocytes (SCH). Pafuramidine, a prodrug of furamidine, and 2, 5-bis [5-(*N*-methoxyamidino)-2-pyridyl] furan (CPD-0868), a prodrug of CPD-0801, were selected for investigation because CPD-0801 exhibits greater systemic exposure than furamidine, despite remarkable structural similarity between these two active metabolites. In both IPLs and SCH, the extent of conversion of CPD-0868 to CPD-0801 was consistently higher than that of pafuramidine to furamidine over time (at most 2.5-fold); area under the curve (AUC) of CPD-0801 in IPL perfusate and SCH medium was at least 7-fold higher than that of furamidine. Pharmacokinetic modeling revealed that the rate constant for basolateral (liver to blood) net efflux ($k_{A\_net\ efflux}$) of total formed CPD-0801 (bound+unbound) was 6-fold higher than that of furamidine. Hepatic accumulation of both active metabolites was extensive (>95% of total formed); hepatic unbound fraction ($f_{u,L}$) of CPD-0801 was 5-fold higher than that of furamidine (1.6 versus 0.3%). Incorporation of $f_{u,L}$ into the pharmacokinetic model resulted in comparable $k_{A\_net\ efflux,u}$ between furamidine and CPD-0801. In conclusion, intrahepatic binding markedly influenced the disposition of these active metabolites. A higher $f_{u,L}$ explained, in part, the enhanced perfusate AUC of CPD-0801 compared to furamidine in IPLs. SCH predicted the disposition of prodrug/metabolite in IPLs.

B. INTRODUCTION

The liver often is the predominant organ for biotransformation of a precursor compound (i.e., prodrug) to active metabolite, which can influence therapeutic and/or toxicologic outcomes (Pang et al., 2008). Once formed, active metabolite can undergo further metabolism, excretion into the systemic circulation or bile, and/or intrahepatic sequestration. Therefore, accurate characterization of the systemic and hepatobiliary exposure of active metabolite is imperative for efficacy and risk assessment. Although physiologically relevant, in vivo studies are cumbersome, costly, and associated with a variety of extrahepatic variables, including metabolic and active uptake/efflux processes in the intestine and kidney. As an alternative methodology, in vitro or ex vivo hepatic models that have strong descriptive and predictive capabilities for the in vivo situation would offer significant advantages.

Isolated perfused livers (IPLs) are considered the closest approximation to the hepatobiliary system in vivo due to maintenance of hepatic architecture, microcirculation, and bile production (Brouwer and Thurman, 1996). Biotransformation pathways, sinusoidal/biliary transport processes, mechanisms underlying drug-drug interactions, and alterations in physiology (blood flow or changes in protein binding that might be associated with disease) can be elucidated by manipulating experimental conditions, in the absence of extrahepatic influence. Despite these advantages, several shortcomings limit widespread use of IPLs, such as the delicate surgical techniques required, the relatively short experimental period in which viability is maintained (≤ 2h), and the time/labor-intensive nature of the procedure (Brouwer and Thurman, 1996).

Sandwich-cultured hepatocytes (SCH) have emerged as an alternative in vitro model of the hepatobiliary system (Swift et al., 2009). Unlike conventional culture, hepatocytes cultured between layers of gelled collagen in a sandwich configuration establish cell polarity and form intact canalicular networks with appropriate localization, expression, and function

of transport proteins (LeCluyse et al., 1994; Liu et al., 1999a). Compared to IPLs, SCH represent a more cost-effective and high-throughput system, allowing for simultaneous monitoring of xenobiotics in both cells and culture medium over an extended period of time (up to 24 h). One limitation of SCH is that catalytic activity of cytochrome P450 enzymes declines with days in culture (Boess et al., 2003). A medium additive, dexamethasone (DEX), has been reported to induce the expression of certain phase I and II enzymes in SCH to levels that more closely approximate in vivo metabolic activity (LeCluyse, 2001; Hewitt et al., 2007a; Hewitt et al., 2007b; Kienhuis et al., 2007).

A large body of literature describes the hepatobiliary disposition of many xenobiotics using IPLs or SCH. However, a comparison of both sinusoidal/canalicular transport and metabolism between these two hepatic models has not been evaluated. In the current study, two antiparasitic prodrugs and derived metabolites were utilized as model drug/metabolite pairs to investigate this unaddressed issue.

Human African trypanosomiasis (HAT), a neglected parasitic disease, consists of two stages. During first stage infection, parasites are restricted to the hemolymphatic system; second stage infection begins once parasites invade the central nervous system, causing serious neurologic dysfunction (Barrett, 2010). Without treatment, HAT is invariably fatal. Pafuramidine (Fig. 3.1), a prodrug of furamidine (Fig. 3.1), is the only orally-active agent that has shown efficacy in clinical trials for the treatment of first stage infection (Paine et al., 2010). CPD-0868 (Fig. 3.1), a structural analog of pafuramidine and prodrug of CPD-0801 (Fig. 3.1), demonstrated a higher cure rate compared to pafuramidine in a second stage mouse model (4/5 versus 1/5 at 50 mg/kg p.o. for 10 days) (Wenzler et al., 2009); systemic exposure to CPD-0801 was higher than that to furamidine in mice given the same dose of respective prodrugs (Wu et al., 2007). These encouraging observations warrant further evaluation of CPD-0868 as an orally-active agent for second stage HAT.

Both furamidine and CPD-0801 are formed in the liver via sequential oxidative *O*-demethylation and reductive *N*-dehydroxylation reactions, producing four intermediate phase I metabolites (Fig. 3.1) (Zhou et al., 2004; Generaux, 2010). Once formed, active metabolites must be excreted from hepatocytes into the systemic circulation to exert antiparasitic activity. These observations led to the hypothesis that improved efficacy of the prodrug, CPD-0868, against second stage infection compared to pafuramidine reflects superior hepatobiliary disposition characteristics, including a greater extent of conversion to the active metabolite (CPD-0801) and/or more efficient efflux of CPD-0801 from hepatocytes into the systemic circulation. This hypothesis was addressed utilizing IPLs and SCH from rats, coupled with mathematical modeling, to elucidate mechanisms underlying the difference in systemic/hepatobiliary exposure of these two antiparasitic active metabolites. Results generated from SCH were compared with IPLs.

C. MATERIALS AND METHODS

Materials and Chemicals. Dulbecco's modified Eagle's medium (DMEM) and insulin were purchased from Invitrogen/GIBCO (Carlsbad, CA). ITS^{+TM} (insulin/transferring/selenium) culture supplement and Matrigel^{TM} were purchased from BD Biosciences (Bedford, MA). Penicillin, streptomycin, fetal bovine serum (FBS), non-essential amino acids (NEAA), dexamethasone (DEX), Krebs-Henseleit buffer, Triton X-100, and taurocholate were purchased from Sigma-Aldrich (St. Louis, MO). The prodrugs pafuramidine and CPD-0868, the intermediate phase I metabolites (M1, M2, and M3) of pafuramidine and CPD-0868, the active metabolites furamidine and CPD-0801, and the internal standards (deuterium-labeled pafuramidine, CPD-0868, furamidine, and CPD-0801) were synthesized in the laboratory of Dr. David W. Boykin (Georgia State University, Atlanta, GA) (Boykin et al., 1996; Ismail et al., 2003; Ismail and Boykin, 2006). All other chemicals and reagents were of analytical grade and were used without further purification.

Animals. Male Wistar rats (250–300 g) were purchased from Charles River Laboratories (Raleigh, NC) for liver perfusion and hepatocyte isolation. Animals had free access to water and food before surgery. All animal procedures were compliant with guidelines of the University of North Carolina Institutional Animal Care and Use Committee.

Disposition of Prodrugs/Metabolites in Isolated Perfused Rat Livers. Recirculating IPLs from rats were prepared using standard techniques; perfusions were conducted *ex situ* over designated times (up to 2 h) in a temperature-controlled chamber with recirculating oxygenated Krebs-Henseleit buffer (80 ml) containing 20% (v/v) rat blood at a flow rate of 20 ml/min (Brouwer and Thurman, 1996). Taurocholate was infused (30 µmol/h) into the perfusate reservoir to maintain bile flow. Prodrug (pafuramidine or CPD-0868) stock solution (80 µl; 10 mM in DMSO) was added as a bolus to the perfusate reservoir to yield an initial concentration of 10 µM (0.1% DMSO). Aliquots of perfusate (~400 µl) were collected from the IPL reservoir at 5-min intervals from 0-40 min and at 10-min intervals thereafter up to 2 h during perfusion; bile

was collected at 10-min intervals; liver was harvested at the end of perfusion. Perfusate plasma, bile, and liver collections were stored at -80°C pending analysis for prodrug and derived metabolites by liquid chromatography with detection by tandem mass spectrometry (LC-MS/MS). The prodrug concentration (10 μM) was based on solubility in perfusate and assay sensitivity to monitor prodrugs/metabolites in perfusate plasma, liver, and bile throughout the 2-h experimental period. The absence-of-liver condition was used to assess nonspecific binding of prodrug and metabolites to the IPL apparatus.

Determination of Unbound Fraction. *Liver*. Livers from IPL experiments (described above) were thawed and homogenized in three volumes (v/w) of 0.1 M phosphate buffered saline (PBS). The unbound fraction of formed active metabolite in liver homogenates was determined using rapid equilibrium dialysis devices (Pierce Biotechnology, ThermoFisher Scientific, Waltham, MA). Liver homogenates (200 μl) and blank PBS (350 μl) were placed in tissue and buffer chambers, respectively, and incubated (37°C) for 6 h on a thermomixer (350 rpm) (Eppendorf AG, Hamburg, Germany). Preliminary testing indicated that 6 h of incubation was sufficient to achieve equilibrium without significant compound degradation. After 6 h, aliquots (100 μl) were collected from the tissue and buffer chambers and analyzed for total (bound+unbound) and unbound formed active metabolite, respectively, by LC-MS/MS. *Perfusate/Plasma.* Blank rat IPL perfusate (composed of 20% rat blood) and plasma were spiked with preformed active metabolite to yield a total concentration of 1 or 10 μM. Spiked perfusate/plasma (200 μl) and blank PBS (350 μl) were placed in corresponding dialysis chambers, incubated for 6 h, and analyzed for total (bound+unbound) and unbound preformed active metabolite, respectively, by LC-MS/MS.

Disposition of Prodrugs/Metabolites in Sandwich-Cultured Rat Hepatocytes. Freshly-isolated rat hepatocytes were seeded at 1.75 x 10^6 cells/well onto 6-well BioCoat™ collagen plates (BD Biosciences, Bedford, MA) in seeding medium (DMEM containing 5% (v/v) FBS, 10 μM insulin, 1 μM DEX, 2 mM L-glutamine, 1% (v/v) NEAA, 100 units penicillin G

sodium, and 100 µg streptomycin sulfate). Approximately 24 hours after seeding (Day 1), cells were overlaid with 0.25 mg/ml Matrigel™ in ice-cold culture medium (DMEM supplemented with 1% (v/v) ITS+™, 1 µM DEX, 2 mM L-glutamine, 1% (v/v) NEAA, 100 units penicillin G sodium, and 100 µg/ml streptomycin sulfate). Thereafter, culture medium was changed every 24 h for two days. On Day 4, cells were incubated with culture medium (1.5 ml) containing pafuramidine or CPD-0868 at a concentration identical to that used for the IPL experiments (10 µM, 0.1% DMSO). At designated times up to 24 h, aliquots of medium (500 µl) were collected, and cells were washed twice and incubated at 37°C for 5 min with HBSS with Ca^{2+} (to maintain bile canalicular networks; cells+bile) or without Ca^{2+} (to open bile canalicular spaces; cells) (Lee et al., 2010). After incubation, buffer was removed, and cells were lysed with ice-cold methanol/water (7:1 v/v) containing 0.1% (v/v) trifluoroacetic acid (TFA). Media, cell lysates, and cells+bile lysates were stored at -80°C pending analysis for prodrug and derived metabolites by LC-MS/MS. The absence-of-cell condition was used to assess nonspecific binding of prodrug and metabolites to Matrigel-overlaid BioCoat™ collagen plates.

Determination of Hepatocyte Viability. Effect of prodrugs/metabolites on hepatocyte viability was assessed by monitoring lactate dehydrogenase (LDH) release to the culture medium using a cytotoxicity detection kit (Roche, Indianapolis, IN) according to the manufacturer's instructions. Briefly, aliquots (25 µl) of medium from vehicle- (0.1% DMSO) and prodrug-treated SCH were collected at 0.5, 2, 4, 8, and 24 h. The degree of LDH release was expressed as percentage of the maximum cellular LDH release, which was measured by adding 2% detergent, Triton X-100, to SCH (Lee et al., 2008).

LC-MS/MS Analysis for Prodrugs and Derived Metabolites. The concentration of prodrug and derived metabolites in perfusate/plasma or medium, liver homogenates or cell lysates, bile, and PBS from IPL or SCH studies (described above) was quantified by LC-MS/MS using a method modified from Wang et al. (2006). Briefly, analytes were extracted by adding methanol/H_2O (7:1) with 0.1% TFA containing 600 nM internal standards, followed by vigorous

mixing and centrifugation at 1800 g for 10 min. The supernatant (100 µl) was transferred to HPLC vials and quantified for prodrug and metabolite using multiple reaction monitoring via an API 4000 triple quadrupole mass spectrometer (Applied Biosystems, Foster City, CA) equipped with a Turbo IonSpray interface (MDS Sciex, San Francisco, CA). Analytes were separated on an Aquasil C18 HPLC column (2.1 mm × 50 mm, 5 µm) (Thermo Electron, Waltham, MA) with a high-pressure linear gradient program consisting of 0.1% formic acid in HPLC-grade water (A) and 0.1% formic acid in HPLC-grade methanol (B) delivered by a Shimadzu pumping system (Shimadzu, Kyoto, Japan) at a flow rate of 0.75 ml/min as follows: after a 0.5-min initial hold at 10% B, mobile phase composition was increased from 10% to 90% B over 3.5 min, and held at 90% B for 0.5 min; the column was re-equilibrated for 0.5 min before the next injection. For all studies except liver binding, prodrugs and metabolites were quantified with calibration standards (1-10,000 nM) prepared in the appropriate matrix; for the liver binding study, both active metabolites were quantified with calibration standards prepared in liver homogenates (0.5-50 µM) and PBS (1-10,000 nM). All calibration curves were linear over the respective range (R^2 > 0.98). Intra- and Inter-day coefficients of variation were <15%.

Pharmacokinetic Modeling. Stepwise nonlinear least-squares regression analysis (WinNonlin 5.0.1, Pharsight Corp., Mountain View, CA) was used to fit a compartmental model (Fig. 3.2, Model 1) to the hepatobiliary disposition of prodrug and derived metabolites mass versus time data obtained from IPLs and SCH. Model 2 (Fig. 3.2) incorporates the unbound fraction of active metabolite in the liver to emphasize the importance of hepatic binding in governing the systemic exposure of these compounds. Goodness of fit was based on randomness of residuals, correlation matrices, standard errors of parameter estimates, and visual comparison of predicted mass/concentration-time profiles with observed data. Because the batch of synthesized pafuramidine standard contained impurities largely as the intermediate metabolite, M3, an initial value of 10% of pafuramidine in the dosing compartment (perfusate for IPLs; medium for SCH) was utilized to describe M3 disposition in IPLs and SCH. Some

intermediate metabolites (specifically, M1 and M2 of pafuramidine and M2 of CPD-0868) were not included in the model if concentrations in the perfusate/medium, liver/cells, and bile were below the limit of quantification (BLQ), or if pure synthesized standards (M4 of pafuramidine and CPD-0868) were not available.

Data Analysis. The hepatic clearance (ml/min) and extraction ratio of prodrug in IPLs were calculated as follows:

Total hepatic clearance (Cl_H) = dose / $AUC_{perfusate,0-\infty}$, where $AUC_{perfusate,0-\infty}$ was calculated as the area under the perfusate concentration-time curve from time 0 to infinity using the trapezoidal method.

Biliary clearance (Cl_b) = $mass_{bile,0-120min}$ / $AUC_{perfusate,0-120min}$, where $mass_{bile,0-120min}$ was calculated as the cumulative amount of compound excreted into bile over 120 min.

Metabolic clearance (Cl_m) = Cl_H - Cl_b

Hepatic extraction ratio (E_H) = Cl_H / Q, where Q represents total perfusate flow rate (20 ml/min). The blood-to-plasma ratio for both prodrugs is 1 (GZY, KLRB, MFP, unpublished observations).

With both IPLs and SCH, hepatic accumulation was calculated as the amount of active metabolite recovered in the liver or cells as a percentage of the total amount formed over time. Extent of formation of active metabolite was determined as the total amount of active metabolite recovered in perfusate, liver and bile as a percentage of the initial amount of prodrug added to the perfusate reservoir (IPLs) or the total amount of active metabolite recovered in medium, cells and bile as a percentage of the initial amount of prodrug added to the culture medium (SCH).

Data showed that distribution of furamidine/CPD-0801 between liver and perfusate in IPLs, and between cells and medium in SCH, reached equilibrium from 100 min and 16 h onward, respectively. Therefore, furamidine/CPD-0801 liver-to-perfusate (IPLs) or cell-to-medium (SCH) partition coefficients ($K_{p,IPLs}$ and $K_{p,SCH}$, respectively) were calculated as the ratio

of concentration in liver (C_L) to that in perfusate (C_{Per}) at the end of the perfusion (120 min), or the ratio of concentration in cells (C_C) to that in medium (C_M) at the end of the incubation (24 h). The hepatocellular volumes used to calculate C_L and C_C were 0.6 ml/g rat liver (Pang et al., 1988) and 6.2 $\times 10^{-6}$ µl/hepatocyte (Swift et al., 2009) for IPLs and SCH, respectively.

A two-tailed Student's t-test was used to compare disposition properties between furamidine and CPD-0801 in IPLs and SCH. A *p*-value < 0.05 was considered statistically significant.

D. RESULTS

Nonspecific Binding of Prodrugs/Metabolites. Nonspecific binding of both prodrugs and all metabolites to collagen-coated culture plates, and to the perfusion tubing and apparatus, was <10% of the initial mass of starting material. Accordingly, nonspecific binding was assumed to be negligible.

Disposition of Prodrugs/Metabolites in Isolated Perfused Rat Livers. Both prodrugs were taken up and metabolized rapidly, as reflected by the prompt appearance of intermediate metabolites in perfusate (Fig. 3.3). Both prodrugs were eliminated in rat liver primarily by metabolism; biliary excretion was negligible (Table 3.1). Pafuramidine had a higher hepatic extraction ratio than CPD-0868 (Table 3.1). Recovery of M1 and M2 metabolites of pafuramidine in perfusate, liver, and bile was BLQ. The M3 metabolite of pafuramidine appeared in the perfusate immediately (Fig. 3.3A), reflecting M3 as an impurity in this batch of synthesized standard of pafuramidine, and then decreased slightly due to uptake into hepatocytes; at ~10 min, M3 began to increase slightly due to efflux of M3 formed from M1. The M1 metabolite of CPD-0868 in perfusate was maximal at ~15 min (Fig. 3.3B), then decreased rapidly, due to reuptake into hepatocytes and further metabolism. The M3 metabolite of CPD-0868 in perfusate was maximal at ~40 min (Fig. 3.3B), then decreased due to reuptake into hepatocytes and further metabolism. The rate constants associated with both basolateral reuptake ($k_{M3\_reuptake}$) and efflux (k_{M3_efflux}) of the M3 metabolite were comparable between prodrugs (Table 3.2). $k_{M3\_reuptake}$ was more than 40-fold higher than k_{M3_efflux} for the M3 metabolite of both prodrugs (Table 3.2). The rate constant associated with biliary excretion of the M3 metabolite (k_{M3_bile}) of CPD-0868 was 4-fold higher than that of the M3 metabolite of pafuramidine (Table 3.2). The rate constant associated with conversion from M3 to the active metabolite ($k_{M3\rightarrow A}$) of CPD-0868 was 3.5-fold higher than that of pafuramidine (Table 3.2).

The extent of formation of furamidine in rat IPLs was at least half that of CPD-0801 (Fig. 3.4A). Perfusate exposure to CPD-0801 was much higher compared to furamidine. The area

under the perfusate concentration-time curve (AUC) PD-0801 was 10-fold higher than that for furamidine (Table 3.3). Pharmacokinetic modeling (Model 1, Fig. 3.2) revealed that the rate constant associated with net basolateral efflux ($k_{A\_net\ efflux}$) of CPD-0801 was 6-fold higher than that of furamidine (Table 3.2).

Hepatic accumulation of both active metabolites in rat IPLs was extensive (Table 3.3). The liver-to-perfusate partition coefficient ($K_{p,IPLs}$) of furamidine at 2 h was 3700 and was approximately 5-fold higher than that of CPD-0801 (Table 3.3). The unbound fractions of both active metabolites in plasma/perfusate were similar at 1 and 10 μM. The unbound fraction of each active metabolite in rat liver ($f_{u,L}$) was ≥24-fold lower than that in plasma ($f_{u,P}$) and perfusate (composed of 20% rat blood; $f_{u,Per}$) (Table 3.3). The $f_{u,L}$ of CPD-0801 was approximately 5-fold higher than that of furamidine (Table 3.3). Assuming that only unbound drug can translocate out of hepatocytes into blood and bile, $f_{u,L}$ was incorporated into the pharmacokinetic model (Model 2, Fig. 3.2) to evaluate further the hepatic excretion of derived active metabolite. Based on Model 2, the rate constant for biliary excretion ($k_{A\_bile,u}$) was 9-fold higher than that of basolateral efflux ($k_{A\_net\ efflux,u}$) for unbound furamidine, whereas $k_{A\_bile,u}$ and $k_{A\_net\ efflux,u}$ for CPD-0801 were more comparable than those for furamidine (Table 3.4). After incorporating $f_{u,L}$, the $k_{A\_net\ efflux,u}$ of furamidine became comparable to that of CPD-0801 (Table 3.4).

Disposition of Prodrugs/Metabolites in Day-4 Sandwich-Cultured Rat Hepatocytes. The disposition profiles of prodrugs and derived metabolites in SCH (Fig. 3.5) were similar to those for rat IPLs (Fig. 3.3), although the time-course in SCH was longer than that in IPLs (24 versus 2 h). As shown in IPLs, the recovery of M1 and M2 metabolites of pafuramidine in medium, cells, and bile was BLQ; the M3 metabolite of pafuramidine appeared in medium immediately (Fig. 3.5A), reflecting M3 as an impurity. The M1 metabolite of CPD-0868 in medium was maximal at 2 h (Fig. 3.5B), and then decreased rapidly due to subsequent reuptake into hepatocytes and metabolism. The M3 metabolite of CPD-0868 in medium was

maximal at 8 h (Fig. 3.5B), then decreased due to reuptake into hepatocytes and further metabolism. The rate constant associated with conversion from M3 to the active metabolite ($k_{M3 \rightarrow A}$) of CPD-0868 was 1.4-fold higher than that of pafuramidine (Table 3.5). Only the M3 metabolite of CPD-0868 was recovered in bile (Table 3.5).

The extent of conversion of CPD-0868 to CPD-0801 was consistently higher than that of pafuramidine to furamidine in SCH over 24 h (Fig. 3.4B). Medium exposure to CPD-0801 was higher compared to furamidine. The area under the medium concentration-time curve (Jin et al.) for CPD-0801 was 7-fold higher than that for furamidine (Table 3.3). As shown in IPLs, $k_{A\_net\ efflux}$ of CPD-0801 was 6-fold greater than that of furamidine. Model 1 adequately described the disposition of furamidine in medium and hepatocytes (solid and dashed lines in Fig 3.5A); the large variability in the parameter estimate for $k_{A\_net\ efflux}$ of furamidine may be due to the marked difference between the amount of furamidine recovered in the medium and that recovered in hepatocytes (>2 orders of magnitude). Hepatocellular accumulation of furamidine and CPD-0801 over 24 hr was extensive (Table 3.3). The cell-to-medium partition coefficients of both active metabolites measured in SCH ($K_{p,SCH}$) was 6- to 7-fold higher than liver-to-perfusate partition coefficients measured in IPLs ($K_{p,IPLs}$); similar to IPL results, $K_{p,SCH}$ of furamidine was approximately 5- to 6-fold higher than that of CPD-0801 (Table 3.3).

Effect of Prodrugs/Metabolites on Hepatocyte Viability. In rat SCH treated with vehicle (0.1% DMSO) or prodrug (pafuramidine or CPD-0868), an elevation in LDH release was not observed over 24 h compared to untreated SCH (data not shown). These data suggested that membrane integrity remained intact as a function of prodrug treatment and time.

E. DISCUSSION

SCH have been used previously to investigate the hepatobiliary disposition of drug/metabolite pairs, including terfenadine and fexofenadine (Turncliff et al., 2006). The current work represents the first systematic comparison of two established hepatic models, IPLs and SCH, to understand mechanisms governing the systemic and hepatobiliary exposure of two antiparasitic active metabolites. Rat IPLs and SCH showed similar disposition profiles of prodrugs and derived metabolites (Fig. 3.3 versus Fig. 3.5). The extent of formation and AUC in perfusate (IPLs) or medium (SCH) of CPD-0801 was consistently higher than that of furamidine (Table 3.3). A stepwise pharmacokinetic modeling approach was utilized to differentiate, quantitatively, between the contribution of hepatic metabolism and transport to the enhanced perfusate/medium AUC of CPD-0801 compared to furamidine. Model 1 described adequately the disposition of both prodrugs and derived metabolites (Fig. 3.3 and Fig. 3.5; Supplemental Fig. 3.S1 and Fig. 3.S2) and predicted a net basolateral efflux rate constant ($k_{A\_net\ efflux}$) for CPD-0801 that was 6-fold higher than that for furamidine in both IPLs (Table 3.2) and SCH (Table 3.5). The extent of formation of CPD-0801 was only ≤2.5-fold higher than that of furamidine (Fig. 3.4A and Fig. 3.4B; Table 3.3). These observations indicated that net basolateral efflux predominated over metabolism in governing perfusate/medium exposure to active metabolite.

The $f_{u,L}$ of CPD-0801 was ~5-fold higher than that of furamidine. Based on Model 2 (Fig. 3.2), the ratio of biliary excretion ($k_{A\_bile,u}$) to basolateral efflux ($k_{A\_net\ efflux,u}$) rate constants for furamidine was 9 (Table 3.4), suggesting that once formed in liver, the predominant process that determines furamidine elimination is excretion into bile, whereas biliary and basolateral excretory processes contribute approximately equally to CPD-0801 hepatic excretion (Table 3.4). Incorporation of $f_{u,L}$ in Model 2 (Fig. 3.2) resulted in a comparable $k_{A\_net\ efflux,u}$ of both active metabolites (Table 3.4), indicating that the 6-fold

difference in the rate constant for net basolateral efflux of total formed active metabolite ($k_{A\_net\ efflux}$) could be attributed largely to the 5-fold difference in hepatic binding.

During an expanded phase I safety study in indigenous African volunteers, pafuramidine demonstrated transiently elevated liver transaminases, a known class effect of diamidines (Paine et al., 2010). In rats administered a single oral dose of pafuramidine (10 mg/kg), liver-to-plasma partitioning (K_p) of furamidine was as high as 1300 (Midgley et al., 2007). As shown in the current study, hepatic accumulation of furamidine was extensive, and the unbound fraction of furamidine in liver was at least 80-fold lower than that in plasma and perfusate (Table 3.3). Thus, binding sites in liver may act as an "intracellular sink" that limit systemic exposure to furamidine. Previous subcellular fractionation studies demonstrated that furamidine accumulated primarily in the mitochondrial fraction of liver tissue (Midgley et al., 2007). Consistent with these observations, preliminary fractionation studies with rat IPLs revealed that furamidine was localized primarily in the mitochondrial fraction (43%); CPD-0801 was localized primarily in the cytosolic fraction (45%), with negligible mitochondrial accumulation (≤1%) (GZY, KLRB, MFP, unpublished observations). Extensive accumulation of furamidine in mitochondria could cause mitochondrial dysfunction and trigger liver signal elevations (Pessayre et al., 1999). Significant hepatic accumulation of furamidine is consistent with previous in vivo data (Midgley et al., 2007) suggesting that hepatocellular sequestration may limit systemic exposure of furamidine and predispose the liver to elevated signals. In contrast, a significantly higher hepatic unbound fraction and less mitochondrial accumulation of CPD-0801, compared to furamidine, could enhance systemic exposure to CPD-0801 and reduce hepatic signals.

Utilizing appropriate preclinical hepatic models to estimate liver-to-plasma partitioning of potential hepatotoxicants has been a topic of interest in toxicologic risk assessment. In the current study, the liver-to-perfusate partition coefficient ($K_{p,IPLs}$) of furamidine measured in IPLs was 3700, about 2.8-fold higher than the in vivo K_p (1300)

measured in rats. This discrepancy can be explained by the 2-fold difference in the extent of protein binding of furamidine in perfusate (composed of 20% blood) versus plasma (Table 3.3). If basolateral membrane barriers are absent, liver-to-plasma partitioning can be estimated as the ratio of the unbound fraction of furamidine in plasma to that in liver (*i.e.*, $K_p = f_{u,P}/f_{u,L} = 24/0.3 = 80$), assuming the liver is a well-stirred organ (Rowland, 1985). Similarly, $K_{p,IPLs} = f_{u,Per}/f_{u,L} = 44/0.3 = 147$. Both estimated K_p and $K_{p,IPLs}$ values are much lower than observed values in IPLs and intact rats, suggesting that active transport may be involved in the increased hepatic partitioning of furamidine in the intact organ. Notably, cell-to-medium partition coefficients of furamidine/CPD-0801 measured in SCH ($K_{p,SCH}$) overestimated corresponding values measured in IPLs ($K_{p,IPLs}$) by approximately 6-fold. This discrepancy could be explained, in part, by the absence of serum in culture medium, which resulted in a higher f_u in medium (approximately unity) than that in perfusate. Therefore, binding differences in transport buffer/medium and plasma need to be considered when using SCH to estimate liver-to-plasma partitioning. Nonetheless, both $K_{p,SCH}$ and $K_{p,IPLs}$ of furamidine were >5-fold higher than those of CPD-0801.

The intermediate metabolite, M3, from both prodrugs was excreted extensively into bile in IPLs; M3 from CPD-0868 was the most extensively excreted compound in bile among all prodrugs and metabolites. Both active metabolites also were recovered in bile, but to a 20- to 50-fold lesser extent than M3 from CPD-0868 (Table 3.2). In contrast, only M3 from CPD-0868 was recovered in bile of SCH. Unlike in IPLs, biliary excretion in SCH was measured indirectly, by determining the difference in substrate accumulation between standard HBSS (cells+bile) and Ca^{2+}-free HBSS (cells) (Liu et al., 1999b). As reported previously, SCH may under-predict in vivo biliary clearance of compounds due to less extensive canalicular network formation relative to whole liver (Liu et al., 1999b; Hoffmaster et al., 2005; Abe et al., 2008). To compare the biliary excretion in SCH and in IPLs, the intrinsic biliary clearance of M3 from CPD-0868 in SCH ($Cl_{M3\_biliary,\ SCH}$) was estimated by

multiplying k_{M3_bile} (Table 3.5) by the hepatocellular volume of 6.2×10^{-6} µl/hepatocyte (Swift et al., 2009), and then scaled up to l/h/g liver based on 110×10^6 hepatocytes/g rat liver (Ito and Houston, 2004) and 1×10^6 hepatocytes/well in 6-well plates. The intrinsic biliary clearance of M3 from CPD-0868 in IPLs ($Cl_{M3\_biliary,\ IPLs}$) was estimated by multiplying k_{M3_bile} (Table 3.2) by the hepatocellular volume of 0.6 ml/g rat liver (Pang et al., 1988). Scaled $Cl_{M3\_biliary,\ SCH}$ approximated $Cl_{M3\_biliary,\ IPLs}$ (3.4×10^{-5} versus 25×10^{-5} l/h/g liver) within an order of magnitude. As shown in rat IPLs, the fraction of total formed furamidine and CPD-0801 excreted into bile at 2 h was ≤3% (calculated by subtraction of percent of hepatic accumulation from unity; Table 3.3); in addition, k_{A_bile} of furamidine and CPD-0801 was 20- to 50-fold lower compared to M3 (k_{M3_bile}) from CPD-0868 (Table 3.2). Therefore, biliary excretion of furamidine/CPD-0801 may be so small that the difference in substrate accumulation between standard and Ca^{2+}-free HBSS was indistinguishable.

A previous study showed that CYP4F2 and CYP4F3B were the major enzymes responsible for pafuramidine *O*-demethylation (M1 formation) in human liver microsomes (Wang et al., 2006). The enzymes involved in this reaction in rats have not been identified. Cyp1a2, Cyp2d2, and Cyp4f1 were reported to catalyze CPD-0868 *O*-demethylation in rat liver microsomes (Generaux, 2010). In the current work, metabolic activity in rat SCH was maintained by supplementing the culture medium with 1 µM DEX, a standard concentration used in metabolism studies with SCH (Turncliff et al., 2006). Further studies are warranted to characterize the effect of DEX concentration on expression/activity of the enzymes involved in the biotransformation of both prodrugs.

In summary, an integrated approach involving two rat hepatic systems (IPLs and SCH) and pharmacokinetic modeling provided a mechanistic understanding of the impact of hepatic binding on the systemic and hepatobiliary exposure of two antiparasitic active metabolites. As hypothesized, despite structural similarities, CPD-0868 had superior hepatobiliary disposition characteristics compared to pafuramidine, as reflected by more

extensive formation of the active metabolite, CPD-0801, together with higher hepatic basolateral efflux (due to a higher hepatic unbound fraction), compared with furamidine. The combined effect of both factors could explain, in part, the enhanced systemic exposure of CPD-0801. Although mechanism(s) of brain penetration for these active metabolites have not been elucidated, an increased systemic exposure of CPD-0801 could lead to improved brain exposure. Based on similar in vitro potencies of both active metabolites against various strains of trypanosomes (Wenzler et al., 2009), increased brain exposure of CPD-0801 may enhance antitrypanosomal efficacy in the central nervous system relative to furamidine. The agreement between results from rat IPLs and SCH further substantiates SCH as a useful in vitro tool to characterize hepatobiliary disposition of xenobiotics. Because human IPLs are not feasible, human SCH could be utilized as a surrogate to predict hepatobiliary disposition of xenobiotics in humans.

F. TABLES

Table 3.1. Hepatic clearance and extraction ratio of prodrugs in rat isolated perfused livers.

Prodrug	Hepatic Clearance (ml/min)			E_H
	Total	Metabolic	Biliary	
Pafuramidine	17.6	17.6	< 0.1	0.88
CPD-0868	12.4	12.4	< 0.1	0.62

Table 3.2. Kinetic parameters[a], generated from Model 1, associated with the disposition of prodrugs (pafuramidine and CPD-0868) and derived metabolites in rat isolated perfused livers.

Parameters	Pafuramidine / Metabolites		CPD-0868 / Metabolites	
	Estimate (h^{-1})	CV (%)	Estimate (h^{-1})	CV (%)
$k_{P\_net\ uptake}$	58	88	13	23
$k_{P \rightarrow M1}$	N.A.[b]	N.A.	3.8	7
$k_{M1\_reuptake}$	N.A.	N.A.	96	55
k_{M1_efflux}	N.A.	N.A.	330	62
$k_{P \rightarrow M3}$	1.7	6	N.A.	N.A.
$k_{M1 \rightarrow M3}$	N.A.	N.A.	108	20
$k_{M3\_reuptake}$	13	69	11	33
k_{M3_efflux}	0.31	72	0.20	29
k_{M3_bile}	0.096	11	0.42	14
$k_{M3 \rightarrow A}$	0.43	8	1.5	12
$k_{A\_reuptake}$	2.7	>100	3.3	>100
k_{A_efflux}	0.0065	>100	0.028	>100
$k_{A\_net\ efflux}$[c]	0.0021	14	0.012	51
k_{A_bile}	0.020	48	0.0084	61

[a]*Defined in the legend to Fig. 3.2. No discernable correlation between parameters was observed by evaluation of the correlation matrix (absolute correlation value ≤0.5). See Supplemental Fig. 3.S1 for the plot of weighted residual* versus *time data.*

[b]*Not applicable.*

[c]*Due to the high variability associated with the parameter estimates for $k_{A,reuptake}$ and k_{A_efflux}, Model 1 was modified to include a net efflux term, $k_{A\_net\ efflux}$.*

Table 3.3. Comparison of hepatic disposition of active metabolites in isolated perfused livers (IPLs) and day-4 sandwich-cultured hepatocytes (SCH) from rats.

Measure[a]	Rat IPLs		Rat SCH	
	Furamidine	CPD-0801	Furamidine	CPD-0801
Hepatic Accumulation (%)	99 ± 1	97 ± 1	99 ± 0	95 ± 1*
Extent of Formation[b] (%)	31 ± 6	72 ± 14*	49 ± 2	61 ± 11
Perfusate or Medium AUC (μM•h)[c]	0.006 ± 0.002	0.06 ± 0.01*	0.6 ± 0.1	4.2 ± 0.3*
Liver-to-perfusate or cell-to-medium partition coefficient	3,700	800	27,000	4,700
$f_{u,L}$[d] (%)	0.3 ± 0.1	1.6 ± 0.3*	N.A.[e]	N.A.
$f_{u,Per}$[f] (%)	44 ± 5	70 ± 6*	N.A.	N.A.
$f_{u,P}$[f] (%)	24 ± 2	38 ± 3*	N.A.	N.A.

[a] *Comparisons between furamidine and CPD-0801 for all outcomes were made using the two-tailed Student's t-test. *p<0.05* versus *furamidine. Values denote mean ± SD.*

[b] *Measured at the end of the perfusion for IPLs (120 min) and at the end of the incubation for SCH (24 h).*

[c] *Calculated as the area under the respective concentration-time curves from 0 to 2 h (IPL) and from 0 to 24 h (SCH), respectively.*

[d] *Unbound fraction of formed active metabolite in liver.*

[e] *Not applicable.*

[f] *Unbound fractions of preformed active metabolite added to perfusate or plasma at 1 μM.*

Table 3.4. Kinetic parameters[a], generated from Model 2, associated with the hepatic excretion of unbound active metabolites in rat isolated perfused livers.

Unbound Active Metabolite	$k_{A\ net\ efflux,u}$		$k_{A\ bile,u}$	
	Estimate (h^{-1})	CV (%)	Estimate (h^{-1})	CV (%)
Furamidine	0.66	16	6.0	19
CPD-0801	0.60	42	0.74	40

[a]*Defined in the legend to Fig. 3.2.*

Table 3.5. Kinetic parameters[a], generated from Model 1, associated with disposition of prodrugs (pafuramidine and CPD-0868) and derived metabolites in Day-4 sandwich-cultured rat hepatocytes.

Parameters	Pafuramidine / Metabolites		CPD-0868 / Metabolites	
	Estimate (h^{-1})	CV (%)	Estimate (h^{-1})	CV (%)
$k_{P\_net\ uptake}$	0.30	7	0.40	4
$k_{P \rightarrow M1}$	N.A.[b]	N.A.	67	37
$k_{M1\_reuptake}$	N.A.	N.A.	3.5	29
k_{M1_efflux}	N.A.	N.A.	71	42
$k_{P \rightarrow M3}$	1.3	26	N.A.	N.A.
$k_{M1 \rightarrow M3}$	N.A.	N.A.	12	40
$k_{M3\_reuptake}$	0.080	90	0.15	30
k_{M3_efflux}	N.A.	N.A.	0.35	27
k_{M3_bile}	N.A.	N.A.	0.050	55
$k_{M3 \rightarrow A}$	0.46	16	0.66	15
$k_{A\_reuptake}$	0.83	>100	0.27	>100
k_{A_efflux}	0.0080	>100	0.015	>100
$k_{A\_net\ efflux}$[c]	0.00076	>100	0.0046	27
k_{A_bile}	N.A.	N.A.	N.A.	N.A.

[a]*Defined in the legend to Fig. 3.2. No discernable correlation between parameters was observed by evaluation of the correlation matrix (absolute correlation value ≤0.5). See Supplemental Fig. 3.S2 for the plot of weighted residual* versus *time data.*

[b]*Not applicable.*

[c]*Due to the high variability associated with the parameter estimates for $k_{A,reuptake}$ and k_{A_efflux}, Model 1 was modified to include a net efflux term, $k_{A\_net\ efflux}$.*

G. FIGURES

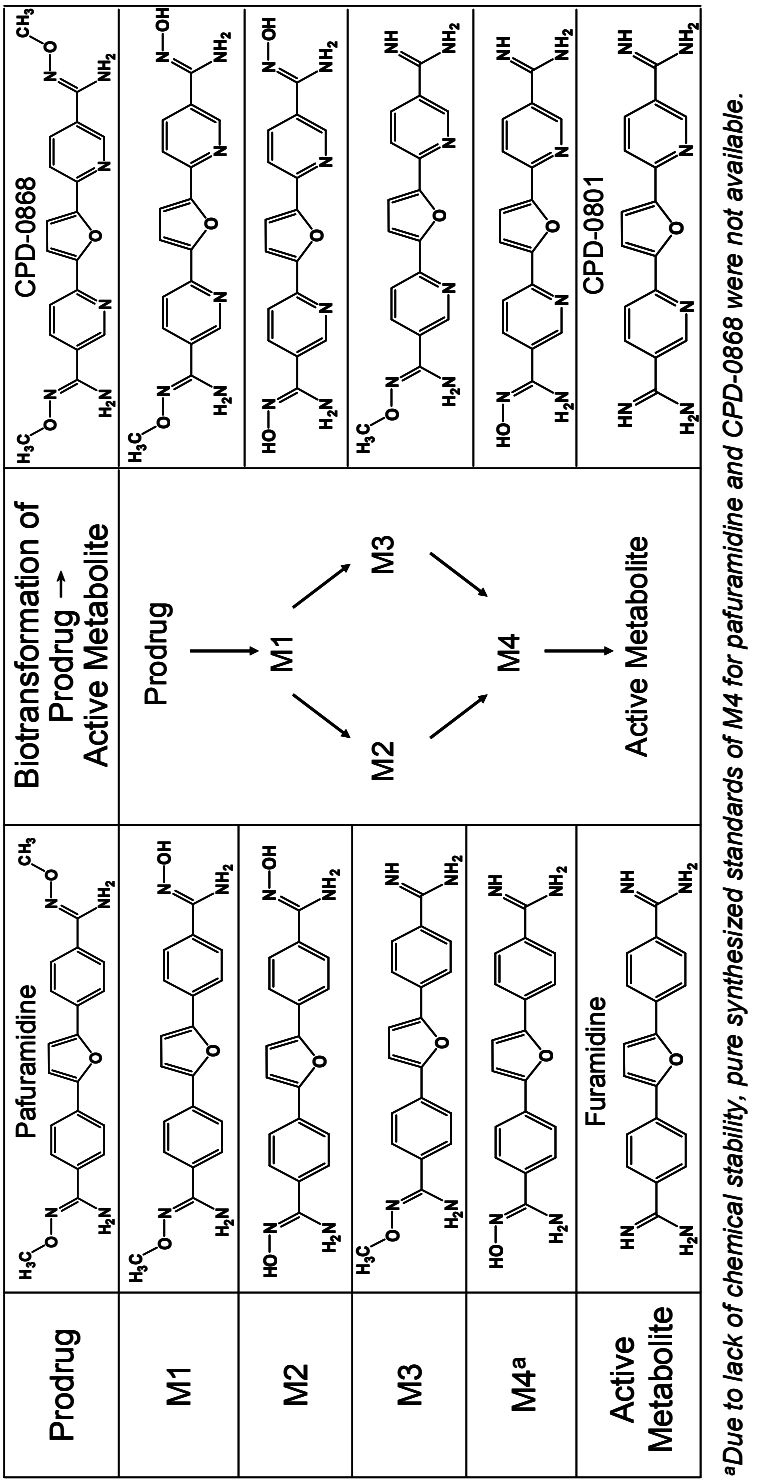

Figure 3.1. Biotransformation of prodrug to active metabolite and corresponding chemical structures.

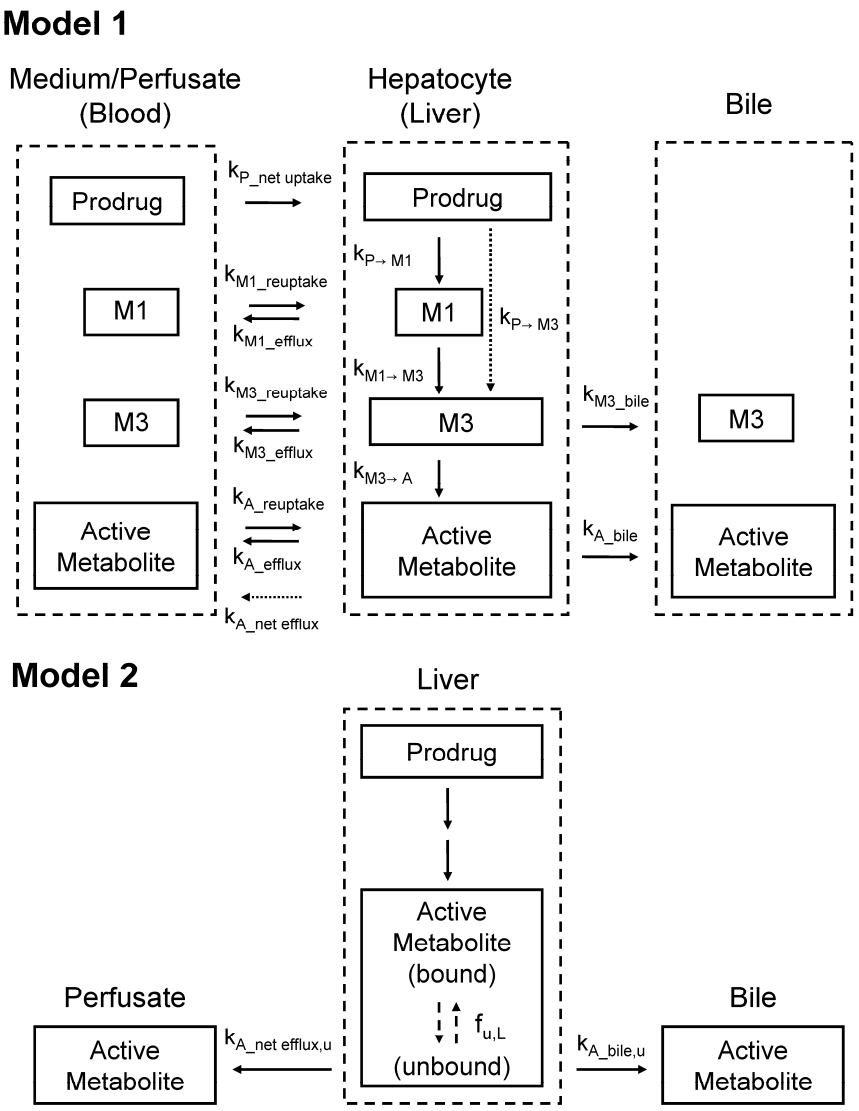

Figure 3.2. Model schemes depicting disposition of prodrugs/metabolites in rat IPLs and SCH (Model 1) and hepatic excretion of unbound active metabolite in rat IPLs (Model 2). $k_{P\_net\ uptake}$ represents the first-order rate constant for net hepatic uptake of prodrug; $k_{P\rightarrow M1}$ represents the first-order rate constant for metabolic conversion from prodrug to intermediate metabolite M1; k_{M1_efflux} and $k_{M1\_reuptake}$ represent the first-order rate constants for hepatic basolateral efflux and reuptake of M1; $k_{P\rightarrow M3}$ represents the first-order rate constant for metabolic conversion from prodrug (pafuramidine only) to intermediate metabolite M3; $k_{M1\rightarrow M3}$ represents the first-order rate constant for metabolic conversion from M1 to M3; k_{M3_efflux}, $k_{M3\_reuptake}$ and k_{M3_bile} represent the first-order rate constants for hepatic basolateral efflux, reuptake and biliary excretion of M3; $k_{M3\rightarrow A}$ represents the first-order rate constant for metabolic conversion from M3 to active metabolite; k_{A_efflux}, $k_{A\_reuptake}$, $k_{A\_net\ effulx}$ and k_{A_bile} represent the first-order rate constants for hepatic basolateral efflux, reuptake, net basolateral efflux and biliary excretion of active metabolite; $f_{u,L}$ represents hepatic unbound fraction of active metabolite; $k_{A\_net\ efflux,u}$ and $k_{A\_bile,u}$ represent first-order rate constants for hepatic basolateral net efflux and biliary excretion of unbound active metabolite.

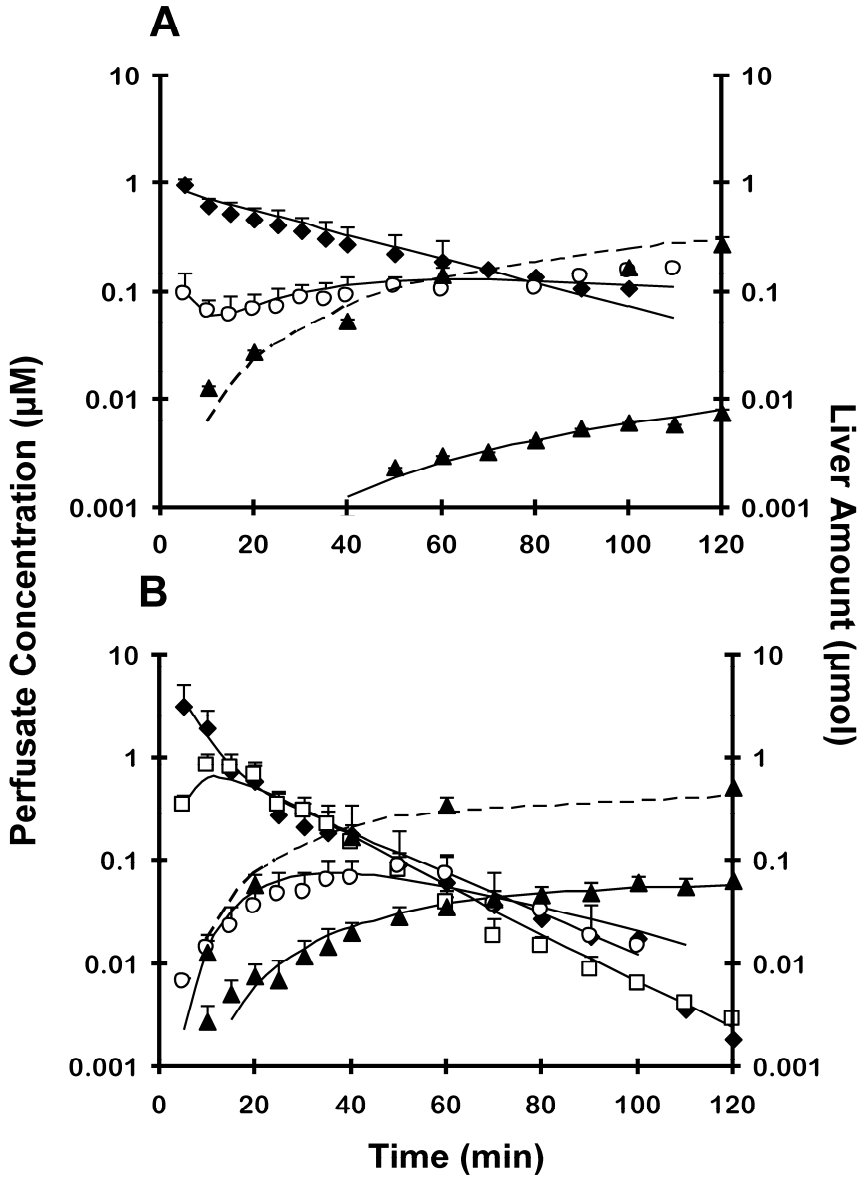

Figure 3.3. Disposition of prodrugs, pafuramidine (A) and CPD-0868 (B), and corresponding metabolites over 120 min in rat isolated perfused livers. Prodrug (10 µM) was administered as a bolus to the perfusion reservoir, which contained 80 ml of 20% (v/v) rat blood. ◆, prodrug; □ , M1; ○ , M3; ▲ , active metabolite. Symbols and error bars for perfusate concentrations denote means and SDs, respectively, of n=5 livers. Symbols and error bars for liver mass denote means and SDs, respectively, of n=5 livers, using a destructive sampling strategy. Solid lines represent perfusate concentration-time profile of prodrug and derived metabolites. Dashed lines represent liver amount-time profile of active metabolite. Solid and dashed Lines represent the computer-generated best fit of the pharmacokinetic scheme depicted in Fig. 3.2 (Model 1) to the data. Note: pafuramidine contained 5-10% impurities, largely as M3; M1 from pafuramidine is not included in (A) because of low recovery in perfusate, as described in Results.

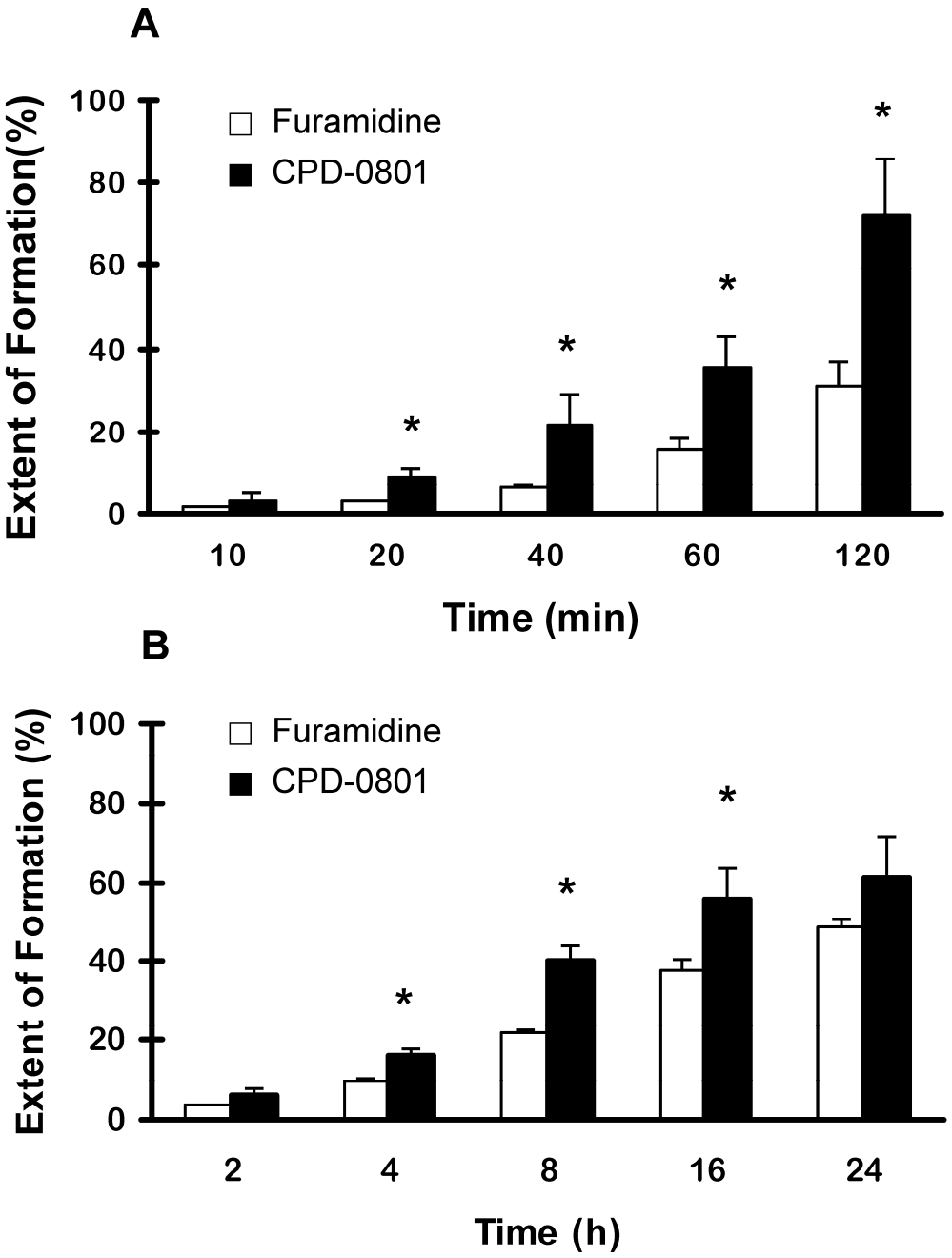

Figure 3.4. Extent of formation of active metabolites represented as total amount of active metabolite recovered in perfusate, liver and bile as a percentage of the initial amount of prodrug added to the perfusate reservoir from isolated perfused rat liver experiments (A; mean ± SD, n=5 livers), and total amount of active metabolite recovered in medium, cells and bile as a percentage of the initial amount of prodrug added to the culture medium from sandwich-cultured rat hepatocyte experiments (B; mean ± SD, n=2 livers in duplicate). *$p<0.05$ versus furamidine (two-tailed Student's *t* test).

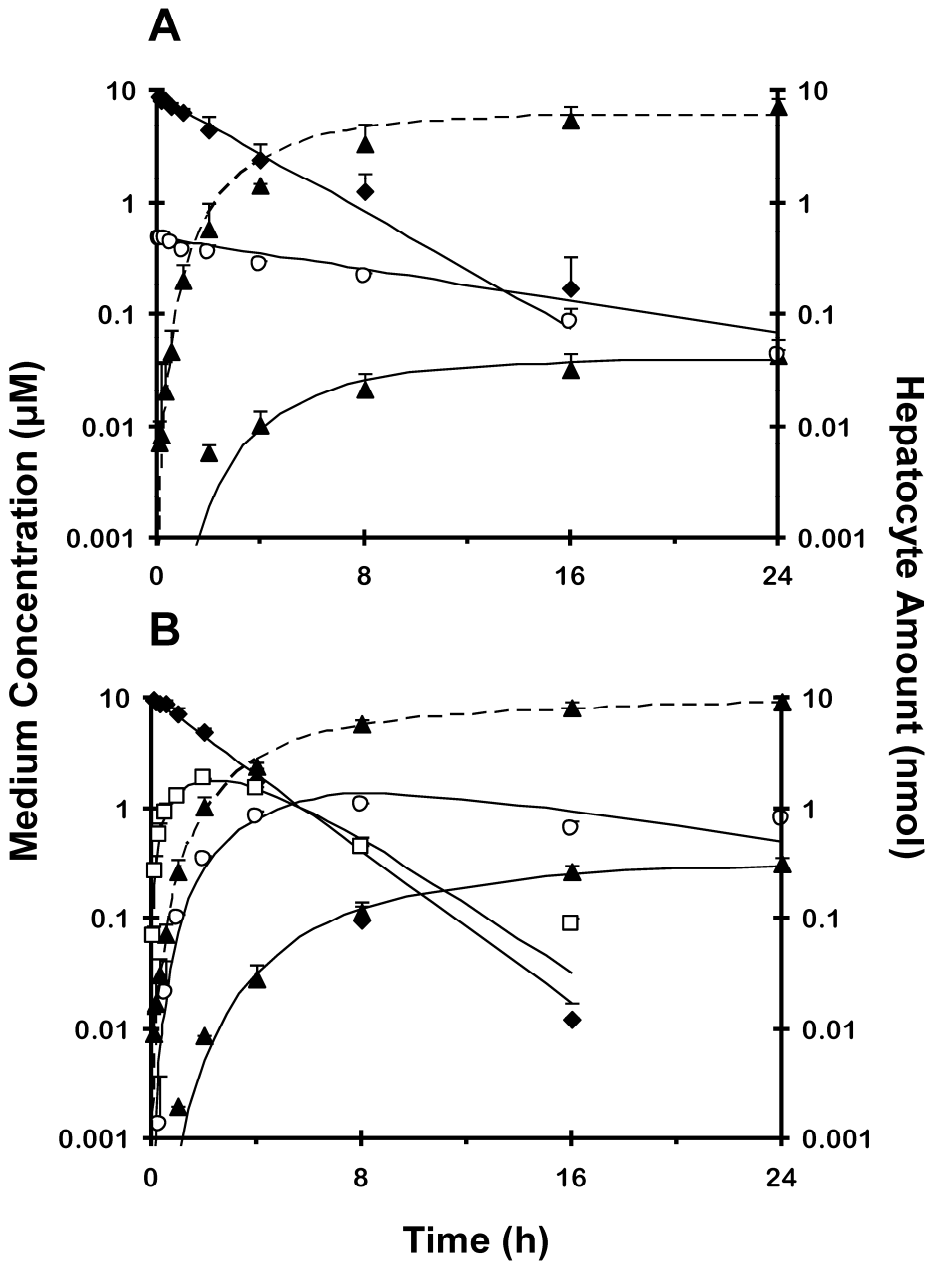

Figure 3.5. Disposition of prodrugs, pafuramidine (A) and CPD-0868 (B) and corresponding metabolites over 24 h in day-4 sandwich-cultured rat hepatocytes. Prodrug (10 μM) was administered as a bolus to each well, which contained 1.5 ml culture medium. ◆, prodrug; □ , M1; ○ , M3; ▲ , active metabolite. Symbols and error bars denote means and SDs, respectively, of n=2 livers in duplicate. Solid lines represent medium concentration-time profile of prodrug and derived metabolites. Dashed lines represent hepatocyte amount-time profile of active metabolite. Solid and dashed lines represent the computer-generated best fit of the pharmacokinetic model depicted in Fig. 3.2 (Model 1) to the data. Note: pafuramidine contained 5-10% impurities, primarily M3; M1 from pafuramidine is not included in (A) because of low recovery in medium, as described in Results.

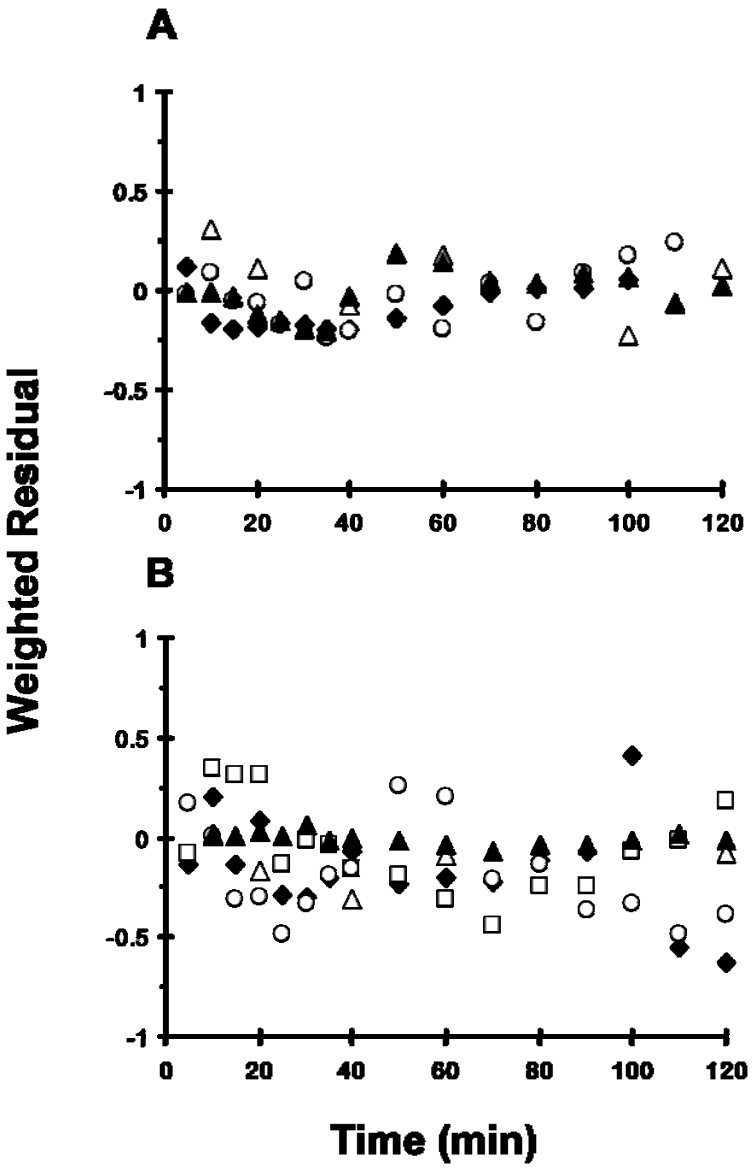

Supplemental Fig. S1. Plot of the weighted residual versus time data from the computer-generated best fit of Model 1 to the rat isolated perfused liver data depicted in Fig. 3.3. Pafuramidine/metabolites (A) and CPD-0868/metabolites (B) are denoted as follows: ◆, prodrug in perfusate; □ , M1 in perfusate; ○ , M3 in perfusate; ▲ , active metabolite in perfusate; △ , active metabolite in liver. A weighting factor of $1/y^2$ was applied.

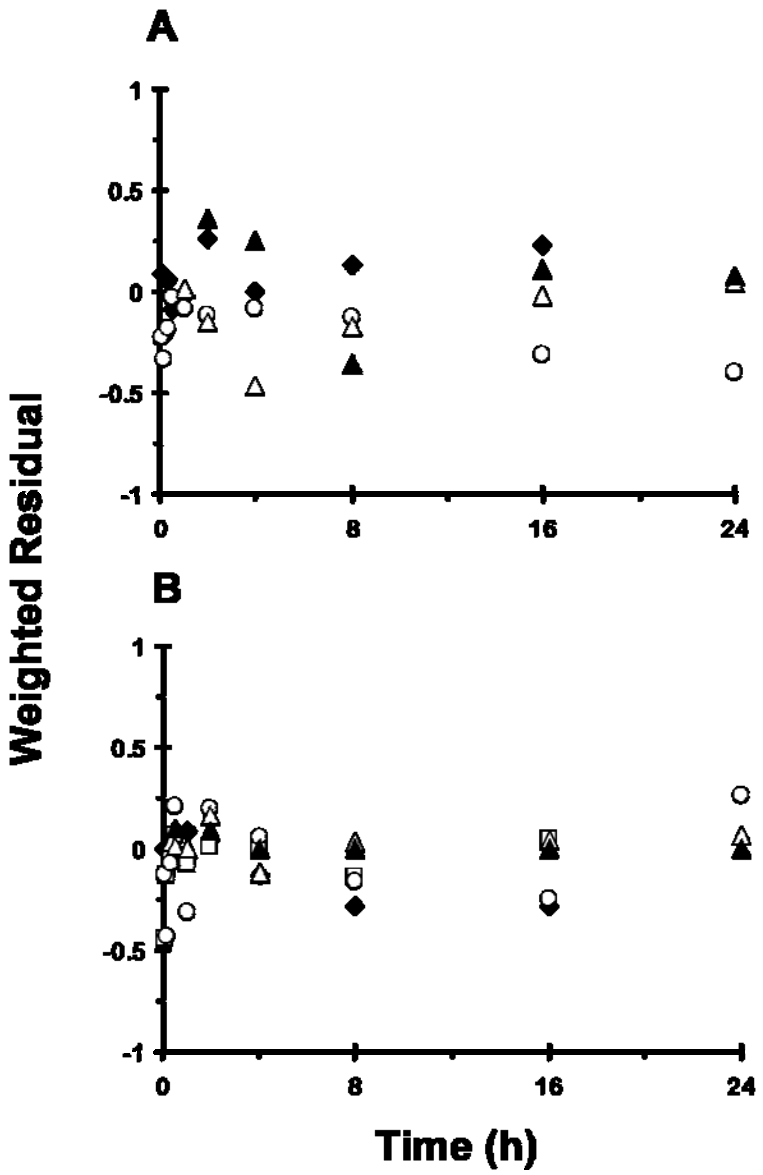

Supplemental Fig. 3.S2. Plot of the weighted residual versus time data from the computer-generated best fit of Model 1 to the rat sandwich-cultured hepatocyte data depicted in Fig. 3.5. Pafuramidine/metabolites (A) and CPD-0868/metabolites (B) are denoted as follows: ◆, prodrug in medium; □ , M1 in medium; ○ , M3 in medium; ▲ , active metabolite in medium; △ , active metabolite in hepatocytes. A weighting factor of $1/y^2$ was applied.

H. REFERENCES

Abe K, Bridges AS, Yue W and Brouwer KLR (2008) In vitro biliary clearance of angiotensin II receptor blockers and 3-hydroxy-3-methylglutaryl-coenzyme A reductase inhibitors in sandwich-cultured rat hepatocytes: comparison with in vivo biliary clearance. *J Pharmacol Exp Ther* **326**:983-990.

Barrett MP (2010) Potential new drugs for human African trypanosomiasis: some progress at last. *Curr Opin Infect Dis* **23**:603-608.

Boess F, Kamber M, Romer S, Gasser R, Muller D, Albertini S and Suter L (2003) Gene expression in two hepatic cell lines, cultured primary hepatocytes, and liver slices compared to the in vivo liver gene expression in rats: possible implications for toxicogenomics use of in vitro systems. *Toxicol Sci* **73**:386-402.

Boykin DW, Kumar A, Hall JE, Bender BC and Tidwell RR (1996) Anti-*Pneumocystis carinii* activity of bis-amidoximes and bis-*O*-alkylamidoxime prodrugs. *Bioorg Med Chem* **6**:3017-3020.

Brouwer KLR and Thurman RG (1996) Isolated perfused liver. *Pharm Biotechnol* **8**:161-192.

Generaux CN (2010) Effects of Parasitic Infection on the Pharmacokinetics and Disposition of Pentamidine Ananalogs. PhD thesis, in *UNC Eshelman School of Pharmacy*, University of North Carolina, Chapel Hill.

Hewitt NJ, Lechon MJ, Houston JB, Hallifax D, Brown HS, Maurel P, Kenna JG, Gustavsson L, Lohmann C, Skonberg C, Guillouzo A, Tuschl G, Li AP, LeCluyse E, Groothuis GM and Hengstler JG (2007a) Primary hepatocytes: current understanding of the regulation of metabolic enzymes and transporter proteins, and pharmaceutical practice for the use of hepatocytes in metabolism, enzyme induction, transporter, clearance, and hepatotoxicity studies. *Drug Metab Rev* **39**:159-234.

Hewitt NJ, Lecluyse EL and Ferguson SS (2007b) Induction of hepatic cytochrome P450 enzymes: methods, mechanisms, recommendations, and in vitro-in vivo correlations. *Xenobiotica* **37**:1196-1224.

Hoffmaster KA, Zamek-Gliszczynski MJ, Pollack GM and Brouwer KL (2005) Multiple transport systems mediate the hepatic uptake and biliary excretion of the metabolically stable opioid peptide [D-penicillamine2,5]enkephalin. *Drug Metab Dispos* **33**:287-293.

Ismail MA and Boykin DW (2006) Synthesis of deuterium and ^{15}N-labelled 2,5-*Bis*[5-amidino-2-pyridyl]furan and 2,5-*Bis*[5-(methoxyamidino)-2-pyridyl]furan. *Journal of Labelled Compounds and Radiopharmaceuticals* **49**:985–996.

Ismail MA, Brun R, Easterbrook JD, Tanious FA, Wilson WD and Boykin DW (2003) Synthesis and antiprotozoal activity of aza-analogues of furamidine. *J Med Chem* **46**:4761-4769.

Ito K and Houston JB (2004) Comparison of the use of liver models for predicting drug clearance using in vitro kinetic data from hepatic microsomes and isolated hepatocytes. *Pharm Res* **21**:785-792.

Kienhuis AS, Wortelboer HM, Maas WJ, van Herwijnen M, Kleinjans JC, van Delft JH and Stierum RH (2007) A sandwich-cultured rat hepatocyte system with increased metabolic competence evaluated by gene expression profiling. *Toxicol* In vitro **21**:892-901.

LeCluyse EL (2001) Human hepatocyte culture systems for the in vitro evaluation of cytochrome P450 expression and regulation. *Eur J Pharm Sci* **13**:343-368.

LeCluyse EL, Audus KL and Hochman JH (1994) Formation of extensive canalicular networks by rat hepatocytes cultured in collagen-sandwich configuration. *Am J Physiol* **266**:C1764-1774.

Lee JK, Leslie EM, Zamek-Gliszczynski MJ and Brouwer KLR (2008) Modulation of trabectedin (ET-743) hepatobiliary disposition by multidrug resistance-associated proteins (Mrps) may prevent hepatotoxicity. *Toxicol Appl Pharmacol* **228**:17-23.

Lee JK, Marion TL, Abe K, Lim C, Pollock GM and Brouwer KLR (2010) Hepatobiliary disposition of troglitazone and metabolites in rat and human sandwich-cultured hepatocytes: use of Monte Carlo simulations to assess the impact of changes in biliary excretion on troglitazone sulfate accumulation. *J Pharmacol Exp Ther* **332**:26-34.

Liu X, LeCluyse EL, Brouwer KR, Gan LS, Lemasters JJ, Stieger B, Meier PJ and Brouwer KLR (1999a) Biliary excretion in primary rat hepatocytes cultured in a collagen-sandwich configuration. *Am J Physiol* **277**:G12-21.

Liu X, LeCluyse EL, Brouwer KR, Lightfoot RM, Lee JI and Brouwer KLR (1999b) Use of Ca2+ modulation to evaluate biliary excretion in sandwich-cultured rat hepatocytes. *J Pharmacol Exp Ther* **289**:1592-1599.

Midgley I, Fitzpatrick K, Taylor LM, Houchen TL, Henderson SJ, Wright SJ, Cybulski ZR, John BA, McBurney A, Boykin DW and Trendler KL (2007) Pharmacokinetics and metabolism of the prodrug DB289 (2,5-bis[4-(N-methoxyamidino)phenyl]furan monomaleate) in rat and monkey and its conversion to the antiprotozoal/antifungal drug DB75 (2,5-bis(4-guanylphenyl)furan dihydrochloride). *Drug Metab Dispos* **35**:955-967.

Paine MF, Wang MZ, Generaux CN, Boykin DW, Wilson WD, De Koning HP, Olson CA, Pohlig G, Burri C, Brun R, Murilla GA, Thuita JK, Barrett MP and Tidwell RR (2010) Diamidines for human African trypanosomiasis. *Curr Opin Investig Drugs* **11**:876-883.

Pang KS, Lee WF, Cherry WF, Yuen V, Accaputo J, Fayz S, Schwab AJ and Goresky CA (1988) Effects of perfusate flow rate on measured blood volume, disse space, intracellular water space, and drug extraction in the perfused rat liver preparation: characterization by the multiple indicator dilution technique. *J Pharmacokinet Biopharm* **16**:595-632.

Pang KS, Morris ME and Sun H (2008) Formed and preformed metabolites: facts and comparisons. *J Pharm Pharmacol* **60**:1247-1275.

Pessayre D, Mansouri A, Haouzi D and Fromenty B (1999) Hepatotoxicity due to mitochondrial dysfunction. *Cell Biol Toxicol* **15**:367-373.

Rowland M (1985) Physiologic pharmacokinetic models and interanimal species scaling. *Pharmacol Ther* **29**:49-68.

Swift B, Pfeifer ND and Brouwer KLR (2009) Sandwich-cultured hepatocytes: an in vitro model to evaluate hepatobiliary transporter-based drug interactions and hepatotoxicity. *Drug Metab Rev* **42**:446-471.

Turncliff RZ, Hoffmaster KA, Kalvass JC, Pollack GM and Brouwer KLR (2006) Hepatobiliary disposition of a drug/metabolite pair: Comprehensive pharmacokinetic modeling in sandwich-cultured rat hepatocytes. *J Pharmacol Exp Ther* **318**:881-889.

Wang MZ, Saulter JY, Usuki E, Cheung YL, Hall M, Bridges AS, Loewen G, Parkinson OT, Stephens CE, Allen JL, Zeldin DC, Boykin DW, Tidwell RR, Parkinson A, Paine MF and Hall JE (2006) CYP4F enzymes are the major enzymes in human liver microsomes that catalyze the O-demethylation of the antiparasitic prodrug DB289 [2,5-bis(4-amidinophenyl)furan-bis-O-methylamidoxime]. *Drug Metab Dispos* **34**:1985-1994.

Wenzler T, Boykin DW, Ismail MA, Hall JE, Tidwell RR and Brun R (2009) New treatment option for second-stage African sleeping sickness: in vitro and in vivo efficacy of aza analogs of DB289. *Antimicrob Agents Chemother* **53**:4185-4192.

Wu H, Ming X, Wang MZ, Tidwell R and Hall JE (2007) Comparative Pharmacokinetics of the Antitrypanosomal Diamidines DB75, DB820 and DB829 Following Oral Administration of Their Dimethamidoximes Prodrugs in Mice. *The AAPS Journal. 2007; 9(S2).*

Zhou L, Thakker DR, Voyksner RD, Anbazhagan M, Boykin DW, Hall JE and Tidwell RR (2004) Metabolites of an orally active antimicrobial prodrug, 2,5-bis(4-amidinophenyl)furan-bis-O-methylamidoxime, identified by liquid chromatography/tandem mass spectrometry. *J Mass Spectrom* **39**:351-360.

CHAPTER 4

A SEMI-PHYSIOLOGICALLY-BASED PHARMACOKINETIC MODELING APPROACH TO PREDICT THE DOSE-EXPOSURE RELATIONSHIP OF AN ANTIPARASITIC PRODRUG/ACTIVE METABOLITE PAIR

This chapter was submitted to the *Drug Metabolism and Disposition.*

A. ABSTRACT

Dose selection during antiparasitic drug development in animal models and humans traditionally has relied on correlations between plasma concentrations obtained at or below maximally tolerated doses that are efficacious. The objective of this study was to improve the understanding of the relationship between dose and plasma/tissue exposure of the model antiparasitic agent, pafuramidine, using a semi-physiologically-based pharmacokinetic (PBPK) modeling approach. Preclinical and clinical data generated during the development of pafuramidine, a prodrug of the active metabolite, furamidine, were utilized. A whole-body semi-PBPK model for rats was developed based on a whole-liver semi-PBPK model using rat isolated perfused liver data. A whole-body semi-PBPK model for humans was developed based on the whole-body rat model. Scaling factors were calculated using metabolic and transport clearance data generated from rat and human sandwich-cultured hepatocytes. Both whole-body models described pafuramidine and furamidine disposition in plasma and predicted furamidine tissue (liver, kidney) exposure and excretion profiles (biliary, renal). The whole-body models predicted that the intestine contributes significantly (30-40%) to first-pass furamidine formation in both rats and humans. The predicted terminal elimination half-life of furamidine in plasma was three- to four-fold longer than that of pafuramidine in rats (170 versus 47 h) and humans (64 versus 19 h). The dose-plasma/tissue exposure relationship for the prodrug/active metabolite pair was determined using the whole-body models. The human model proposed a dose regimen of pafuramidine (40 mg once daily) based on a pre-defined efficacy-safety index. A similar strategy could be used to guide dose-ranging studies in humans for next-in-class compounds.

B. INTRODUCTION

The primary goal of preclinical drug development is to identify compounds with optimal efficacy and safety profiles and desirable pharmacokinetic properties to advance to clinical trials. The design of safe and effective dosage regimens that are compatible with the target patient population and disease remains a major challenge. Suboptimal dose selection can adversely influence progression of a drug development program, resulting in additional time and expense for the dose-ranging study (dose too low), or a poor understanding of risk/benefit, causing unnecessary early termination of promising drug candidates (dose too high).

Human African trypanosomiasis (HAT), a life-threatening parasitic disease, afflicts the world's poorest populations (Barrett, 2010). HAT is characterized by a first stage, when parasites proliferate in the hemolymphatic system, and a second stage, when parasites cross the blood brain barrier and invade the central nervous system. The disease is fatal if untreated. All current chemotherapies are unsatisfactory due to toxicity and/or inconvenient parenteral administration regimens (Barrett, 2010). Pafuramidine, a prodrug of furamidine, is the only orally-active agent that has shown efficacy in clinical trials for treatment of first stage infection (Paine et al., 2010). However, clinical development of pafuramidine was placed on hold due to transiently elevated liver transaminases observed in an expanded Phase I safety trial (www.immtechpharma.com/documents/news_022208.pdf) (Paine et al., 2010). Bioconversion of pafuramidine to furamidine is believed to occur primarily in the liver. The metabolic pathway involves sequential oxidative and reductive reactions, producing four intermediate metabolites (Zhou et al., 2004). Following a single oral dose of ^{14}C-pafuramidine (10 mg/kg) to rats, tissue retention of total radioactivity, predominately as furamidine, was extensive (Midgley et al., 2007). The highest concentration of radioactivity was detected in liver, which was three orders of magnitude higher than that measured in plasma 24 h post-administration; radioactivity was still detectable in liver after seven days.

Unlike with animal models, collection of liver tissue from human subjects over a prolonged period of time is impossible due to obvious ethical reasons. Alternatively, a semi-physiologically-based pharmacokinetic (PBPK) modeling approach could be used to predict the furamidine hepatic exposure-time profile in humans, permitting an improved understanding of the relationship between the dose of pafuramidine and plasma/hepatic exposure of furamidine.

Hepatic clearance is a fundamental PBPK model parameter. Several approaches have been developed to predict human hepatic clearance, including 1) empirical allometric scaling; 2) physiologically-based direct scaling of in vitro human clearance; and 3) normalized scaling of in vivo animal clearance based on in vitro animal and human data (Luttringer et al., 2003; Ito and Houston, 2005). Empirical allometric scaling, a conventional technique based on body weight, frequently fails when drug disposition demonstrates large species differences (Lave et al., 1999). With physiologically-based direct scaling, intrinsic clearance, determined from human hepatocytes or liver microsomes, is corrected by a physiologically-based scaling factor, and subsequently scaled up based on a liver model (well-stirred or parallel-tube) (Ito and Houston, 2004). Although preferred to empirical allometric scaling, physiologically-based direct scaling consistently underestimates human clearance due to decreased enzyme activity or incomplete enzyme composition associated with in vitro systems (Ito and Houston, 2005). Normalized scaling, via integration of in vivo and in vitro data, represents an alternative approach to predict human pharmacokinetics (Lave et al., 1997; Luttringer et al., 2003). Application of these approaches has been limited primarily to the estimation of metabolic clearance of parent compounds; interspecies extrapolation of both metabolic and transport clearance values are reported rarely for metabolites (Pang et al., 2008). In the current work, normalized scaling was applied to isolated perfused rat liver (IPL) and rat/human sandwich-cultured hepatocyte (SCH) data to predict the metabolic/transport clearance of pafuramidine/furamidine. The following

modeling strategy was used: 1) develop a whole-liver PBPK model using rat IPL data; 2) develop and validate a whole-body PBPK model for rats based on the IPL model; 3) develop a whole-body PBPK model for humans to predict furamidine plasma and tissue exposure under various multiple-dose scenarios of pafuramidine. This strategy could be used to guide dose-ranging human studies for next-in-class compounds.

C. MATERIALS AND METHODS

Materials and Chemicals. Dulbecco's modified Eagle's medium (DMEM) was purchased from Invitrogen/GIBCO (Carlsbad, CA). ITS^{+TM} (insulin/transferring/selenium) culture supplement and Matrigel^{TM} were obtained from BD Biosciences (Bedford, MA). Penicillin, streptomycin, non-essential amino acids (NEAA), dexamethasone (DEX), Hanks' balanced salt solution (HBSS), modified HBSS (HBSS without Ca^{2+} and Mg^{2+}, with 0.38 g/l EGTA), and phosphate buffered saline (PBS) were purchased from Sigma-Aldrich (St. Louis, MO). Human plasma was obtained from Biological Specialty Corporation (Colmar, PA). Pafuramidine, furamidine, and internal standards (d_8-pafuramidine and d_8-furamidine) were synthesized in the laboratory of Dr. David W. Boykin (Georgia State University, Atlanta, GA) as described (Boykin et al., 1996). All other chemicals and reagents were of analytical grade and were used without further purification.

Animals. Male Wistar and Sprague-Dawley (SD) rats (250-300 g) were purchased from Charles River Laboratories (Raleigh, NC). Animals had free access to water and food before surgery. All animal procedures were compliant with guidelines of the University of North Carolina Institutional Animal Care and Use Committee.

Disposition of Pafuramidine and Furamidine in Isolated Perfused Livers (IPLs) from Rats. Data were obtained from a previous recirculating rat IPL study, in which pafuramidine was added as a bolus to the perfusate reservoir to yield an initial concentration of 10 μM (Yan et al., 2011). In brief, perfusions were conducted ex situ over designated times (up to 2 h) in a temperature-controlled chamber. Aliquots of perfusate (~400 μl) were collected from the IPL reservoir at 5-min intervals from 0-40 min and at 10-min intervals thereafter, and bile was collected at 10-min intervals; the liver was harvested at the end of perfusion.

Determination of Unbound Fraction. The unbound fractions of furamidine in liver and perfusate from rat IPL experiments and rat plasma, determined using rapid equilibrium

dialysis devices (Pierce Biotechnology, ThermoFisher Scientific, Waltham, MA), were provided from a previous study (Yan et al., 2011). In the present study, the unbound fractions of pafuramidine in liver and perfusate from rat IPL experiments and rat plasma, as well as unbound fractions of pafuramidine and furamidine in human plasma, were determined using the same method. In brief, pafuramidine or furamidine was added to thawed rat liver homogenates/perfusate/plasma to yield a concentration of 1 μM, and a 200-μl aliquot, and 350 μl of 0.1 M PBS, was placed in tissue and buffer chambers, respectively, and incubated (37°C) on a thermomixer (350 rpm) (Eppendorf AG, Hamburg, Germany). After 6 h, aliquots (100 μl) were collected from the sample and buffer chambers and analyzed for total (bound+unbound) and unbound pafuramidine or furamidine, respectively, by LC-MS/MS.

Determination of Blood-to-Plasma (B/P) Ratio in Rats. The B/P ratios of pafuramidine and furamidine in rats were determined using an in vitro method described previously (Berry et al., 2010). In brief, pafuramidine or furamidine was added to pre-warmed fresh rat blood and reference (blank) plasma to yield a concentration of 0.1 μM. After incubation at 37 °C for 1 h in a humidified and oxygenated incubator, compound-treated rat blood was centrifuged at 1500 g for 10 min, and plasma was separated from blood cells. Plasma was analyzed for pafuramidine and furamidine by LC-MS/MS. The B/P ratios were calculated by dividing the peak area observed in the reference plasma (representing nominal blood concentration) by the peak area observed in the compound-treated plasma (representing plasma concentration).

Disposition of Pafuramidine and Furamidine in Rat and Human Sandwich-Cultured Hepatocytes (SCH). Rat SCH data were obtained from a previous study (Yan et al., 2011). Freshly-isolated suspended human hepatocytes, provided by Invitrogen (Durham, NC), were seeded at 1.5 x 10^6 cells/well onto 6-well plates and overlaid with Matrigel™ in the same manner as described for rat hepatocytes (Yan et al., 2011). The liver donors were

reported as Caucasian (two women and one man; 50, 56, and 57 years old, respectively). Culture medium (DMEM supplemented with 1% (v/v) ITS^{+TM}, 1 μM DEX, 2 mM L-glutamine, 1% (v/v) NEAA, 100 units penicillin G sodium, and 100 μg/ml streptomycin sulfate) was changed daily for 5-7 days until extensive canalicular networks were formed. On the day of experimentation, SCH were incubated with culture medium (1.5 ml) containing pafuramidine at the same concentration (10 μM) as that used in rat SCH experiments (Yan et al., 2011). At designated times up to 24 h, aliquots of medium (500 μl) were collected, and cells were washed twice and incubated at 37°C for 5 min with 2 ml standard HBSS (to maintain bile canalicular networks; cells+bile) or Ca^{2+}-free HBSS (to open bile canalicular spaces; cells) (Turncliff et al., 2006). After incubation, buffer was removed, and cells were washed three times with 2 ml ice-cold standard HBSS and lysed with 1 ml ice-cold methanol/water (7:1 v/v) containing 0.1% (v/v) trifluoroacetic acid (TFA). Media and cell lysates were stored at -80°C pending analysis for pafuramidine and furamidine by LC-MS/MS.

In Vivo Studies

Rats. Data were provided from a previous study, in which four Sprague Dawley rats were administered a single dose of pafuramidine (7.5 μmol/kg) by oral gavage (Generaux, 2010). Pafuramidine was prepared as a suspension in acidified water (pH = 3)/70% Tween 80 in ethanol (7:3 v/v). Blood (0.2 ml) was collected via a jugular vein cannula over 24 h after pafuramidine administration. Plasma was separated from blood cells by centrifugation (1500 g for 10 min) and analyzed for pafuramidine and furamidine by LC-MS/MS.

Humans. Data were provided from a previous clinical study (Olson, 2008). The Institutional Review Board reviewed and approved the study protocol. In brief, male Caucasian volunteers (n=6) were administered a single oral dose of ^{14}C-pafuramidine (100 mg). The dose was prepared in capsule form, containing 0.7 MBq (19 μCi) of radioactivity, and administered following a high fat meal to facilitate absorption. After administration of ^{14}C-pafuramidine, blood was collected at designated times over 168 h. Urine and feces were

collected for up to 14 and 21 days, respectively, post pafuramidine administration. Total radioactivity was measured in whole blood, plasma, urine, and feces by high performance liquid radiochromatography; pafuramidine and furamidine concentrations in plasma were measured by LC-MS/MS.

LC-MS/MS Analysis. *In vitro samples and rat plasma.* Pafuramidine and furamidine were quantified using an API 4000 triple quadrupole mass spectrometer (Applied Biosystems, Foster City, CA) equipped with a Turbo IonSpray interface (MDS Sciex, San Francisco, CA). The sample preparation procedure and LC-MS/MS conditions for the quantification of pafuramidine and furamidine were detailed previously (Yan et al., 2011). Briefly, pafuramidine/furamidine and internal standards (d_8-pafuramidine/d_8-furamidine) were separated on an Aquasil C18 HPLC column (2.1 mm × 50 mm, 5 µm) (Thermo Electron, Waltham, MA) with a high-pressure linear gradient program. Calibration curves were prepared in appropriate matrices (0.05-5 µM in liver homogenates; 1-10,000 nM in perfusate, medium, cell lysates, human plasma, and PBS) and were linear over the respective ranges ($R^2 > 0.98$). The limit of quantification was 5 nM for both compounds. *Human plasma.* Quantification of pafuramidine and furamidine was carried out by Tandem Labs (Salt Lake City, UT). The stock solutions of analytes (pafuramidine and furamidine) and internal standards (d_8-pafuramidine and d_8-furamidine) were prepared in 100% methanol to yield concentrations of 0.37, 0.41, 0.21, and 0.3 mg/ml, respectively. Stock solutions of pafuramidine and furamidine were diluted in blank human plasma to yield working concentrations of 5000 and 2000 ng/ml for preparation of calibration standards and quality controls, respectively. Calibration standards (0.25-250 ng/ml) and quality controls (0.75, 75, and 200 ng/ml) for pafuramidine and furamidine were prepared by serial dilution of the corresponding working solution with blank human plasma. The working internal standards (100 ng/ml for d_8-pafuramidine and d_8-furamidine) were prepared by diluting the respective stock solution with 0.05% TFA in water:methanol (5:5 v/v); 50 µl of the diluted stock solution and 500 µl of 50 nM ammonium acetate buffer (pH = 3) were added to 100 µl of

human plasma, standards, and quality controls. After vortex-mixing, all samples were loaded onto Polycrom B1000 1cc, 20-mg extraction cartridges (Cera, Inc., Baldwin Park, CA), followed by serial washing of the solid phase with 300 µl of 50 mM ammonium acetate buffer (pH 3), followed by 300 µl of 50 mM ammonium acetate buffer (pH = 3):methanol (8:2 v/v). Analytes were eluted with 300 µl of acetonitrile, followed by 300 µl of 0.1% hydrochloric acid in methanol. After evaporation at 45°C (TurboVap®; Zymark Corp., Hopkinton, MA), samples were reconstituted with 50 µl of 0.05% TFA in water:acetonitrile (9:1 v/v) and transferred to HPLC vials. Pafuramidine and furamidine were quantified on an API 3000 triple quadrupole mass spectrometer (PE Sciex, Concord, Ontario). Analytes were separated on a BDS Hypersil Phenyl HPLC column (2 mm x 50 mm, 5 µm) at 35°C with a high-pressure linear gradient program consisting of 0.05% TFA in HPLC-grade water (A) and HPLC-grade acetonitrile (B) delivered by a Hewlett Packard HP 1100 pumping system (Hewlett Packard, Palo Alto, CA) at a flow rate of 300 µl/min. Mobile phase composition was increased from 10% to 70% B from 0 to 3.5 min, and then decreased to 10% B from 3.5 to 3.6 min; the column was re-equilibrated for 2 min before the next injection. Calibration curves for pafuramidine and furamidine were linear from 0.25-250 ng/ml (R^2 > 0.99). Intra- and Inter-day precision (expressed as CV%) and accuracy (expressed as bias%) of quality controls for both compounds were <15%. The mass spectrometers were operated in positive ion mode using multiple reaction monitoring: pafuramidine, 365.1→334.1 *m*/*z*; furamidine, 305.3→288.1 *m*/*z*; d_8-pafuramidine, 373.1→242.0 *m*/*z*; d_8-furamidine, 313.3→296.1 *m*/*z*.

Semi-Physiologically-Based Pharmacokinetic (PBPK) Modeling

Modeling Strategy

Kinetic parameters associated with hepatic disposition of pafuramidine and furamidine were generated from the whole-liver semi-PBPK model and utilized to develop the whole-body rat semi-PBPK model. Preclinical data on preformed furamidine kidney-to-plasma partitioning and renal excretion were incorporated to predict formed furamidine

disposition in rats. In vivo rat data were used to develop the semi-PBPK model structure and associated parameters. Kinetic parameters for humans (see model parameterization) were utilized to predict the disposition of pafuramidine and furamidine and, ultimately, to predict the relationship between dose and plasma or tissue exposure.

Model Structure

Rats. *Whole-liver.* Pafuramidine and furamidine submodels were linked by pafuramidine metabolism in the liver (Fig. 4.1A). The pafuramidine submodel for rat IPLs was composed of two compartments: perfusate reservoir and liver (Fig. 4.1A). The furamidine submodel was composed of three compartments: perfusate reservoir, liver, and bile. Pafuramidine is highly lipophilic (Log D_{pH_7} = 4.3) (Zhou et al., 2002) and poorly-soluble, qualifying as a class II compound according to the Biopharmaceutics Classification System (BCS) (Wu and Benet, 2005). As such, pafuramidine was assumed to diffuse passively through the hepatic basolateral membrane. In contrast to pafuramidine, furamidine is hydrophilic (Log D_{pH_7} = -3) (Zhou et al., 2002). Furamidine basolateral reuptake and efflux clearances ($Cl_{F\_up,\ u}$ and $Cl_{F\_eff,\ u}$; Table 4.1) estimated by the whole-liver model (Fig. 4.1A) were at least two-fold lower than perfusate flow rate (4 l/h/kg), suggesting that diffusional barriers exist for furamidine. Therefore, distribution of pafuramidine and furamidine in liver was assumed to be flow- and diffusion-limited, respectively (Fig. 4.1A).

Whole-body. The whole-liver rat model was expanded into a whole-body rat model by substituting the perfusion reservoir with the blood compartment (Fig. 4.1B). Based on the high lipophilicity of pafuramidine, fat was added as a storage organ in the pafuramidine submodel. The kidney was incorporated as an additional storage organ in the furamidine submodel based on the significant kidney retention of furamidine (Midgley et al., 2007; Goldsmith, 2011); all other tissues were grouped together as “rest of body” in both submodels to maintain mass balance (Fig. 4.1B). Pafuramidine distribution into the liver was assumed to be flow-limited, whereas furamidine distribution into the liver was assumed to be

diffusion-limited. To avoid over-parameterization, distribution of both compounds into all other organs was assumed to be flow-limited (Fig. 4.1B).

Based on the high hepatic extraction ratio calculated from IPL data (E_H = 0.88) (Yan et al., 2011), pafuramidine was assumed to be cleared from the body primarily via hepatic metabolism. Based on in vivo data, furamidine was assumed to be eliminated via both biliary and renal excretion (Midgley et al., 2007; Goldsmith, 2011). To simulate pafuramidine and furamidine plasma concentration-time profiles, the model incorporated a single gut compartment for pafuramidine absorption following oral administration. Absorption of pafuramidine from gut to liver was assumed to be a first-order process. Because the initial model failed to describe the prompt appearance of furamidine in plasma, the model was modified to include the gut as a site of furamidine formation during pafuramidine absorption.

Humans. The final whole-body rat model was utilized initially to predict the disposition of pafuramidine/furamidine in humans. However, model predictions failed to describe the delayed absorption of pafuramidine observed in humans, which may be attributed to the capsule formulation and concurrent administration of a high fat meal. Therefore, three consecutive transit compartments were added between the site of administration (oral route) and site of absorption (gut) in the pafuramidine submodel (Fig. 4.1B) to represent dissolution from the dosage form (capsule), stomach emptying, and/or partitioning from the fat components of the concomitant high fat meal.

Model Parameterization

Absorption and Metabolism in the Gut. Absorption and metabolism of pafuramidine/furamidine in the gut have not been characterized extensively in rats and humans. Thus, the relevant kinetic parameters, including the fraction of the dose absorbed into enterocytes (f_a), the rate constants associated with absorption of pafuramidine or furamidine (k_{a_P} or k_{a_F}), and the rate constant associated with metabolic conversion from

pafuramidine to furamidine in the gut ($k_{G\_P\rightarrow F}$) were estimated by fitting the semi-PBPK models (Fig. 4.1B) to in vivo rat and human data.

Tissue Distribution. Tissue-to-perfusate/plasma partition coefficients were optimized by fitting relevant PBPK models (Fig. 4.1A and 4.1B) to IPL and in vivo rat data. The pafuramidine liver-to-plasma partition coefficient in rats was calculated based on the liver-to-perfusate partition coefficient generated from the rat IPL data after correction for the 5-fold difference in unbound fraction between plasma and perfusate (Table 4.1). Due to the lack of human tissue data, tissue partition coefficients and liver binding for pafuramidine/furamidine in humans were assumed to be equal to those in rats (Table 4.1).

Clearances

Hepatic. Rat hepatic clearance (Cl_{rat_liver}) values were derived by fitting the whole-liver rat model to the rat IPL data. Cl_{rat_liver}, which represented metabolic and/or active transport capacities, was normalized by a scaling factor (SF) and corrected for liver weight (LW) to estimate the human hepatic clearance value:

$$Cl_{human\_liver} = Cl_{rat\_liver} \times SF \times (LW_{human}/LW_{rat)}),$$

where $SF = Cl_{human\ SCH} / Cl_{rat\ SCH}$ or $k_{human\ SCH} / k_{rat\ SCH}$

Because biliary Cl of formed furamidine was too small to measure in both rat and human SCH, in vivo human biliary Cl was estimated by scaling in vivo rat biliary Cl based on liver weight.

Renal. Furamidine unbound renal clearance from plasma in rat ($Cl_{R\_rat,u}$) was calculated based on preclinical data in rats administered furamidine intravenously (10 μmol/kg) (Goldsmith, 2011). In brief, rats (n = 3-7) were sacrificed at designated timepoints up to 16 days post furamidine administration, after which kidneys were harvested and homogenized; urine was collected at 0-3, 3-6, 6-12, and 12-24 h intervals post furamidine administration. $Cl_{R\_rat,u}$ was calculated by dividing the total amount of furamidine recovered in urine from 0-24 h by the area under the concentration-time curve (AUC) in plasma within

the same time interval, and was corrected by the unbound fraction of furamidine in plasma (Table 4.1). The unbound renal clearance of furamidine from plasma in humans ($Cl_{R\_human,u}$; l/h/kg) was estimated by the "glomerular filtration rate (GFR) ratio approach" (Lin, 1998):

$Cl_{R\_human,u} = Cl_{R\_rat,u}$ / GFR ratio, where the GFR ratio between rats and humans is 4.8.

PBPK Modeling and Simulation

Pharmacokinetic Analysis. PBPK modeling and simulation were performed with Berkeley Madonna (v 8.0.2, University of California, Berkeley, CA), a differential equation-based modeling software program used extensively in the development of PBPK models (Rowland et al., 2004). The goodness-of-fit of model simulations was assessed based on visual comparison of predicted mass/concentration-time profiles and observed in vivo rat and human data. Observed and predicted plasma/tissue concentration-time profiles were analyzed for plasma/tissue AUC values and terminal half-lives ($t_{1/2,terminal}$) of pafuramidine/furamidine by non-compartmental analysis using WinNonlin (v 5.0.1, Pharsight Corp., Mountain View, CA).

Prediction of Dose-Exposure Relationship. Furamidine plasma concentration-time profiles were simulated under different multiple-dose regimens based on the single-dose human semi-PBPK model (Fig. 4.1B). The efficacy and safety indices of furamidine were defined by a minimum effective concentration ($C_{eff,min}$) and a hypothetical no observable adverse effect level (NOAEL), respectively. Selection of an optimal multiple-dose regimen of pafuramidine was based on the assumption that furamidine concentrations in plasma must be above $C_{eff,min}$ at least 80% of the time during the dosing interval, whereas the average steady-state and maximum concentrations in plasma ($C_{ss,ave}$ and $C_{ss,max}$) must be less than the NOAEL. $C_{eff,min}$ was determined based on an in vitro 50% inhibitory concentration (IC_{50}; 1 ng/ml ≈ 3 nM) of furamidine against the *Trypanosoma brucei rhodesiense* strain, STIB900 (Wenzler et al., 2009). This trypanosome strain is used routinely at the Swiss Tropical and Public Health Institute to assess in vitro and in vivo

activity of diamidine compounds (Ismail et al., 2005). The IC_{50}, determined with culture medium containing 15% heat-inactivated horse serum, was converted to $C_{eff,min}$ based on the following assumptions: 1) no species differences in plasma binding (f_{u,p_F} = 25%, Table 4.1); 2) binding in 15% horse serum (f_{u,ser_F}) approximated that in rat perfusate (f_{u,per_F}), which consisted of 20% rat blood; that is, $f_{u,ser\_F} = f_{u,per\_F}$ = 44% (Table 4.1). $C_{eff,min}$ for total (bound+unbound) furamidine in plasma was corrected to 5 nM ($C_{eff,min} = IC_{50} \times f_{u,ser\_F} / f_{u,p\_F}$ = 3 nM x 44% / 25% = 5 nM). The NOAEL has not been determined for furamidine. A concentration of 100 nM, which is 20% less than the predicted $C_{ss,ave}$ under the dosage regimen used in the expanded Phase I safety study (100 mg twice daily for 14 days), was selected to define the NOAEL. Dose safety was evaluated by comparing the furamidine concentrations in plasma with the hypothetical NOAEL, and comparing furamidine exposure in liver between the clinically-used and semi-PBPK model-predicted dosage regimens.

D. RESULTS

Whole-Liver Rat PBPK Model Prediction. The disposition of pafuramidine and furamidine in rat IPLs was characterized in a previous study (Yan et al., 2011). In summary, pafuramidine was taken up by IPLs and eliminated primarily by metabolism, with negligible biliary excretion; at the end of the 2-h perfusion, >98% of total formed furamidine was recovered in the liver. Pafuramidine distribution between perfusate and liver reached equilibrium after ~20 min. The liver-to-perfusate partition coefficient for pafuramidine, generated based on the whole-liver model (Fig. 4.1A), was 70 (Table 4.1). Pafuramidine was highly bound to proteins in plasma, perfusate (composed of 20% blood), and liver tissue (Table 4.1), whereas furamidine was highly bound only to liver tissue. The unbound fraction of furamidine in liver (f_{u,L_F}) was at least 80-fold lower than that in plasma (f_{u,p_F}) and perfusate (f_{u,per_F}) (Table 4.1). The hepatic unbound intrinsic formation clearance of furamidine ($Cl_{L\_P\rightarrow F,\ u}$) accounted for approximately one-third of total hepatic unbound intrinsic clearance of pafuramidine ($Cl_{L\_P\rightarrow F,\ u}$ + $Cl_{L\_P\rightarrow M,\ u}$) (Table 4.1). The unbound intrinsic clearance for furamidine hepatic basolateral reuptake ($Cl_{F\_up,\ u}$) was 24-fold higher than that for basolateral efflux ($Cl_{F\_eff,\ u}$) (Table 4.1), whereas the unbound intrinsic clearance for furamidine biliary excretion ($Cl_{F\_bile,\ u}$) was similar to $Cl_{F\_eff,\ u}$ (Table 4.1).

Disposition of Pafuramidine and Furamidine in Rat and Human Sandwich-Cultured Hepatocytes. The disappearance of pafuramidine from medium was faster in human compared to rat SCH (Fig. 4.2), as reflected by the 3-fold higher intrinsic clearance of pafuramidine in human compared to rat SCH (Table 4.2). Disposition profiles of formed furamidine were similar between rat and human SCH (Fig. 4.2). The kinetic parameters associated with pafuramidine and furamidine hepatic disposition in rat and human SCH were derived from a previously developed compartmental model (Yan et al., 2011). The rate constants for furamidine basolateral efflux were similar between rats and humans, whereas

the rate constant for furamidine basolateral reuptake in human SCH was three-fourths of that in rat SCH (Table 4.2). Furamidine was not detected in bile in both rat and human SCH.

Disposition of Pafuramidine and Furamidine in Rats. Pafuramidine was absorbed and metabolized to furamidine rapidly after oral administration; both compounds in plasma reached a maximum concentration at ~1 h and declined approximately in parallel for up to 12 h (Fig. 4.3A, inset). The apparent terminal half-life ($t_{1/2,app}$) of pafuramidine, based on the 0-12 h plasma concentration-time profile, was similar to that of furamidine (4 h).

Whole-Body Rat Semi-PBPK Model Prediction. Physiologic and pafuramidine- and furamidine-specific parameters (Table 4.1) were utilized to develop the rat semi-PBPK model (Fig. 4.1B). Pafuramidine and furamidine hepatic disposition parameters were obtained from the rat whole-liver model (Fig. 4.1A). The partition coefficient of pafuramidine in fat was much higher than that in other tissues, which could be due to the high lipophilicity (Zhou et al., 2002; Andersen et al., 2008). Based on previous data from rats administered preformed furamidine intravenously, the furamidine kidney-to-plasma partition coefficient was estimated to be as high as 4000 (Table 4.1); the renal clearance of furamidine from plasma ($Cl_{F\_renal,u}$) in rats was approximately 3-fold less than GFR (Table 4.1) (Goldsmith, 2011). The rate constant for pafuramidine absorption (k_{a_P}) was 7-fold higher than that for metabolic conversion of pafuramidine to furamidine in the gut ($k_{G\_P\rightarrow F}$). The overall fraction of furamidine formed from pafuramidine in the rat was about 40%, of which the liver contributed approximately twice as much as the gut (Table 4.3). The semi-PBPK model (Fig. 4.1B) adequately described pafuramidine/furamidine disposition observed in plasma up to 12 h (Fig. 4.3A, inset). Based on model predictions through 360 h, the terminal elimination half-lives ($t_{1/2,terminal}$) of both pafuramidine and furamidine were at least 10-fold longer than those measured from the 0-12 h observed in vivo data ($t_{1/2,app}$); $t_{1/2,terminal}$ of furamidine was ~4-fold longer than that of pafuramidine (170 versus 47 h) (Fig. 4.3A). The semi-PBPK model predicted that liver and kidney accumulation of furamidine was extensive, accounting

for 63 and 32% of total formed at 12 h, respectively; ~1% of furamidine was recovered in plasma at 12 h. Furamidine exposure in liver and kidney reached a maximum at ~24 h (Fig. 4.3B), and then declined in parallel with that in plasma (Fig. 4.3A). Furamidine was eliminated in rat primarily by biliary excretion; renal excretion was <10% (Table 4.3 and Fig. 4.3B).

Disposition of Pafuramidine and Furamidine in Humans. Following oral administration, pafuramidine was detected in plasma at 0.5 h in five of the six subjects. Pafuramidine concentrations increased to maximum values between 1.5-4 h (median T_{max} = 2.8 h). Pafuramidine concentrations declined, with apparent terminal half-lives of 4-46 h (harmonic mean $t_{1/2,app}$ = 11.5 h). Furamidine was not consistently detected in plasma until 2 h after pafuramidine administration and increased to a maximum concentration between 4-10 h (median T_{max} = 6 h). Furamidine concentrations declined, with a harmonic mean half-life ($t_{1/2,app}$) of 14.5 h. Both pafuramidine and furamidine were above the limit of quantification (BLQ) in plasma of all subjects up to 24 h post-administration. Within 168 h of dosing (during which complete collections of excreta were available), the major route of elimination of radioactivity was via feces (a mean of 36% of the dose, primarily as furamidine, and one of the intermediate metabolites, M3), with a mean of 13% of the dose eliminated in urine (primarily as M3). Extrapolations of the data available after 168 h indicated that about 13% and 39% of the dose (a total of 52%) would be eliminated in urine and feces, respectively.

Whole-Body Human Semi-PBPK Model Prediction. Physiologic and pafuramidine/furamidine-specific parameters (Table 4.1) were utilized to develop the human semi-PBPK model. No significant difference in plasma binding of pafuramidine and furamidine was observed between rats and humans (Table 4.1). Pafuramidine/furamidine hepatic clearance values in humans were predicted by scaling the corresponding in vivo rat values normalized by scaling factors derived from rat and human SCH studies, as described in Materials and Methods. Similar to rats, the renal clearance of furamidine from plasma

($Cl_{F\_renal,u}$), estimated by the GFR approach, was approximately 3-fold less than GFR (Table 4.1). Because a one-compartment oral absorption model failed to predict the delayed absorption of pafuramidine, transit compartments were added to the human semi-PBPK model (Fig. 4.1B). The rate constants for pafuramidine absorption along the transit compartments (k_{P_12}, k_{P_23}, k_{P_3g}) were similar (Table 4.1); the rate constant for pafuramidine absorption from gut to liver (k_{a_P}) was comparable to k_{P_12}, k_{P_23}, and k_{P_3g}, but was 5-fold higher than that for furamidine absorption (k_{a_F}) (Table 4.1); the rate constant for metabolic conversion of pafuramidine to furamidine in the gut ($k_{G\_P\rightarrow F}$) was approximately 4-fold lower than k_{a_P} (Table 4.1). The overall fraction of furamidine generated from pafuramidine in the gut and liver was about 50%; similar to rats, the contribution by the liver was higher than that by the gut (Table 4.3). Model predictions, based on the scheme depicted in Fig. 4.1B, adequately described pafuramidine and furamidine disposition observed in plasma up to 24 h (Fig 4.4A, inset). Prolonged (up to 240 h) predictions indicated that the $t_{1/2,terminal}$ of both pafuramidine and furamidine were 1.5- and 4-fold longer, respectively, than those measured from the 24-h observed in vivo data; the $t_{1/2,terminal}$ of furamidine was ~3-fold longer than that of pafuramidine (64 versus 19 h) (Fig. 4.4A). Similar to rats, the semi-PBPK model for human disposition predicted that the liver and kidney are the major organs for furamidine accumulation. Furamidine distribution between tissues (liver, kidney) and plasma reached equilibrium after ~36 h, as reflected by the parallel terminal plasma concentration- and tissue mass-time profiles (Fig. 4.4A and 4.4B). Furamidine was eliminated in humans primarily by biliary excretion; renal excretion was negligible (Table 4.3 and Fig. 4.4B).

Prediction of Dose-Exposure Relationship. The human semi-PBPK model (Fig. 4.1B) was used to simulate plasma- and liver-time profiles associated with various pafuramidine oral dosing regimens. Based on the pre-defined hypothetical efficacy and safety indices, a regimen (40 mg once daily for 14 days) that maintained furamidine plasma concentrations above the $C_{eff,min}$ for ~99% of the time throughout the 14 days was selected

(Fig. 4.5). Based on the predicted plasma $t_{1/2,terminal}$ of furamidine, plasma concentrations of furamidine reached steady-state at approximately 12-13 days; $C_{ss,ave}$ was approximately 4-fold higher than the $C_{eff,min}$ and was 4-fold lower than the hypothetical NOAEL (Fig. 4.5). Predicted furamidine liver exposure, expressed as the area under the liver concentration-time curve ($AUC_{0\text{-}14\ d}$), was 5-fold lower with this alternate dosage regimen compared to the dosage regimen administered in the expanded Phase I safety study (100 mg twice daily for 14 days) (Fig. 4.5).

E. DISCUSSION

Accurate prediction of the pharmacokinetics of generated active metabolites in humans is essential in the selection of appropriate prodrug doses prior to clinical trials. Pafuramidine is a prodrug of the antiparasitic agent, furamidine, that demonstrated efficacy in animal models of first stage human African trypanosomiasis (Mdachi et al., 2009; Wenzler et al., 2009). Dose selection for antiparasitic drug development traditionally has relied on achieving efficacious plasma drug concentrations in humans that correlate with those in animal models. A similar strategy was applied to pafuramidine, only plasma concentrations of furamidine were correlated between species. The current work represents the first attempt to optimize this prodrug dose-selection strategy using whole-body semi-PBPK models for rats and humans to predict plasma and tissue exposure and excretion profiles of the active metabolite. Preclinical and clinical data generated during pafuramidine development were used as a training set to demonstrate the utility of PBPK modeling to examine the relationship between pafuramidine dose and furamidine plasma/tissue exposure, which could be used to guide clinical dose-ranging studies of next-in-class compounds.

The final model structure and pafuramidine absorption characteristics in rats were used initially to predict pafuramidine and furamidine disposition in humans. However, the model prediction underestimated the C_{max} and T_{max} of pafuramidine and furamidine, which possibly could be attributed to differences in dosage formulation (suspension versus capsule) and/or concomitant diet (standard versus high fat meal) between rats and humans. Either or both of these factors could extend the T_{max} of pafuramidine in humans. As such, three transit compartments were added sequentially to the pafuramidine human submodel to describe the dissociation of pafuramidine from the dosage form and the high fat meal before reaching the absorption site (gut). Pafuramidine is a BCS class II compound (Zhou et al., 2002); the high fat meal was administered intentionally to facilitate pafuramidine absorption

(Wu and Benet, 2005). This food effect was substantiated by the enhanced f_a estimated from the human compared to the rat semi-PBPK model (Table 4.1). These observations emphasized that formulation/diet may be significant determinants of pafuramidine/furamidine disposition.

Tissue-to-plasma partitioning (K_p) is another factor that influences the disposition of compounds in the body. The in vivo K_p values for pafuramidine and furamidine were not available for human tissues. Unbound K_p values in rats and humans were assumed to be similar ($K_{p,u,rat} = K_{p,u,human}$) (Arundel, 1997). Because no significant species difference in plasma binding of pafuramidine/furamidine was observed (Table 4.1), K_p values derived from the rat model were applied to describe the distribution of pafuramidine/furamidine in humans.

Extrapolation of metabolite kinetics from animals to humans remains a major challenge in PBPK modeling. Disposition of furamidine in the liver involves formation from pafuramidine, hepatocellular binding, basolateral efflux/reuptake, and biliary excretion. Empirical allometric scaling and physiologically-based direct scaling were not utilized for the following reasons: 1) marked species differences in pafuramidine metabolism (Table 4.2); 2) physiologically-based direct scaling using rat SCH underestimated metabolic Cl of pafuramidine in rat IPLs; and 3) in vitro biliary Cl of furamidine was too small to measure in rat and human SCH (Table 4.2) (Yan et al., 2011). Normalized scaling via integration of IPL and SCH data was utilized in the current work, as this method successfully predicted hepatic metabolic Cl of ten extensively metabolized drugs in humans (Lave et al., 1997). In addition, incorporation of Cl, predicted by normalized scaling using conventionally-cultured hepatocytes, into the PBPK model of an antimalarial drug, epiroprim, provided more accurate predictions of epiroprim disposition in humans (Luttringer et al., 2003). SCH, rather than conventionally-cultured hepatocytes, were utilized in the current study due to the ability to characterize both sinusoidal/biliary transport and metabolism (Swift et al., 2009). The human semi-PBPK model, based on these scaled parameters, adequately described

pafuramidine/furamidine concentration-time profiles in human plasma and predicted the dose-plasma/tissue exposure relationship and excretion profiles (Fig. 4.4). To the authors' knowledge, the current work represents the first effort to extrapolate metabolism/transport clearance from rats to humans for a prodrug/active metabolite pair.

Previous studies in rats and monkeys indicated that pafuramidine has a low oral bioavailability (10-20%) (Midgley et al., 2007), suggesting that pafuramidine could undergo extensive first-pass biotransformation in the gut, as well as in the liver. One report examined pafuramidine metabolism in the gut; the intrinsic formation clearance of the first intermediate metabolite (M1) from pafuramidine in human intestinal microsomes was at least 10-fold lower than that in human liver microsomes (Wang et al., 2007). As such, the liver was assumed initially to be the sole site of furamidine formation. However, in vivo studies showed a near-simultaneous appearance of furamidine with pafuramidine in plasma in both rats and humans (Fig. 4.3A and 4.4A, insets). Initial model predictions showed a marked delay in the appearance of furamidine relative to pafuramidine. This discrepancy suggested that furamidine may be formed during pafuramidine absorption through the gut before entering the liver. Bioconversion from pafuramidine to furamidine involves sequential oxidative and reductive reactions mediated by cytochrome P450 enzymes and cytochrome b_5/NADH cytochrome b_5 reductases (Saulter et al., 2005; Wang et al., 2006). These enzymes are expressed in both the liver and gut. Previous studies demonstrated that CYP4F, a major catalyst of M1 formation, represented a significant portion of the human intestinal P450 "pie" (Wang et al., 2007). These observations prompted incorporation of a gut compartment, representing furamidine formation during pafuramidine absorption, in the furamidine rat/human submodel (Fig. 4.1B). The model described furamidine plasma disposition adequately (Fig. 4.3A and 4.4A, insets). Concordant with in vivo observations, the model predicted that, once absorbed, pafuramidine was converted efficiently to furamidine in rats and humans, as reflected by nearly 50% conversion from pafuramidine;

the gut contributed approximately 30-40% to furamidine formation in both species (Table 4.3). These data suggested that the gut contributes significantly to furamidine formation after pafuramidine administration, and substantiated the value of PBPK modeling to uncover potentially important biologic determinants of drug disposition. Further studies are warranted to confirm that the gut is a major pre-systemic site of furamidine formation following oral administration of pafuramidine.

In rats and humans administered a single oral dose of pafuramidine, the apparent terminal half-life ($t_{1/2,app}$) of furamidine was approximately 4 and 14.5 h, respectively, similar to pafuramidine (Fig. 4.3A and 4.4A, insets). However, one week after ^{14}C-pafuramidine administration, a considerable amount of radioactivity was retained in rats (Midgley et al., 2007) and humans (CAO, unpublished observations), largely as furamidine. Due to LC-MS/MS assay sensitivity limitations in the current study, furamidine was BLQ in plasma beyond 8 and 24 h after pafuramidine administration to rats and humans, respectively. As such, the observed plasma profile of furamidine (Fig. 4.3A and 4.4A insets) represents the distribution phase. In the absence of a more sensitive assay, the "true" terminal half-life ($t_{1/2,terminal}$) of furamidine was predicted using semi-PBPK modeling. The model predicted that furamidine $t_{1/2,terminal}$ in rats was approximately 40-fold longer than $t_{1/2,app}$ (7 d versus 4 h). After intravenous administration of preformed furamidine (10 μmol/kg) to rats, furamidine was detected in the kidney for up to 16 days. The corresponding kidney $t_{1/2,terminal}$ was estimated to be 7 d (Goldsmith, 2011). The human plasma and tissue $t_{1/2,terminal}$ of furamidine was predicted to be 64 h (~2.5 d), demonstrating the utility of PBPK modeling to estimate long-term plasma and tissue exposure, which may not be possible to measure directly in vivo due to analytical sensitivity and/or inaccessibility to sampling sites such as the liver.

A semi-PBPK modeling approach was used in the current work to examine the relationship between dose and plasma/tissue exposure for an antiparasitic prodrug/active metabolite pair in humans. The model predicted that the $C_{ss,ave}$ of the active metabolite,

furamidine, was 25-fold higher than the estimated $C_{eff,min}$ in plasma (Fig. 4.5) based on the dose administered (100 mg twice daily) in the expanded Phase I safety study. An alternate dosage regimen (40 mg once daily) was predicted to maintain furamidine plasma concentrations half-way between the pre-defined hypothetical efficacy and safety indices ~99% of the time throughout the entire 14-day dosing period (Fig. 4.5), while reducing furamidine hepatic exposure (Fig. 4.5). Model predictions suggested that, if a patient were to inadvertently miss or double the projected dose, only modest fluctuations in plasma furamidine concentrations within the efficacy-safety range would result. Next-in-class compounds in development for both stages of HAT are under investigation (Wenzler et al., 2009). This PBPK modeling-based strategy, which requires estimated or known efficacy (*e.g.,* $C_{eff,min}$) and safety (*e.g.,* NOAEL) indices, could be applied to next-in-class compounds to predict plasma/tissue disposition and guide dose-ranging studies in humans.

F. APPENDIX

MODEL PARAMETER ABBREVIATIONS

D_{oral}: oral dose;

$A_{tissue/compartment}$: amount in whole organ or compartment;

AA: amount in arterial blood;

CA: arterial blood concentration;

CV: venous blood concentration;

CVP: venous plasma concentration;

B/P: blood-to-plasma ratio;

CV_{tissue}: vascular tissue concentration;

C_{tissue}: tissue concentration;

CO: cardiac output;

Q_{tissue}: tissue blood flow;

V_{tissue}: tissue volume;

$K_{p,tissue}$: tissue-to-plasma partition coefficient

k_{P_12}, k_{P_23}, k_{P_3g}: first-order rate constants for pafuramidine distribution along the transit compartments of gut;

k_{a_P} and k_{a_F}: first-order rate constants for the movement from gut to liver of pafuramidine and formed furamidine, respectively;

$k_{G\_P\rightarrow F}$: first-order rate constant for metabolic conversion from pafuramidine to furamidine in the gut;

$f_{u,L,}$ and $f_{u,p}$: unbound fractions in liver and plasma, respectively;

$Cl_{L\_P\rightarrow F,\ u}$: hepatic unbound intrinsic clearance for the formation of furamidine from pafuramidine; $Cl_{L\_P\rightarrow M,\ u}$: hepatic unbound intrinsic clearance for metabolic conversion from pafuramidine to other metabolites;

$Cl_{F\_up,\ u}$: unbound intrinsic clearance for hepatic basolateral uptake of furamidine;

$CL_{F\_eff,\ u}$: unbound intrinsic clearance for hepatic basolateral efflux of furamidine;

$CL_{F\_bile,\ u}$: unbound intrinsic clearance for biliary excretion of furamidine;

$CL_{F\_renal,\ u}$: unbound renal clearance of furamidine from plasma;

R_{abs_P}: rate of pafuramidine movement from gut to liver

R_{abs_F}: rate of intestinally-formed furamidine movement from gut to liver

$R_{gut\ formation\_F}$: rate of furamidine formation in the gut;

$R_{liver\ formation\_F}$: rate of furamidine formation in the liver;

$R_{liver\ formation\_M}$: rate of other metabolite formation in the liver;

R_{renal_F}: rate of furamidine renal excretion;

R_{bile_F}: rate of furamidine biliary excretion;

Brown et al., 1997P, pafuramidine; M, other metabolites; F, furamidine.

Note: The volume of tissue and vascular blood in the liver represents 95% and 5%, respectively, of total liver volume (Nong et al., 2008).

HUMAN SEMI-PBPK MODEL EQUATIONS

Pafuramidine

Disposition in the gut:

1) Amount in transit compartment 1 (T1):

Single-dose: $dA_{T1}/dt = -(k_{p\_12} \times A_{T1}) + D_{oral}\ (t = 0)$;

Multiple-dose: $dA_{T1}/dt = -(k_{p\_12} \times A_{T1}) + D_{oral}$ (at the beginning of each dosing interval)

2) Amount in transit compartment 2 (T2):

$dA_{T2}/dt = (k_{p\_12} \times A_{T1}) – (k_{p\_23} \times A_{T2})$

3) Amount in transit compartment 3 (T3):

$dA_{T3}/dt = (k_{p\_23} \times A_{T2}) – (k_{p\_3g} \times A_{T3})$

4) Amount in the gut:

$$dA_{gut\_P}/dt = (k_{p\_3g} \times A_{T3}) - R_{abs\_P} - R_{gut\ formation\_F}$$

$$R_{abs\_P} = k_{a\_P} \times A_{gut\_P}$$

$$R_{gut\ formation\_F} = k_{G\_P \rightarrow F} \times A_{gut\_P}$$

Disposition in the liver (flow-limited):

$$dA_{liver\_P}/dt = Q_{liver} \times (CA_P - CV_{liver\_P}) - R_{liver\ formation\_F} - R_{liver\ formation\_M} + R_{abs\_P}$$

$$C_{liver\_P} = A_{liver\_P}/V_{liver}$$

$$CV_{liver\_P} = C_{liver\_P}/K_{p\_liver\_P}$$

$$R_{liver\ formation\_F} = C_{liver\_P} \times f_{u,L\_P} \times Cl_{L\_P \rightarrow F,\ u}$$

$$R_{liver\ formation\_M} = C_{liver\_P} \times f_{u,L\_P} \times Cl_{L\_P \rightarrow M,\ u}$$

Disposition in the fat (flow limited):

$$dA_{fat\_P}/dt = Q_{fat} \times (CA_P - CV_{fat\_P})$$

$$C_{fat\_P} = A_{fat\_P}/V_{fat}$$

$$CV_{fat\_P} = C_{fat\_P}/K_{p\_fat\_P}$$

Disposition in the rest of body (rest) (flow limited):

$$dA_{rest\_P}/dt = Q_{rest} \times (CA_P - CV_{rest\_P})$$

$$C_{rest\_P} = A_{rest\_P}/V_{rest}$$

$$CV_{rest\_P} = C_{rest\_P}/K_{p\_rest\_P}$$

Blood and plasma concentration:

1) Venous blood concentration:

$$CV_P = (Q_{liver} \times CV_{liver\_P} + Q_{fat} \times CV_{fat\_P} + Q_{rest} \times CV_{rest\_P})/CO$$

2) Venous plasma concentration:

$$CVP_P = CV_P/(B/P_P)$$

3) Arterial blood concentration:

$$dAA_P/dt = QC \times (CV_P - CA_P)$$

$$CA_P = AA_P/V_{blood}$$

Furamidine

Disposition in the gut:

$$dA_{gut\_F}/dt = R_{gut\ formation\_F} - R_{abs\_F}$$

$$R_{abs\_F} = k_{a\_F} \times A_{gut\_F}$$

Disposition in the liver (diffusion-limited):

1) Liver blood:

$$dAV_{liver\_F}/dt = Q_{liver} \times (CA_F - CV_{liver\_F}) + R_{abs\_P} - R_{uptake\_F} + R_{efflux\_F}$$

$$CV_{liver\_F} = AV_{liver\_F}/(0.05 \times V_{liver})$$

2) Liver tissue:

$$dA_{liver\_F}/dt = R_{liver\ formation\_F} + R_{uptake\_F} - R_{efflux\_F} - R_{bile\_F}$$

$$C_{liver\_F} = A_{liver\_F}/(0.95 \times V_{liver})$$

$$R_{uptake\_F} = CV_{liver\_F} \times f_{u,p\_F} \times Cl_{F\_up,\ u}$$

$$R_{efflux\_F} = C_{liver\_F} \times f_{u,L\_F} \times Cl_{F\_eff,\ u}$$

$$R_{bile\_F} = C_{liver\_F} \times f_{u,L\_F} \times Cl_{F\_bile,\ u}$$

Disposition in the kidney (flow limited):

$$dA_{kidney\_F}/dt = Q_{kidney} \times (CA_F - CV_{kidney\_F})$$

$$C_{kidney\_F} = A_{kidney\_F}/V_{kidney}$$

$$CV_{kidney\_F} = C_{kidney\_F}/K_{p,kidney\_F}$$

Disposition in the rest of body (rest) (flow limited):

$$dA_{rest\_F}/dt = Q_{rest} \times (CA_F - CV_{rest\_F})$$

$$C_{rest\_F} = A_{rest\_F}/V_{rest}$$

$$CV_{rest\_F} = C_{rest\_F}/K_{p,rest\_F}$$

Blood and plasma concentration:

1) Venous blood concentration:

$$CV_F = (Q_{liver} \times CV_{liver\_F} + Q_{kidney} \times CV_{kidney\_F} + Q_{rest} \times CV_{rest\_F})/CO$$

2) Venous plasma concentration:

$$CVP_F = CV_F/(B/P_F)$$

3) Arterial blood concentration:

$$dAA_F/dt = QC \times (CV_F - CA_F) - R_{renal\_F}$$

$$R_{renal\_F} = CA_F \times f_{u,p\_F} \times Cl_{F\_renal,\ u}$$

$$CA_F = AA_F/V_{blood}$$

Urine:

$$dA_{urine\_F}/dt = R_{renal\_F}$$

Feces:

$$dA_{feces\_F}/dt = R_{bile\_F}$$

G. TABLES

Table 4.1. Semi-physiologically-based pharmacokinetic model parameters associated with the disposition of pafuramidine and furamidine in rats and humans.

Parameters	Value		Source
	Rat	Human	
Physiologic			
Body weight (kg)	0.3	70	Measured
Cardiac output (l/h/kg)	14	5	Brown et al., 1997
Blood and tissue volumes[a]			
Blood	0.074	0.077	Brown et al., 1997
Fat	0.07	0.2	Brown et al., 1997
Liver	0.03	0.03	Brown et al., 1997
Kidney	0.007	0.004	Brown et al., 1997
Tissue blood flows[a]			Brown et al., 1997
Fat	0.07	0.05	Brown et al., 1997
Liver	0.17	0.25	Brown et al., 1997
Kidney	0.14	0.19	Brown et al., 1997
Rest of body	0.62	0.51	Calculated
Chemical specific			
Pafuramidine			
Unbound fractions (%)			
Liver (f_{u,L_P})[b]	0.07 ± 0.02	Same as rats	Measured
Perfusate (f_{u,per_P})	1.1 ± 0.1	N.A.[c]	Measured
Plasma (f_{u,p_P})	0.2 ± 0.02	0.2 ± 0.01	Measured
Liver-to-perfusate partition coefficient	70	N.A.	Fitted
Tissue-to-plasma partition coefficients			
Liver	14	Same as rats	Calculated
Fat	260	Same as rats	Fitted
Rest of body	2	Same as rats	Fitted
Blood-to-plasma (B/P) ratio[d]	1.1 ± 0.1	Same as rats	Measured
Fraction of dose absorbed into enterocytes (f_a)	0.3	1	Fitted
Gastrointestinal rate constants (h^{-1})[e]			
k_{P_12}, k_{P_23}, k_{P_3g}	N.A.	1.1	Fitted
k_{a_P}	0.5	1.1	Fitted
$k_{G\_P \rightarrow F}$	0.07	0.3	Fitted

Hepatic clearance (l/h/kg BW)[f]			
$Cl_{L\_P\rightarrow M,u}$	70	124	Fitted (Rat) Scaled (human)
$Cl_{L\_P\rightarrow F,u}$	40	71	Fitted (Rat) Scaled (human)
Furamidine			
Unbound fractions (%)			
Liver (f_{u,L_F})[b]	0.3 ± 0.1	Same as rats	Measured
Perfusate (f_{u,per_F})	44 ± 5	N.A.	Measured
Plasma (f_{u,p_F})	24 ± 2	25 ± 3	Measured
Tissue-to-plasma partition coefficients			
Kidney	4000	Same as rats	Fitted
Rest of body	1	Same as rats	Fitted
Blood-to-plasma (B/P) ratio[d]	0.9 ± 0.1	Same as rats	Measured
Gastrointestinal rate constants (h^{-1})[e]			
k_{a_F}	2.4	0.2	Fitted
Hepatic and renal clearances (l/h/kg BW)[e]			
$Cl_{F\_up,u}$	1.9	1	Fitted (Rat) Scaled (human)
$Cl_{F\_eff,u}$	0.08	0.05	Fitted (Rat) Scaled (human)
$Cl_{F\_bile,u}$	0.08	0.05	Fitted (Rat) Scaled (human)
$Cl_{F\_renal,u}$	0.12	0.024	Calculated
GFR[g]	0.4	0.08	Lin, 1998

[a] *Tissue volumes and blood flows denote fractions of total body weight and cardiac output, respectively.*

[b] *Liver unbound fractions in humans were assumed equal to those in rats.*
[c] *Not applicable.*

[d] *B/P ratio of pafuramidine or furamidine at 0.1 μM in rat blood (see Materials and Methods).*

[e] *Rate constants associated with pafuramidine and furamidine absorption and metabolism in the gut are defined in the legend to Fig. 4.1 and were optimized by fitting the semi-PBPK model (schemed depicted in Fig. 4.1B) to* in vivo *rat and human data.*

[f] *Clearance values associated with the disposition of both pafuramidine and furamidine in rat livers are defined in the legend to Fig. 4.1 and were optimized by fitting the semi-PBPK model (schemed depicted in Fig. 4.1A) to rat IPL data; corresponding hepatic clearances in humans were calculated as described in Methods; furamidine renal clearance in rats was calculated based on* in vivo *rat data; human renal clearance was estimated using a 'GFR ratio approach' proposed by Lin, 1998 (see Materials and Methods).*

[g] *GFR, glomerular filtration rate, was obtained from Lin,1998.*

Table 4.2. Kinetic parameters associated with disposition of pafuramidine and furamidine in rat and human sandwich-cultured hepatocytes (SCH).

Parameter[a]	Rat SCH	Human SCH	Scaling Factor[b]
$Cl_{L\_P\rightarrow M}$	0.0047	0.013	3
$Cl_{L\_P\rightarrow F}$	0.0023	0.0067	3
k_{F_up}	0.8	0.6	0.75
k_{F_eff}	0.008	0.008	1
k_{F_bile}[c]	N.A.[d]	N.A.	N.A.

[a] *$Cl_{L\_P\rightarrow M}$ and $Cl_{L\_P\rightarrow F}$ represent* in vitro *intrinsic clearance (ml/min/10^6 cells) for the metabolic conversion of pafuramidine to other metabolites and furamidine, respectively. k_{F_up}, k_{F_eff}, and k_{F_bile} represent first-order rate constants (h^{-1}) for furamidine hepatic basolateral uptake, efflux and biliary excretion, respectively. SCH values denote mean data from n = 3 separate livers.*

[b] *Determined by the ratio of rat-to-human hepatic clearances or rate constants determined with SCH. The scaling factor was used to normalize* in vivo *clearance values from rats prior to scaling to human clearance values (see Materials and Methods).*

[c] *Furamidine biliary excretion was undetectable in both rat and human SCH.*

[d] *Not applicable.*

Table 4.3. PBPK Model prediction of furamidine formation and excretion in rats and humans after administration of a single oral dose of pafuramidine (7.5 μmol/kg and 100mg, respectively).

Measure	Rat	Human
f_m (%)[a]	40	52
Formation (%)[b]		
Gut	30	40
Liver	70	60
Excretion (%)[c]		
Bile	93	96
Urine	7	4

[a]*f_m represents the total fraction of pafuramidine converted to furamidine in gut and liver.*

[b]*Formation (%) represents percent contribution of gut or liver in furamidine formation.*

[c]*Percent excretion was calculated based on the cumulative amount of furamidine excreted in bile or urine up to time infinity.*

H. FIGURES

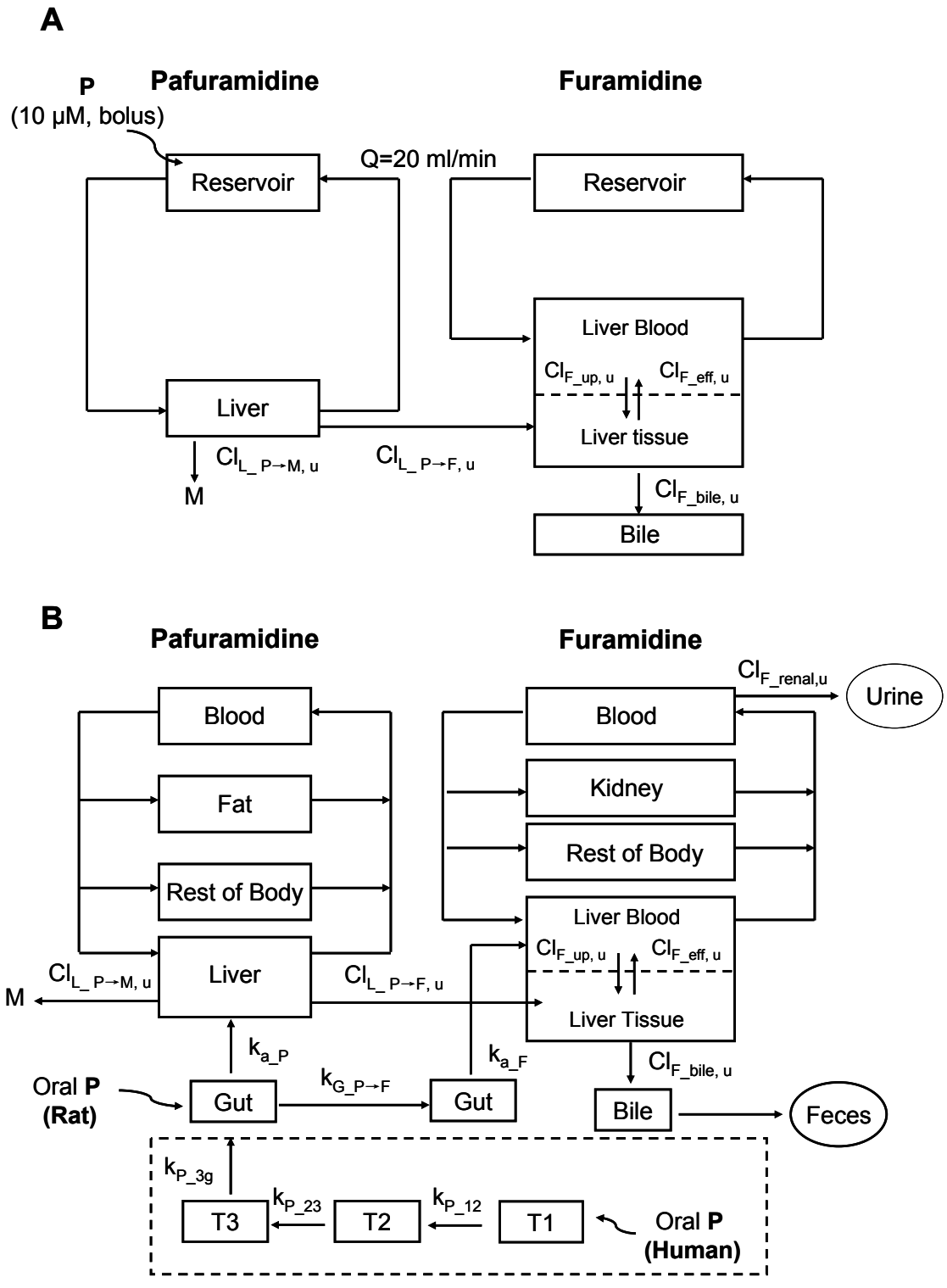
A
P
(10 μM, bolus)
Pafuramidine
Furamidine
Reservoir
Q=20 ml/min
Reservoir
Liver Blood
$Cl_{F\_up,\,u}$
$Cl_{F\_eff,\,u}$
Liver
Liver tissue
$Cl_{L\_P\rightarrow M,\,u}$
$Cl_{L\_P\rightarrow F,\,u}$
M
$Cl_{F\_bile,\,u}$
Bile
B
Pafuramidine
Furamidine
$Cl_{F\_renal,u}$
Urine
Blood
Blood
Fat
Kidney
Rest of Body
Rest of Body
Liver Blood
$Cl_{F\_up,\,u}$
$Cl_{F\_eff,\,u}$
$Cl_{L\_P\rightarrow M,\,u}$
Liver
$Cl_{L\_P\rightarrow F,\,u}$
M
Liver Tissue
k_{a_P}
k_{a_F}
$Cl_{F\_bile,\,u}$
Oral **P**
(Rat)
Gut
$k_{G\_P\rightarrow F}$
Gut
Bile
Feces
k_{P_3g}
k_{P_23}
k_{P_12}
T3
T2
T1
Oral **P**
(Human)

Figure 4.1. Semi-PBPK model schemes depicting disposition of pafuramidine and furamidine in rat IPLs (A) and in vivo in rats and humans (B). Distinct PBPK structures were developed for the prodrug, pafuramidine, and the derived active metabolite, furamidine, and linked by liver (and gut) metabolism. Pafuramidine distribution in all tissue compartments was assumed to be flow-limited. Furamidine distribution in the liver was described as diffusion-limited, as depicted by the dashed line in the liver compartment; furamidine distribution in all other tissue compartments was assumed to be flow-limited. Compartments T1, T2, and T3 in the dashed square represent three consecutive transit compartments for pafuramidine before reaching the absorption site in the gut after oral administration in humans, where k_{P_12}, k_{P_23}, k_{P_3g} represent the first-order rate constants for pafuramidine distribution along the transit compartments and gut. $k_{G\_P\rightarrow F}$ represents the first-order rate constant for metabolic conversion from pafuramidine to furamidine in the gut; k_{a_P} and k_{a_F} represent the first-order rate constants for the movement from gut to liver of pafuramidine and formed furamidine, respectively. $Cl_{L\_P\rightarrow F,\ u}$ represents hepatic unbound intrinsic clearance for the formation of furamidine from pafuramidine; $Cl_{L\_P\rightarrow M,\ u}$ represents hepatic unbound intrinsic clearance for metabolic conversion from pafuramidine to other metabolites; $Cl_{F\_up,\ u}$ represents unbound intrinsic clearance for hepatic basolateral uptake of furamidine; $Cl_{F\_eff,\ u}$ represents unbound intrinsic clearance for hepatic basolateral efflux of furamidine; $Cl_{F\_bile,\ u}$ represents unbound intrinsic clearance for biliary excretion of furamidine; $Cl_{F\_renal,\ u}$ represents unbound renal clearance of furamidine from plasma. P, pafuramidine; M, other metabolites; F, furamidine.

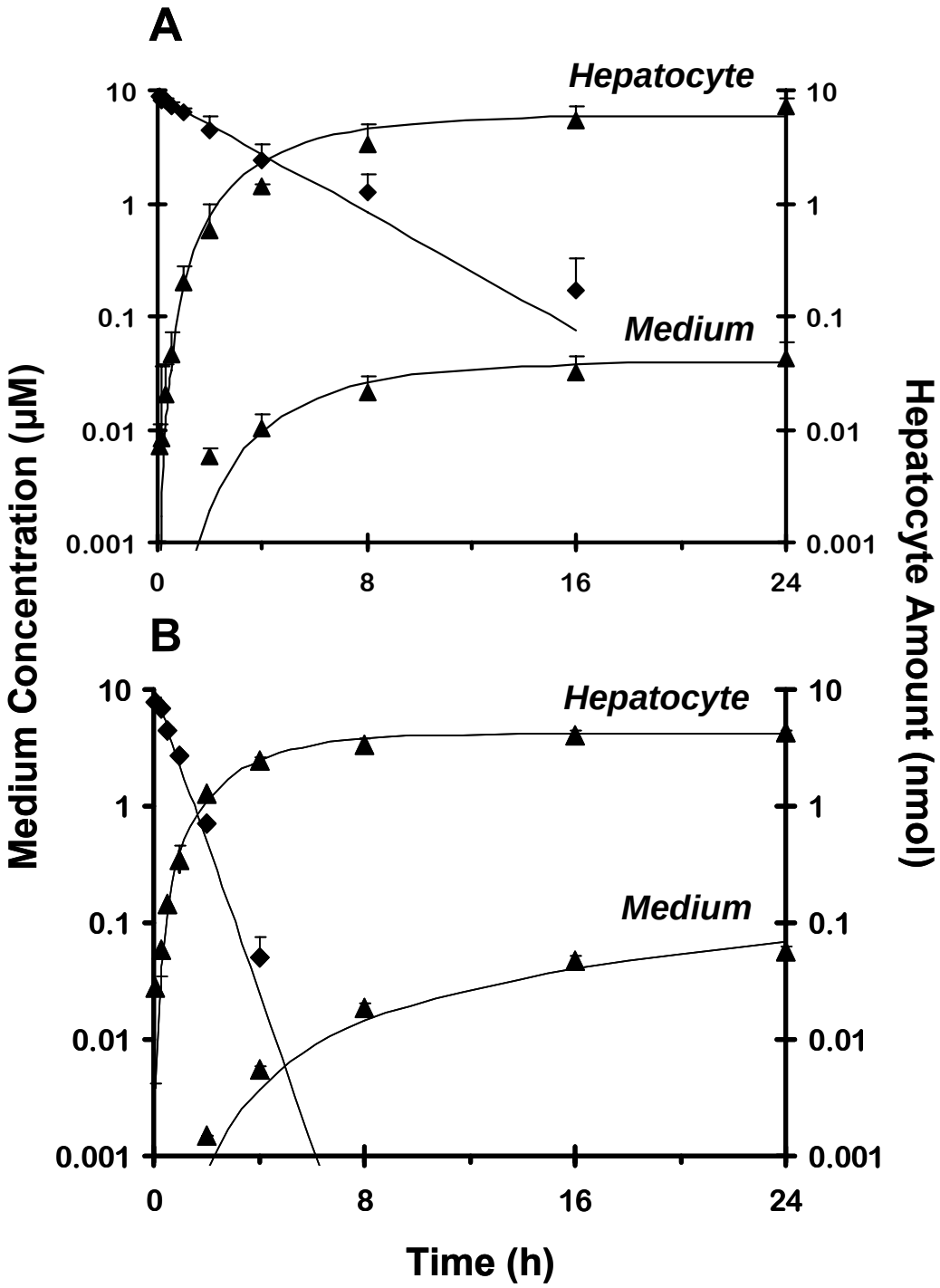

Figure 4.2. Disposition of pafuramidine (diamonds) and furamidine (triangles) over 24 h in sandwich-cultured hepatocytes (SCH) from (A) rats and (B) humans. Rat SCH data were obtained from a previous study (Yan et al., 2011); human SCH data were obtained using a similar study design. Pafuramidine (10 μM) was administered as a bolus to each well, which contained 1.5 ml culture medium. Symbols and error bars denote mean values and SDs, respectively of n=3 livers. Lines represent the computer-generated best fit of a previously developed pharmacokinetic model (Yan et al., 2011) to the data.

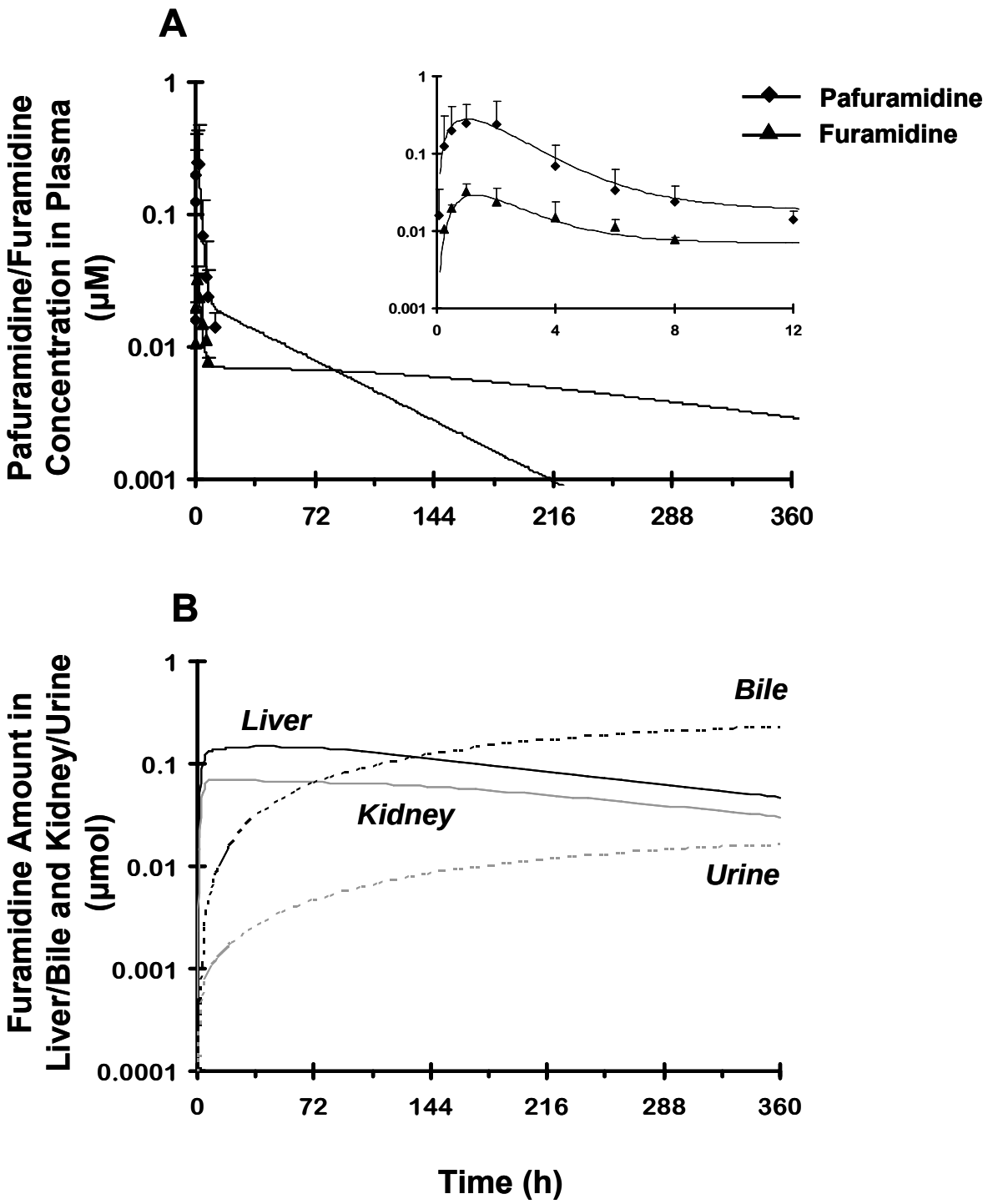

Figure 4.3. Disposition of pafuramidine (diamonds) and furamidine (triangles) in rats administered a single oral dose of pafuramidine (7.5 μmol/kg). (A) Comparison of observed (symbols) and semi-PBPK model-predicted (scheme depicted in Fig. 4.1B) plasma concentration-time profiles of pafuramidine and furamidine over 12 h (inset) and 360 h. Symbols and error bars denote mean values and SD, respectively, of 4 rats. (B) Semi-PBPK model-predicted (scheme depicted in Fig. 4.1B) amount-time profiles of furamidine in liver/kidney (solid lines) and bile/urine (dashed lines) over 360 h.

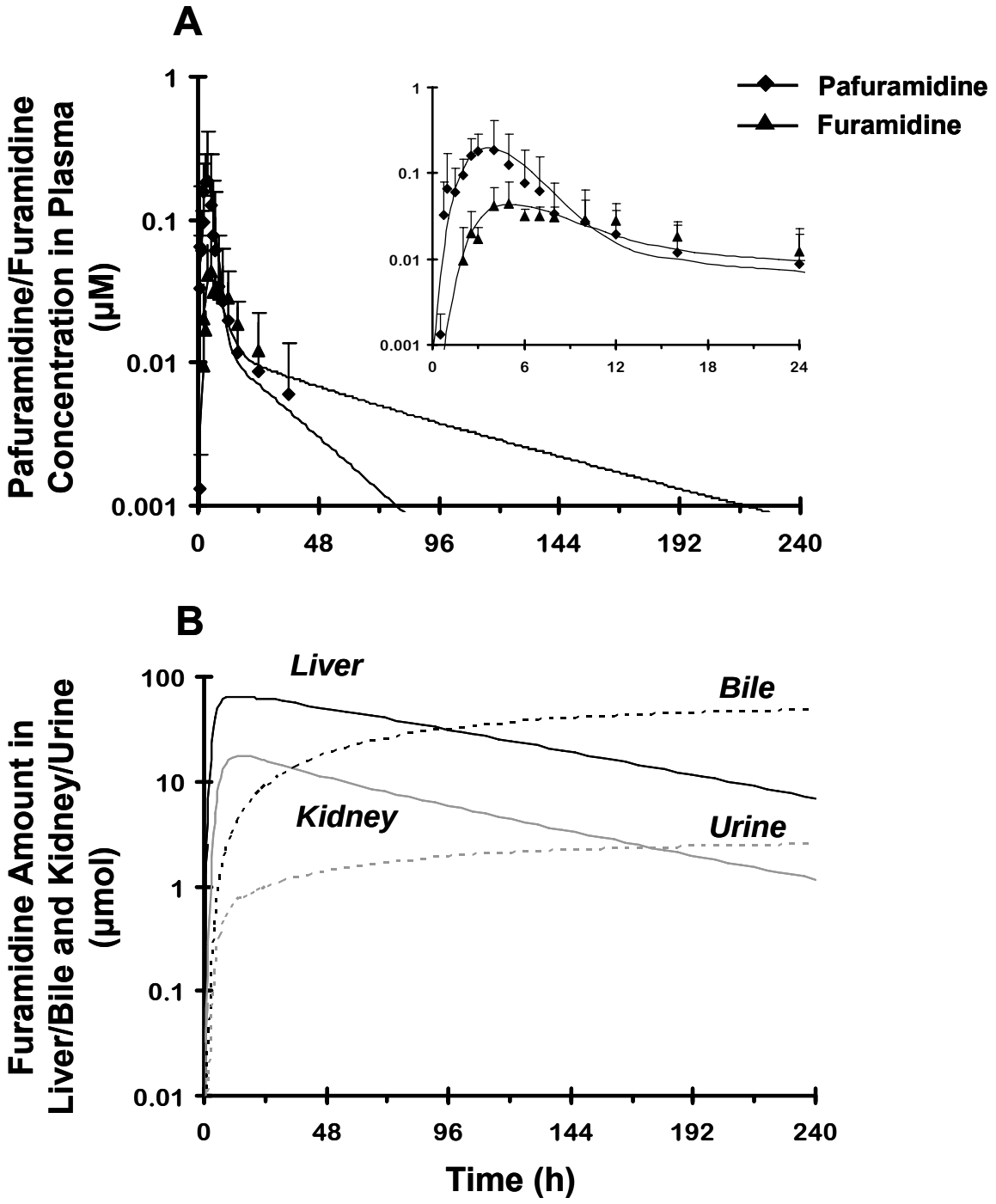

Figure 4.4. Disposition of pafuramidine (diamonds) and furamidine (triangles) in healthy male subjects administered a single oral dose of ^{14}C-pafuramidine (100 mg, equivalent to 274 μmol) in capsule form. (A) Comparison of observed (symbols) and semi-PBPK model-predicted (scheme depicted in Fig. 4.1B) (lines) plasma concentration-time profiles of pafuramidine and furamidine over 24 h (inset) and 240 h. Symbols and error bars denote mean values and SD, respectively, of 6 subjects. (B) Semi-PBPK model-predicted (scheme depicted in Fig. 4.1B) amount versus time profiles of furamidine in liver/kidney (solid lines) and bile/urine (dashed lines) over 240 h.

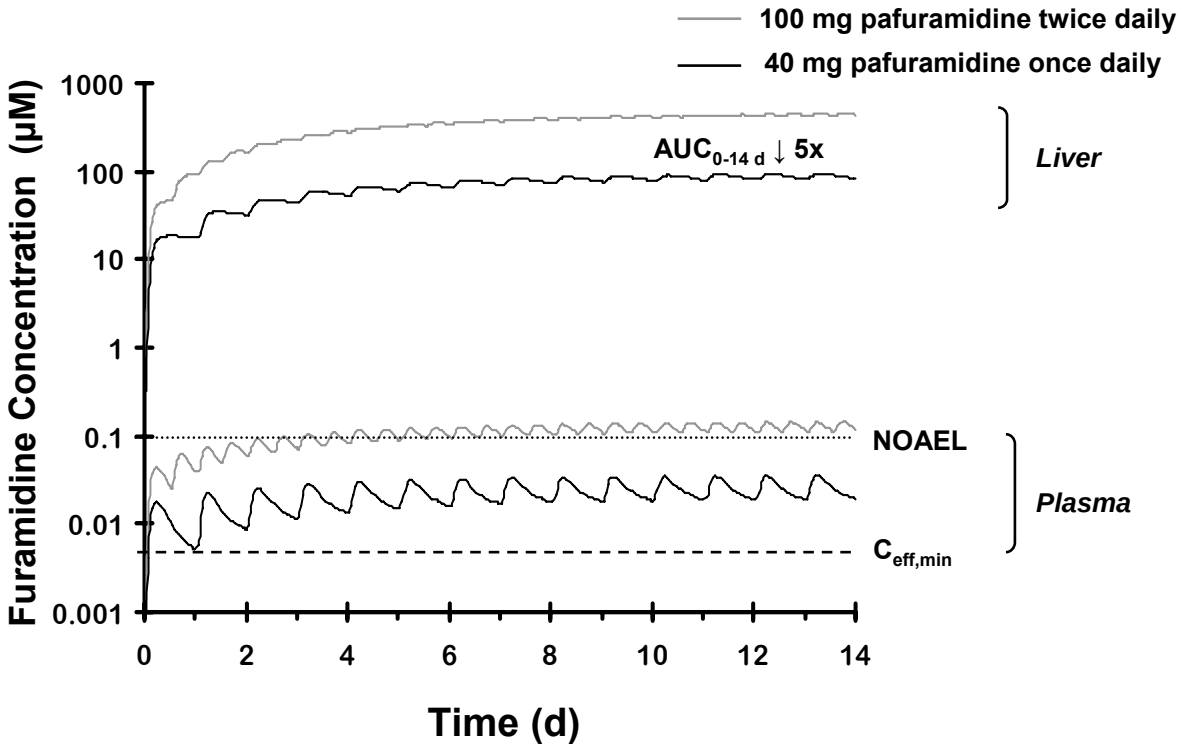

Efficacy Index	$C_{eff,min}$ = 5 nM	
Safety Index	NOAEL = 100 nM	
Dosage Regimen	100 mg twice daily	40 mg once daily
Time > $C_{eff,min}$	~100%	~99%
$C_{ss,ave}$	125 nM	26 nM

Figure 4.5. Semi-PBPK model-predicted (scheme depicted in Fig. 4.1B) plasma and liver concentration-time profiles of furamidine in humans following oral administration of 100 mg pafuramidine twice daily (gray lines) and 40 mg pafuramidine once daily (black lines). Dotted and dashed lines represent safety and efficacy indices defined by a hypothetical no-observable-adverse-effect-level (NOAEL) and a minimum effective concentration ($C_{eff,min}$) of furamidine in plasma, respectively. NOAEL and $C_{eff,min}$ were determined as described in Materials and Methods. Time > $C_{eff,min}$ denotes the time that furamidine concentrations in plasma were above the $C_{eff,min}$ as a percentage of the entire dosing period (14 days); $C_{ss,ave}$ denotes average plasma concentration of furamidine at steady-state; "AUC_{0-14d} ↓ 5x" denotes liver exposure of furamidine, expressed as the area under the liver concentration-time curve ($AUC_{0-14\ d}$), which was 5-fold lower with the modified pafuramidine dosage regimen (40 mg once daily) compared to the dosage regimen administered in the expanded Phase I safety study (100 mg twice daily).

I. REFERENCES

Andersen ME, Reddy MB and Plotzke KP (2008) Are highly lipophilic volatile compounds expected to bioaccumulate with repeated exposures? *Toxicol Lett* **179**:85-92.

Arundel PH (1997) A multi-compartmental model generally applicable to physiologically-based pharmacokinetics. (Astra-Zeneca, UK), in *3rd IFAC symposium: modelling and control in biomedical systems*, University of Warwick, UK, 23–26 March.

Barrett MP (2010) Potential new drugs for human African trypanosomiasis: some progress at last. *Curr Opin Infect Dis* **23**:603-608.

Berry LM, Roberts J, Be X, Zhao Z and Lin MH (2010) Prediction of V(ss) from in vitro tissue-binding studies. *Drug Metab Dispos* **38**:115-121.

Boykin DW, Kumar A, Hall JE, Bender BC and Tidwell RR (1996) Anti-*Pneumocystis carinii* activity of bis-amidoximes and bis-*O*-alkylamidoxime prodrugs. *Bioorg Med Chem* **6**:3017-3020.

Brown RP, Delp MD, Lindstedt SL, Rhomberg LR and Beliles RP (1997) Physiological parameter values for physiologically based pharmacokinetic models. *Toxicol Ind Health* **13**:407-484.

Generaux CN (2010) Effects of Parasitic Infection on the Pharmacokinetics and Disposition of Pentamidine Ananalogs. PhD thesis, in *UNC Eshelman School of Pharmacy*, University of North Carolina, Chapel Hill.

Goldsmith RB (2011) Detection and mechanistic comparison of two anti-trypanosomal diamidines in a rat renal model. PhD thesis, in *School of Medicine* University of North Carolina, Chapel Hill.

Ismail MA, Batista-Parra A, Miao Y, Wilson WD, Wenzler T, Brun R and Boykin DW (2005) Dicationic near-linear biphenyl benzimidazole derivatives as DNA-targeted antiprotozoal agents. *Bioorg Med Chem* **13**:6718-6726.

Ito K and Houston JB (2004) Comparison of the use of liver models for predicting drug clearance using in vitro kinetic data from hepatic microsomes and isolated hepatocytes. *Pharm Res* **21**:785-792.

Ito K and Houston JB (2005) Prediction of human drug clearance from in vitro and preclinical data using physiologically based and empirical approaches. *Pharm Res* **22**:103-112.

Lalonde RL, Kowalski KG, Hutmacher MM, Ewy W, Nichols DJ, Milligan PA, Corrigan BW, Lockwood PA, Marshall SA, Benincosa LJ, Tensfeldt TG, Parivar K, Amantea M, Glue P, Koide H and Miller R (2007) Model-based drug development. *Clin Pharmacol Ther* **82**:21-32.

Lave T, Dupin S, Schmitt C, Chou RC, Jaeck D and Coassolo P (1997) Integration of in vitro data into allometric scaling to predict hepatic metabolic clearance in man: application to 10 extensively metabolized drugs. *J Pharm Sci* **86**:584-590.

Lave T, Portmann R, Schenker G, Gianni A, Guenzi A, Girometta MA and Schmitt M (1999) Interspecies pharmacokinetic comparisons and allometric scaling of napsagatran, a low molecular weight thrombin inhibitor. *J Pharm Pharmacol* **51**:85-91.

Lin JH (1998) Applications and limitations of interspecies scaling and in vitro extrapolation in pharmacokinetics. *Drug Metab Dispos* **26**:1202-1212.

Luttringer O, Theil FP, Poulin P, Schmitt-Hoffmann AH, Guentert TW and Lave T (2003) Physiologically based pharmacokinetic (PBPK) modeling of disposition of epiroprim in humans. *J Pharm Sci* **92**:1990-2007.

Mdachi RE, Thuita JK, Kagira JM, Ngotho JM, Murilla GA, Ndung'u JM, Tidwell RR, Hall JE and Brun R (2009) Efficacy of the novel diamidine compound 2,5-Bis(4-amidinophenyl)- furan-bis-O-Methlylamidoxime (Pafuramidine, DB289) against Trypanosoma brucei rhodesiense infection in vervet monkeys after oral administration. *Antimicrob Agents Chemother* **53**:953-957.

Midgley I, Fitzpatrick K, Taylor LM, Houchen TL, Henderson SJ, Wright SJ, Cybulski ZR, John BA, McBurney A, Boykin DW and Trendler KL (2007) Pharmacokinetics and metabolism of the prodrug DB289 (2,5-bis[4-(N-methoxyamidino)phenyl]furan monomaleate) in rat and monkey and its conversion to the antiprotozoal/antifungal drug DB75 (2,5-bis(4-guanylphenyl)furan dihydrochloride). *Drug Metab Dispos* **35**:955-967.

Nong A, Tan YM, Krolski ME, Wang J, Lunchick C, Conolly RB and Clewell HJ, 3rd (2008) Bayesian calibration of a physiologically based pharmacokinetic/pharmacodynamic model of carbaryl cholinesterase inhibition. *J Toxicol Environ Health A* **71**:1363-1381.

Olson CA (2008) ^{14}C Pafuramidine Maleate Absorption, Metabolism and Excretion in Healthy Men after a Single Oral Dose – a Summary of the Plasma Pharmacokinetics, Excretion and Metabolism Data in, Immtech Pharmaceuticals, Inc.

Paine MF, Wang MZ, Generaux CN, Boykin DW, Wilson WD, De Koning HP, Olson CA, Pohlig G, Burri C, Brun R, Murilla GA, Thuita JK, Barrett MP and Tidwell RR (2010) Diamidines for human African trypanosomiasis. *Curr Opin Investig Drugs* **11**:876-883.

Pang KS, Morris ME and Sun H (2008) Formed and preformed metabolites: facts and comparisons. *J Pharm Pharmacol* **60**:1247-1275.

Rowland M, Balant L and Peck C (2004) Physiologically based pharmacokinetics in drug development and regulatory science: a workshop report (Georgetown University, Washington, DC, May 29-30, 2002). *AAPS PharmSci* **6**:E6.

Saulter JY, Kurian JR, Trepanier LA, Tidwell RR, Bridges AS, Boykin DW, Stephens CE, Anbazhagan M and Hall JE (2005) Unusual dehydroxylation of antimicrobial amidoxime prodrugs by cytochrome b5 and NADH cytochrome b5 reductase. *Drug Metab Dispos* **33**:1886-1893.

Swift B, Pfeifer ND and Brouwer KLR (2009) Sandwich-cultured hepatocytes: an in vitro model to evaluate hepatobiliary transporter-based drug interactions and hepatotoxicity. *Drug Metab Rev* **42**:446-471.

Turncliff RZ, Hoffmaster KA, Kalvass JC, Pollack GM and Brouwer KLR (2006) Hepatobiliary disposition of a drug/metabolite pair: Comprehensive pharmacokinetic modeling in sandwich-cultured rat hepatocytes. *J Pharmacol Exp Ther* **318**:881-889.

Wang MZ, Saulter JY, Usuki E, Cheung YL, Hall M, Bridges AS, Loewen G, Parkinson OT, Stephens CE, Allen JL, Zeldin DC, Boykin DW, Tidwell RR, Parkinson A, Paine MF and Hall JE (2006) CYP4F enzymes are the major enzymes in human liver microsomes that catalyze the O-demethylation of the antiparasitic prodrug DB289 [2,5-bis(4-amidinophenyl)furan-bis-O-methylamidoxime]. *Drug Metab Dispos* **34**:1985-1994.

Wang MZ, Wu JQ, Bridges AS, Zeldin DC, Kornbluth S, Tidwell RR, Hall JE and Paine MF (2007) Human enteric microsomal CYP4F enzymes O-demethylate the antiparasitic prodrug pafuramidine. *Drug Metab Dispos* **35**:2067-2075.

Wenzler T, Boykin DW, Ismail MA, Hall JE, Tidwell RR and Brun R (2009) New treatment option for second-stage African sleeping sickness: in vitro and in vivo efficacy of aza analogs of DB289. *Antimicrob Agents Chemother* **53**:4185-4192.

Wu CY and Benet LZ (2005) Predicting drug disposition via application of BCS: transport/absorption/ elimination interplay and development of a biopharmaceutics drug disposition classification system. *Pharm Res* **22**:11-23.

Yan GZ, Brouwer KLR, Pollack GM, Wang MZ, Tidwell RR, Hall JE and Paine MF (2011) Mechanisms Underlying Differences in Systemic Exposure of Structurally Similar Active Metabolites: Comparison of Two Preclinical Hepatic Models
J Pharmacol Exp Ther **In press**.

Zhou L, Lee K, Thakker DR, Boykin DW, Tidwell RR and Hall JE (2002) Enhanced permeability of the antimicrobial agent 2,5-bis(4-amidinophenyl)furan across Caco-2 cell monolayers via its methylamidoidme prodrug. *Pharm Res* **19**:1689-1695.

Zhou L, Thakker DR, Voyksner RD, Anbazhagan M, Boykin DW, Hall JE and Tidwell RR (2004) Metabolites of an orally active antimicrobial prodrug, 2,5-bis(4-amidinophenyl)furan-bis-O-methylamidoxime, identified by liquid chromatography/tandem mass spectrometry. *J Mass Spectrom* **39**:351-360.

CHAPTER 5

CONCLUSIONS

A. SUMMARY AND DISCUSSION

An important objective in drug development is to identify the concentration/exposure range that provides the optimal benefit-to-risk ratio. An inadequate dose will result in ineffective therapy; an excessive dose will lead to unacceptable toxicity, which may prevent further development of a promising drug candidate. The clinical response (pharmacological and toxic effects) is a function of the dose. Thus, selection of appropriate dosage regimens for clinical trials is the key to successful transition of preclinical drug candidates to clinical drug development (Reigner and Blesch, 2002). Accurate prediction of an efficacious and safe dose for humans relies on integration of pharmacokinetic/pharmacodynamic data from multiple sources, both in vitro and in vivo from animals and humans, using a variety of methods and approaches. For this reason, proper selection of validated preclinical models is imperative.

Human African trypanosomiasis (HAT), also called sleeping sickness, is a parasitic disease caused by *Trypanosoma brucei* species; the disease is endemic throughout tropical Africa (Barrett, 2010). Almost all of the current chemotherapies for treatment of both first (hemolymphatic infection) and second (central nervous system infection) stages of HAT were introduced more than half a century ago and require complicated treatment regimens via parenteral administration (Fairlamb, 2003). An orally-active agent with a convenient dosing regimen would be beneficial in resource-constrained areas of Africa.

Diamidine prodrugs have exhibited satisfactory oral activity against both stages of HAT (Paine et al., 2010). Pafuramidine and CPD-0868 are bis-*O*-methylamidoxime prodrugs of pentamidine analogs, furamidine and CPD-0801, respectively. To date, pafuramidine is the first and only orally-active agent that has entered clinical trials (phase I-III) for the treatment of first stage infection. However, during an expanded phase I safety study, transient elevation of liver transaminases was observed in 25% of subjects five days post completion of the dosage regimen of pafuramidine (100 mg twice daily for 14 days), which

placed pafuramidine program on clinical hold (http://www.immtechpharma.com/documents/news_022208.pdf) (Paine et al., 2010). Although pafuramidine is no longer under development, lessons learned from pafuramidine highlighted the need for an improved understanding of the dose-exposure relationship of these orally-active antiparasitic prodrugs. Preclinical studies showed that furamidine accumulated extensively in the liver and remained in this organ for a prolonged time following a single oral dose of pafuramidine; furamidine concentrations in plasma were lower by three orders of magnitude than those in the liver (Midgley et al., 2007). Both pafuramidine and furamidine were ineffective in a second stage (CNS) mouse model (Wenzler et al., 2009). Structural analogs of pafuramidine/furamidine were synthesized and screened in vitro and in vivo to identify clinical candidates for the treatment of second stage HAT. To date, the most potent analog is CPD-0868, a prodrug of CPD-0801. Despite the structural similarity, CPD-0868 demonstrated superior efficacy against second stage infection (Wenzler et al., 2009), and the systemic exposure of CPD-0801 was higher than that of furamidine in mice given the same dose of respective prodrug (Wu et al., 2007).

Prior to this dissertation research, the mechanism responsible for the large differences in tissue and plasma exposure of furamidine, the reason for the improved systemic exposure of CPD-0801 compared to furamidine, and the relationship between dose of pafuramdine and plasma or tissue exposure of furamidine were unknown. In addition, pafuramidine preclinical and clinical studies in pharmacokinetics, efficacy, and safety were carried out by different researchers from various laboratories and institutes within the Consortium for Parasitic Drug Development (CPDD). Given the large body of experimental data obtained from a variety of sources, there was no quantitative strategy for leveraging prior knowledge to inform the dose selection of antiparasitic prodrugs. These unaddressed but important questions and issues guided the direction of this dissertation project. A variety of in vitro, ex vivo, and in vivo models, together with comprehensive

pharmacokinetic modeling approaches were utilized to address the following objectives: 1) gain a mechanistic understanding of the overall disposition of these antiparasitic prodrugs and metabolites; 2) develop a quantitative strategy that allows preclinical data to be integrated and combined with historical information from clinical studies to predict the dose-plasma/exposure relationship in humans.

A.1. Characterization and Comparison of the Intestinal and Hepatobiliary Disposition of Pafuramidine and CPD-0868 and Derived Metabolites in Preclinical Models.

Using a well-established human intestine-derived absorption model, Caco-2 cell monolayers, absorption of pafuramidine and CPD-0868 through the intestinal epithelium was elucidated. In the absence of serum in the incubation medium, A→B and B→A translocation profiles of both pafuramidine and CPD-0868 were nearly superimposable (Fig. 2.3), corresponding permeability coefficients of both prodrugs in both directions of transport were not significantly different, and efflux ratios were near unity (Table 2.1). These observations indicated that both prodrugs cross the intestinal epithelium by passive diffusion, without involvement of efflux transporters, which was consistent with previous results with pafuramidine using a different Caco-2 cell source (Zhou et al., 2002).

To examine further the difference in the extent of absorption between the two prodrugs, the basolateral compartment (representing the blood side) was supplemented with 4% bovine serum albumin (BSA), to mimic plasma protein binding. Under this more physiologically-relevant condition, absorptive (A→B) permeability of pafuramidine increased greatly, whereas that of CPD-0868 remained unchanged (Table 2.1). As a consequence, the $P_{app,A\rightarrow B}$ values of both prodrugs become comparable (Table 2.1). These findings were consistent with published observations that the presence of BSA increased the absorptive permeability of only highly lipophilic (logP > 3.0) and extensively protein bound (f_u < 5%)

compounds (Aungst et al., 2000). Regardless of structural similarity, pafuramidine is more lipophilic than CPD-0868, as reflected by a 2-fold higher logP (4.0 versus 2.2) and 35-fold lower f_u in human plasma (0.2 versus 7%). The results from Chapter 2 suggested that plasma protein binding may have a much greater impact on pafuramidine absorption in vivo. In addition, comparable permeability coefficients of both prodrugs under "sink" conditions suggested that the extent of absorption between pafuramidine and CPD-0868 may be similar in vivo. Results presented in Chapter 2 further substantiated Caco-2 cells as a valuable screening tool to assess absorption properties of compounds across the intestinal epithelium, as well as emphasized the need of application of BSA in the basolateral compartment to evaluate more accurately the intestinal permeability of highly lipophilic compounds. Moreover, results from this study suggested that the enhanced systemic exposure of CPD-0801 compared to furamidine was not due to a higher intestinal permeability of the prodrug CPD-0868 compared to pafuramidine. The mechanisms underlying the difference in the systemic exposure of respective active metabolites were, therefore, investigated further in two well-established hepatic models, isolated perfused livers (IPLs) and sandwich-cultured hepatocytes (SCH) from rats, to characterize and compare the hepatic disposition of pafuramidine/CPD-0868 and derived metabolites.

In both rat IPLs and SCH, the disposition profiles of both prodrugs and respective derived metabolites were similar (Fig. 3.3 and 3.5), whereas the extent of formation and AUC of CPD-0801 in perfusate (IPLs) or medium (SCH) were consistently higher compared to furamidine (Fig. 3.4 and Table 3.3). Initial compartmental modeling showed that the net basolateral efflux (6-fold difference) played a more important role than metabolism (2-fold difference) in the enhanced perfusate/medium exposure of CPD-0801 compared to furamidine (Table 3.2, 3.3 and 3.5). In addition, both active metabolites accumulated in the liver and hepatocytes at substantially higher concentrations compared to perfusate and medium (Fig. 3.3 and 3.5). Nevertheless, in both IPL and SCH, CPD-0801 exhibited less

hepatic retention compared to furamidine, as reflected by the 5- to 6-fold lower liver-to-perfusate and hepatocyte-to-medium partition coefficients (Table 3.3), which substantiated SCH as a valuable in vitro tool to predict in vivo liver-to-plasma partitioning. Limited perfusate/medium exposure of both active metabolites, relative to liver, led to a subsequent investigation of the plasma/perfusate and liver binding properties of these compounds. The unbound fractions (f_u) of both active metabolites in the liver were much lower (≥24-fold) than those in the plasma and perfusate; f_u of CPD-0801 in the liver was >5-fold higher than that of furamidine (Table 3.3). Assuming that only unbound compound can translocate out of cells to the perfusate and bile, liver f_u was, therefore, incorporated into the model (scheme displayed in Fig. 3.2B), which resulted in comparable rate constants associated with the net basolateral efflux of unbound active metabolites. These results provided further evidence that the enhanced perfusate/medium exposure of CPD-0801 was attributed largely to the 5-fold lower hepatic binding compared to furamidine.

The integrated approach involving two rat hepatic systems (IPLs and SCH) and pharmacokinetic modeling provided an improved mechanistic understanding of the impact of hepatic binding on the systemic and hepatobiliary exposure of these two antiparasitic active metabolites. A higher extent of formation and lower hepatic binding of CPD-0801, compared to furamidine (Table 3.3), at least in part, explained the enhanced systemic exposure of CPD-0801 (≥2-fold) observed in vivo. In addition, a ~2-fold higher f_u in plasma (Table 3.3) can result in a further increase (~4-fold) in the systemic exposure of unbound CPD-0801 compared to furamidine. Assuming only unbound compound can cross the blood brain barrier and both active metabolites have the similar membrane permeability, a higher systemic exposure of unbound CPD-0801 could lead to an increased brain exposure (~4-fold) compared to furamidine. Tissue binding studies showed that CPD-0801 has a consistently higher f_u (≥5-fold) in both liver and kidney than furamidine (Goldsmith, 2011; Yan et al., 2011). If the similar trend holds in brain, a much greater (≥one order of magnitude)

brain exposure of unbound CPD-0801 can be expected. In vitro studies showed that CPD-0801 and furamidine had similar trypanocidal potency (Wenzler et al., 2009). Assuming that only unbound compound can be taken up by the parasites and both active metabolites have similar uptake properties, higher unbound concentrations of CPD-0801 in the brain could lead to an enhanced antitrypanosomal effect in the CNS. The insights gained from this study not only supported CPD-0868 as a hopeful orally-active agent for treatment of second stage HAT, but also substantiated SCH as a useful tool to study hepatobiliary disposition of xenobiotics in preclinical species, and highlighted the potential application of this hepatic model in human studies.

A.2. Prediction of the Dose-Exposure Relationship via Semi-PBPK Modeling

PBPK modeling takes into account the physiologic, metabolic, and chemical-specific parameters to simulate quantitatively the absorption, distribution, metabolism, and excretion of a compound under different dosing scenarios (Poulin and Theil, 2002). For this reason, a systematic strategy combining preclinical/clinical data and semi-PBPK modeling was developed to improve the understanding of the relationship between prodrug dose and plasma/tissue exposure of active metabolite using pafuramidine/furamidine as model compounds (Chapter 4). Because a large body of in vitro and in vivo data on pafuramidine and furamidine disposition was available for rats, the model strategy began with development of a whole-body rat semi-PBPK model. The liver is a major site of furamidine formation/accumulation in rats. Thus, a whole-liver semi-PBPK model (scheme depicted in Fig. 4.1A) was developed first using the data generated from the rat IPL study (Yan et al., 2011) to estimate parameters associated with the hepatic disposition of pafuramidine/furamidine in rats. The whole-body rat semi-PBPK model (scheme depicted in Fig. 4.1B) was developed based on the liver model, with addition of major organs of absorption, storage, and elimination for pafuramidine/furamidine. In vivo rat pharmacokinetic

data generated in a previous study (Generaux, 2010) were utilized to validate and refine the model structure and to optimize associated parameters.

The whole-body rat semi-PBPK model adequately described the disposition of pafuramidine and furamidine in the plasma (Fig. 4.3A), and predicted furamidine disposition in key organs (liver and kidney) and excretion profiles (biliary and renal) (Fig. 4.3B). Consistent with in vivo results (Midgley et al., 2007; Generaux, 2010), predicted furamidine exposure in liver and kidney was much higher than that in plasma by 2-3 orders of magnitude (Fig. 4.3A and 4.3B); furamidine was cleared predominately by biliary excretion, accounting for >90% of the total excreted, whereas renal excretion played a minor role in furamidine elimination (<10%) (Table 4.3 and Fig. 4.3B).

Upon development of the rat model, efforts focused on building a whole-body human semi-PBPK model. Without prior knowledge of pafuramidine/furamidine disposition in humans, the same model structure and pafuramidine absorption properties (f_a and k_a) for rats were applied initially to the human model. However, model predictions underestimated both T_{max} and C_{max} of pafuramidine in humans, which may be attributed to the differences in the dosage form of pafuramidine (suspension versus capsule), and concomitant diet (regular versus high fat meal) between rats and humans. Pafuramidine is a poorly water-soluble compound, for this reason, the dosage forms used in the animal studies were often prepared as a suspension in DMSO or acidified ethanol containing Tween 80 (Midgley et al., 2007; Wenzler et al., 2009). The capsules used in human studies may delay the absorption of pafuramidine while passing through the intestine due to dissolution from the dosage form, causing an increased T_{max}. It has been well documented that food and gastrointestinal (GI) motility can affect drug absorption (Welling, 1977; Evans, 2000; Jamei et al., 2009). As such, patient instructions for drug administration often include a direction to either take with food or on an empty stomach. Previous studies showed that food can delay gastric emptying and therefore delays absorption of antimicrobial agents, tetracyclines and penicillins (Welling

and Tse, 1982). The extent of absorption of poorly water-soluble but highly lipophilic antimicrobial agents, such as spironotactone and griseofulvin, was enhanced when administered together with a fat-containing meal as compared to with water or in the fasting state (Palma et al., 1986). Based on these results, the concomitant high-fat meal also could have a significant impact on the rate and extent of absorption of the highly lipophilic antiparasitic agent, pafuramidine.

To account for the formulation and food effect on the absorption of pafuramidine in humans, a three transit compartments were added sequentially between site of administration (oral route) and absorption (gut) into the pafuramidine human submodel (Fig. 4.1B), which could represent dissolution from the capsule, gastric emptying, and/or partitioning from the fat components of accompanying meal. Model predictions showed that addition of these compartments was adequate to describe the delayed appearance of both pafuramidine and furamidine in the plasma (Fig. 4.4A). Consistent with previous observations on the other lipophilic antimicrobial agents, f_a of pafuramidine predicted by the semi-PBPK model was near 100% in humans, which was much higher than that in rats (~30%). These results highlighted the importance of formulation/diet in the disposition of these antiparasitic prodrugs and active metabolites.

The disposition profiles of pafuramidine/furamidine in SCH from rats and humans were similar between these two species. However, pafuramidine was metabolized in human SCH more quickly than in rat SCH, as reflected by a 3-fold higher intrinsic clearance (Table 4.2) and faster appearance of furamidine in the hepatocytes (Fig. 4.2). The rate constant associated with reuptake of furamidine in human SCH was 25% lower than that in rat SCH (Table 4.2), which resulted in a decreased hepatocyte-to-medium partitioning of furamidine (Fig. 4.2). These observations suggested a species difference in the hepatic disposition of pafuramidine/furamidine between rats and humans. Traditionally, human clearance values have been predicted using empirical allometric scaling and physiologically-based direct

scaling from in vitro-derived intrinsic clearance values (Ito and Houston, 2004; Jones et al., 2006). Allometric scaling, which is empirical in nature, fails to account for differences in pharmacokinetics across species (Mahmood, 2000). Physiologically-based direct scaling from in vitro-derived intrinsic clearance values offers a more physiological rationale by incorporating blood flow and plasma protein binding, however, this method relies on an assumption of liver models (well-stirred, parallel tube, and/or dispersion) selected in the scaling process to relate the clearances obtained in vitro to in vivo conditions (Ito and Houston, 2004; Ito and Houston, 2005). In addition, scaling directly from in vitro derived metabolic clearance often underestimates in vivo values due to decreased enzyme activity associated with the in vitro systems (Ito and Houston, 2005). To balance between these two methods, normalized scaling, rat clearance determined from IPL data corrected with in vitro derived scaling factors, was utilized to account for species differences in the hepatic disposition of pafuramidine/furamidine between rats and humans (Fig. 4.2 and Table 4.2). To authors' knowledge, prior to this dissertation project, there have been no reports utilizing this approach to extrapolate metabolic and transport clearance values for both parent and metabolites from rats to humans. SCH offer significant advantages over conventionally-cultured hepatocytes, including the ability to characterize both metabolic and sinusoidal/biliary transport processes in a single cellular system (Turncliff et al., 2006; Swift et al., 2009), and in particular, the ability to predict the biliary clearance ($Cl_{biliary}$) in humans, which remains a challenge in drug development (Abe et al., 2008). The biliary clearance of furamidine was too low to measure in rat and human SCH (Table 4.2); however, for compounds that exhibit large interspecies differences in biliary excretion, scaling of rat in vivo $Cl_{biliary}$ corrected by a scaling factor derived from rat and human SCH could be utilized for interspecies extrapolation of $Cl_{biliary}$.

Insights from the rat and human semi-PBPK models revealed two major findings: 1) the gut may play an important role in pre-systemic furamidine formation. The contribution of

the GI tract to the first-pass metabolism of pafuramidine, and the overall formation of furamidine, has not been characterized extensively. To date, only one report showed that the intrinsic formation clearance for the first intermediate metabolite (M1) from pafuramidine in human intestinal microsomes was at least 10-fold lower than that in human liver microsomes (Wang et al., 2007). PBPK models, for the first time, predicted that the intestine may contribute 30-40% of total furamidine formation from pafuramidine in both rats and humans. Corresponding confirmation experiments using appropriate intestinal models are warranted and represent a major focus for future studies. 2) The "true" terminal half-life of furamidine may be days, rather than hours (Fig. 4.3A and 4.4A). The terminal half-life of compounds is an important factor that determines the frequency of dosage regimens. However, due to the limitation of analytical assays, plasma concentrations of furamidine were not measurable 12 and 24 hours post oral administration of pafuramidine in rats and humans, respectively. Thus, previous studies failed to identify the "true" elimination phase of furamidine, resulting in an underestimation of the "true" terminal half-life ($t_{1/2,terminal}$). The semi-PBPK model-predicted plasma $t_{1/2,terminal}$ was verified further based on the measured tissue (kidney) $t_{1/2,terminal}$ in rats following IV administration of preformed furamidine, assuming the pharmacokinetic behavior did not differ between preformed and generated furamidine. The approach demonstrated the ability of PBPK modeling to predict drug disposition in plasma and tissue over a prolonged period of time without conducting the actual long-term in vivo experiments.

Previous studies showed that the exposure time may contribute to the more pronounced inhibitory effect of another diamidine, pentamidine, against *T. b. gambiense* in vivo, whereas peak concentrations (C_{max}) of short duration may be less important (Miezan et al., 1994). As a pentamidine analog, furamidine may exhibit the antiparasitic effect in a similar time-dependent manner. The mechanism of pafuramidine-induced transiently elevated hepatic transaminases in humans is not known. If hepatic accumulation of

furamidine is the cause of this adverse effect, the elevated hepatic signals could be either concentration- or time-dependent, or a combination of both. Based on these assumptions, the following criteria were utilized in the dose selection for pafuramidine: 1) plasma concentrations of furamidine must be above a hypothetical therapeutic index ($C_{eff,min}$) >80% of the time throughout the dosing period (14 days); 2) average steady-state concentrations ($C_{ss,ave}$) of furamidine must be below a hypothetical safety index (NOAEL). Hepatic exposure of furamidine was estimated by the human PBPK model and compared with the dosage regimen of 100 mg twice daily used in the expanded safety study. Accordingly, a modified dosage regimen of pafuramidine, 40 mg once daily, was predicted via model simulations of plasma and tissue concentration-time profiles of furamidine (Fig. 4.5). With this alternative daily regimen, plasma concentrations of furamidine could be maintained within the pre-defined hypothetical therapeutic-safety window while the hepatic exposure of furamidine was reduced by ~5-fold.

In rats infected with *T. b. brucei*, furamidine systemic exposure increased markedly (up to 3-fold) compared to control animals administered the same oral dose of pafuramidine (Generaux, 2010). Simulations based on the IPL compartmental model described in Chapter 3 (scheme depicted in Fig. 3.2B) showed that the perfusate exposure of furamidine was most sensitive to the rate constant associated with net basolateral efflux (a combination effect of basolateral uptake and efflux) and liver f_u. Furamidine is a potent substrate for an uptake transporter, human OCT1, which is localized primarily on the sinusoidal membrane of hepatocytes (Ming et al., 2009). Nitric oxide, an inflammatory mediator of immunity, can down-regulate OCT1 expression during inflammation and infection (Heemskerk et al., 2008). Compromised activity of OCT1 could decrease the reuptake of furamidine after excretion from liver to blood, hence, increase systemic exposure of furamidine. As shown in Chapter 3, furamidine was highly bound to liver tissues from rats, as reflected by a much lower f_u compared to plasma (Table 3.3). Based on model simulations, perturbation in tissue binding

that leads to a higher f_u of furamidine in the liver can cause a proportional increase in systemic exposure. Whether infection can decrease the binding capacity of furamidine in the liver currently is unknown. However, with the aid of the developed tissue/plasma binding assay in this dissertation project, this issue can be addressed by measuring the f_u in the liver from the infected animals and comparing with that from control animals (Table 3.3). Whether trypanosomal infection can alter the pharmacokinetics of pafuramidine/furamidine in humans remains unclear. If infection causes a similar effect on the systemic exposure of furamidine in humans, a further reduction in the amount and/or frequency of pafuramidine based on healthy individuals may be needed for infected patients.

Significance: This dissertation project, via a quantitative integration of preclinical/clinical data with pharmacokinetic modeling/simulation, addressed key issues regarding the pharmacokinetics (including the absorption, metabolism, transport, plasma/tissue binding, biliary/renal excretion profiles) and the dose-exposure relationship of antiparasitic prodrugs and active metabolites. Future directions will include using these multifaceted tools and models, coupled with pharmacokinetic modeling/simulation, to predict the disposition profiles, and guide dose-ranging studies in humans for next-in-class compounds for oral treatment of HAT.

B. FUTURE DIRECTIONS

B.1. Characterize the Intracellular localization of Active Metabolites in the Liver

As noted in the current studies, extensive and prolonged hepatic accumulation of active metabolites, furamidine and CPD-0801, was observed in both IPLs and SCH from rats. Previous studies using centrifugal fractionation showed that furamidine was mainly localized in the mitochondrial fraction (Midgley et al., 2007). In the rat IPL study, subcellular fractions of liver homogenates (n=1 liver/compound) were collected using a differential centrifugation method described previously (Studenberg and Brouwer, 1993). Consistent with in vivo observations, furamidine was localized primarily in the mitochondrial fraction (43%) in rat IPLs; in contrast, CPD-0801 was localized primarily in the cytosolic fraction (45%), with negligible mitochondrial accumulation ($\leqslant$1%) (Fig. 5.1). These observations suggested that the active metabolite formed inside the hepatocyte may not reside in a single homogeneous compartment, but may bind to certain intracellular compartments; moreover, the difference in intracellular localization could provide a potential mechanism for differences in the hepatobiliary disposition as well as hepatotoxic potential of these active metabolites.

The subcellular localization of active metabolites showed in Fig. 5.1 was only based on one liver per compound. The reproducibility of these findings needs to be verified in future studies. It is worth noting that there are several concerns associated with the fractionation approach including: *a) some degree of cross-contamination among isolated cellular fractions.* Therefore, activity/content of specific organelle markers will need to be assessed to define the exact composition and purity of each fraction, i.e., ethidium bromide binding (nucleus) assays, marker enzymes of the main organelles, namely, lactate dehydrogenase (cytosol), inosine 5'-diphosphatase (plasma and endoplasmic reticulum membranes) and succinate dehydrogenase (mitochondria). If contamination is severe in

target organelles (e.g. mitochondria), alternative fractionation strategies will need to be employed: e.g. subfractionation of cytoplasmic organelles by isopycnic centrifugation in a sucrose gradient (Duvvuri et al., 2004); *b) potential disruption of binding equilibrium between cellular compartments during fractionation procedures.* This problem will be more evident for drugs that partition into cellular spaces and compartments is primarily via passive diffusion driven by the concentration gradient (Duvvuri et al., 2004). The cationic and hydrophilic properties of furamidine/CPD-0801, together with in vivo evidence of extensive and prolonged accumulation in cellular organelles, suggests that these active metabolites may bind to intracellular compartments with high affinity, therefore, the potential diffusion between cellular fractions during isolation would be expected to be negligible.

These diamidine active metabolites are fluorescent compounds, which allows for monitoring of the hepatocellular trafficking by fluorescence microscopy. One advantage of SCH is that intracellular disposition of fluorescent substrates can be examined by confocal imaging (Bow et al., 2008). The experimental procedure is proposed as following: freshly isolated rat hepatocytes will be seeded onto collagen-coated 35-mm glass-bottomed culture dishes and cultured as described in Chapter 3. On day-4, cells will be incubated with either pafuramidine or CPD-0868 (10 μM) over 24 h. The real-time intracellular distribution of active metabolites will be imaged with a laser scanning confocal microscope at excitation and emission wavelengths of 359 nm and 461 nm, respectively. Using confocal imaging with SCH, the dynamic intracellular disposition of fluorescent active metabolites can be visualized, which will provide further evidence supporting the results from subcellular fractionation study. Furthermore, confocal imaging together with fractionation studies will improve our ability to investigate how changes in drug structure influence drug distribution within cellular compartments. An understanding of these structure-distribution relationships could lead to novel drug design for the treatment of HAT.

B.2. Identify Transport Protein(s) Involved in the Hepatobiliary Disposition of Furamidine

Once formed in the liver, furamidine needs to be excreted to the systemic circulation for antiparasitic effect and to the bile for elimination. Given the cationic and hydrophilic nature, it is likely that active transporters are involved in the translocation of furamidine from hepatocytes to the blood and bile. Pharmacokinetic modeling in both rat IPLs and SCH showed that the rate constant for basolateral reuptake were much higher that that for basolateral efflux, albeit the large variability associated with the parameter estimates (Fig. 3.2 and 3.5), indicating that reuptake predominated over efflux in governing the basolateral transport of furamidine. Previous studies using stably-transfected Chinese hamster ovary (CHO) cells demonstrated that furamidine is a good substrate for human OCT1 (Ming et al., 2009). OCT1, an uptake transporter localized mainly on the sinusoidal membrane of hepatocytes, could be involved in the basolateral reuptake of furamidine in humans. To date, little is known with regards to transporters involved in the basolateral and canalicular efflux of furamidine in the liver. Previous studies with Caco-2 cells showed that the efflux ratio of furamidine was 2.25, suggesting that furamidine may be a substrate for an efflux pump (e.g., P-gp) on the apical membrane of Caco-2 cells (Zhou et al., 2002). Ranitidine, also a cationic hydrophilic compound, was shown to be a substrate for P-gp and OCT1 (Bourdet et al., 2005; Bourdet et al., 2006). Pentamidine, a structural analog of furamidine, demonstrated a significantly higher (up to 3-fold) brain exposure in P-gp knockout mice compared to control animals (Sanderson et al., 2009). In the same study, coadministration of indomethacin, an inhibitor of MRP, increased pentamidine accumulation in choroid plexus of P-gp knockout mice; coadministration of adenosine, a nucleoside analog and a substrate for concentrative/ equilibrative nucleoside transporters (CNT and ENT) and MRP4/5 (Schuetz et al., 1999; Wijnholds et al., 2000; Molina-Arcas et al., 2009), also caused the similar effect (Sanderson et al., 2009). Previous studies showed that ENTs, but not CNTs, were expressed on the

basolateral membrane of human hepatocytes (Molina-Arcas et al., 2009; Fukuchi et al., 2010), indicating that CNTs are unlikely to be involved in the furamidine uptake into hepatocytes. 4',6-diamidino-2-phenylindole (DAPI), another furamidine analog, was shown to be a substrate for hOCT1 and multidrug and toxin extrusion protein 1 (MATE1), which is an efflux transporter expressed mainly on the canalicular membrane of hepatocytes and the brush border of the renal epithelium (Yasujima et al., 2010). These candidate transporters could be responsible for the basolateral (MRP4/5, OCT1, and ENT) and canalicular (P-gp and MATE1) transport of furamidine in the liver. Future studies on identification of the role of these transporters in the hepatobiliary disposition of furamidine are warranted. Appropriate in vitro and in vivo models include, but are not limited to: stably-transfected cell lines (e.g., CHO), membrane vesicles, isolated perfused rat livers (in the presence or absence of inhibitors), and P-gp/MRP knockout animals.

B.3. Characterize First-Pass Metabolism of Prodrugs in the Gut

The PBPK modeling study (Chapter 4) suggested that the gut may contribute significantly (30-40%) to furamidine formation in rats and humans following oral administration of pafuramidine (Table 4.3). These observations lead to a re-evaluation of the role of gut in the observed difference in the systemic exposure of furamidine and CPD-0801. Like liver, CPD-0801 may have a greater extent of formation during prodrug (CPD-0868) absorption in the gut compared to furamidine, which also could contribute to the enhanced systemic exposure of CPD-0801. Additional experiments would be needed to elucidate the differential role of the gut and liver in the first-pass metabolism of these prodrugs, and the overall formation of respective active metabolites.

Previous studies showed that formation of a furamidine analog, CPD-0801, was negligible when the prodrug, CPD-0868, was incubated with liver microsomes, whereas CPD-0801 was detected readily in hepatocytes from both rats and humans (Generaux,

2010). In the current study (Chapter 3 and 4), both pafuramidine and CPD-0868 were biotransformed efficiently to the respective active metabolites, furamidine and CPD-0801, in rat and human SCH (Fig. 3.5 and Fig. 4.2). Phenotyping studies showed that biotransformation of pafuramidine/CPD-0868 to furamidine/CPD-0801 requires two enzyme systems: cytochrome P450s (CYP4F2/3B and possibly CYP3A4) and cytochrome b_5/NADH cytochrome b_5 reductases (Saulter et al., 2005; Wang et al., 2006). These reductases are essential in the final step of furamidine formation (Fig. 1.3) (Saulter et al., 2005). Cytochrome b_5/NADH cytochrome b_5 reductases are localized primarily in microsomes and other cellular organelles, including mitochondrial and cytosol (Saulter et al., 2005). In order to characterize the pre-systemic formation of furamidine and CPD-0801 in the gut, whole-cell systems would be required, such as, 1α,25-$(OH)_2$-D_3-treated Caco-2 cells, Ussing chambers, single-pass perfused intestine from rats, or portal vein-cannulated rats (Fisher et al., 1999; Sinko et al., 2004; Masaki et al., 2007; Pang et al., 2008; Clarke, 2009). General experimental procedures for selected in vitro and in vivo studies are proposed as following:

In 1α,25-$(OH)_2$-D_3-treated Caco-2 cells, midazolam, a probe substrate for CYP3A, showed similar absorption and metabolism characteristics as observed in vivo, which substantiated this modified Caco-2 cells as a suitable model system for studying drug absorption and first-pass intestinal metabolism (Fisher et al., 1999). For this reason, this modified system also could be useful to study the intestinal disposition of these antiparasitic prodrugs/active metabolites. Briefly, 1α,25-$(OH)_2$-D_3-treated Caco-2 cells will be incubated with pafuramidine or CPD-0868. At designated times, apical, cellular, and basolateral samples will be collected for quantification of prodrugs and active metabolites. A catenary model encompassing the apical, cellular, and basolateral compartments will be developed to quantitatively characterize and compare the distribution and intestinal metabolism of prodrugs/active metabolites (Fan et al., 2010).

For in vivo study, portal and jugular vein cannulated rats will be given a single dose of pafuramidine/CPD-0868 by oral gavage. Blood will be sampled via the portal and jugular vein cannulas at designated times over 24 h. Intestine and liver will be harvested and homogenized at the end of experiment. Plasma and tissue samples will be analyzed for prodrug and derived active metabolites by LC-MS/MS. For prodrugs, portal vein concentrations represent the amount of prodrug absorbed across the gut, while concentrations in the jugular vein represent the amount of systemically available prodrug. Thus, the difference represents the extent of first-pass metabolism of prodrug in the liver. For active metabolites, portal vein concentrations represent the amount of active metabolite formed during prodrug absorption and escaped from the gut, while concentrations in the jugular vein represent the total amount of active metabolite formed and escaped from both formation sites (gut and liver). Tissue concentrations present the amount of generated active metabolites sequestered in the gut and liver over 24 h. Results from this study will provide mechanistic information on the relative contribution of gut and liver to the overall formation of these active metabolites.

B.4. Determine the Therapeutic-Safety Index of the Active Metabolites Furamidine and CPD-0801

Due to the lack of knowledge regarding the dose-exposure relationships, the modified dosage regimen of pafuramidine (Chapter 4) was based on a hypothetical NOAEL (20% less than the $C_{ss,ave}$ achieved with the dosage regimen that caused transiently elevated liver transaminases in the clinical trial Fig 4.5). The mechanism of elevated hepatic signals and the relationship with the dose of pafuramidine currently are being investigated in rodent models. The study results will provide a qualitative or semi-quantitative description of site(s), severity, and reversibility of this adverse effect, as well as the dose threshold associated with the NOAEL where no overt adverse effects can be observed. Once this

maximal-tolerated dose is determined, the rat PBPK model developed in the current study (Chapter 4, scheme depicted in Fig. 4.1B) can be utilized to predict the corresponding $C_{ss,ave}$ of furamidine (NOAEL) via simulations, and hence, the safety margin of furamidine in rats. IC_{50} of furamidine against *T.b. brucei* strain was determined in the presence of 15% horse serum. Because the f_u of furamidine in this matrix was unknown, the therapeutic index, $C_{eff,min}$, was corrected by the f_u in perfusate (composed of 20% rat plasma) assuming the binding properties of furamidine were similar between the two matrices. In the future study, the f_u of furamidine in 15% horse serum will need to be determined using the binding assay developed in this dissertation project (Chapter 3) to refine further the therapeutic-safety window.

B.5. Apply the PBPK Model-based Strategy to Future Drug Development

Preclinical safety profiling is built on the assumption that similar drug exposures will result in similar preclinical and clinical outcomes. However, species-specific adverse events may not be realized until the results of preclinical and clinical studies are compared (Reigner and Blesch, 2002). Results from the expanded phase I safety study suggested that humans may be more sensitive to pafuramidine-induced elevated hepatic signals than rats and/or monkeys. As such, the human equivalent dose for safety will be considered to be the dose that leads to furamidine $C_{ss,ave}$ similar to the NOAEL in rats corrected by a "sensitivity" factor, which adjusts for anticipated differences in sensitivity to pafuramidine between rats and humans. Empirically, the maximum starting dose for the first-in-human study is the smallest of the following three doses: 1/10 of the NOAEL dose in rodents, 1/6 of the NOAEL dose in dogs, or 1/3 of the NOAEL dose in monkeys (Boxenbaum and DiLea, 1995; Mahmood, 2000). However, one rule cannot apply to all. A more rational and mechanistic approach is needed to determine the "sensitivity" factor in a compound-specific manner. Rat SCH have demonstrated success in prediction of the hepatotoxicity of trabectedin observed in vivo

using lactate dehydrogenase (LDH) as a biomarker (Lee et al., 2008). Similarly, differences in the LDH release measured in rat and human SCH could be utilized to estimate the "sensitivity" factor, and thus predict a safe dosage regimen for humans.

In conclusion, the PBPK models developed and the studies proposed in this dissertation project can facilitate development of the therapeutic-safety index for future drug candidates in the treatment of HAT. With the aid of PBPK modeling, preclinical/clinical data on pharmacokinetics, efficacy, and safety can be leveraged quantitatively to guide dose-ranging studies for next-in-class antiparasitic compounds. As new data from early clinical studies become available, the PBPK models can be updated and refined, and guide dose selection for later phase II/III trials, allowing for a more precise evaluation of toxicity and efficacy.

C. FIGURES

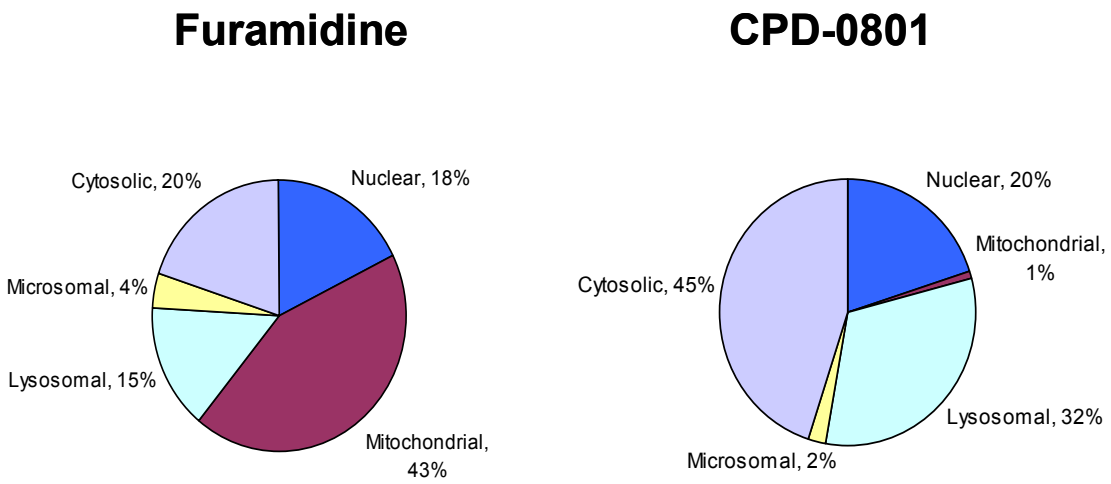

Figure 5.1. Subcellular localization of generated active metabolites, furamidine and CPD-0801, in rat isolated perfused livers. Prodrug, pafuramidine or CPD-0868 (10 μM) was administered as a bolus to the perfusion reservoir.

D. REFERENCES

Abe K, Bridges AS, Yue W and Brouwer KLR (2008) In vitro biliary clearance of angiotensin II receptor blockers and 3-hydroxy-3-methylglutaryl-coenzyme A reductase inhibitors in sandwich-cultured rat hepatocytes: comparison with in vivo biliary clearance. *J Pharmacol Exp Ther* **326**:983-990.

Andersen ME and Krishnan K (1994) Physiologically based pharmacokinetics and cancer risk assessment. *Environ Health Perspect* **102 Suppl 1**:103-108.

Annaert PP and Brouwer KL (2005) Assessment of drug interactions in hepatobiliary transport using rhodamine 123 in sandwich-cultured rat hepatocytes. *Drug Metab Dispos* **33**:388-394.

Ansede JH and Brouwer KR (2008) Transport of Naloxone Glucuronide in B-Clear (Sandwich-Cultured Rat Hepatocytes) and its Application as an In Vitro Model for Determining the Directional Transport of Metabolites, in *10th European ISSX Meeting*, Vienna, Austria.

Artursson P (1990) Epithelial transport of drugs in cell culture. I: A model for studying the passive diffusion of drugs over intestinal absorptive (Caco-2) cells. *J Pharm Sci* **79**:476-482.

Artursson P (1999) Cell cultures as models for drug absorption across the intestinal mucosa. *Crit Rev Ther Drug Carrier Syst.* **8**:305-330.

Artursson P and Karlsson J (1991) Correlation between oral drug absorption in humans and apparent drug permeability coefficients in human intestinal epithelial (Caco-2) cells. *Biochem Biophys Res Commun* **175**:880-885.

Artursson P, Palm K and Luthman K (2001) Caco-2 monolayers in experimental and theoretical predictions of drug transport. *Adv Drug Deliv Rev* **46**:27-43.

Aungst BJ, Nguyen NH, Bulgarelli JP and Oates-Lenz K (2000) The influence of donor and reservoir additives on Caco-2 permeability and secretory transport of HIV protease inhibitors and other lipophilic compounds. *Pharm Res* **17**:1175-1180.

Balimane PV, Chong S and Morrison RA (2000) Current methodologies used for evaluation of intestinal permeability and absorption. *J Pharmacol Toxicol Methods* **44**:301-312.

Barrett MP (2010) Potential new drugs for human African trypanosomiasis: some progress at last. *Curr Opin Infect Dis* **23**:603-608.

Barrett MP, Boykin DW, Brun R and Tidwell RR (2007) Human African trypanosomiasis: pharmacological re-engagement with a neglected disease. *Br J Pharmacol* **152**:1155-1171.

Barrett MP, Burchmore RJ, Stich A, Lazzari JO, Frasch AC, Cazzulo JJ and Krishna S (2003) The trypanosomiases. *Lancet* **362**:1469-1480.

Bjorkman S, Wada DR, Berling BM and Benoni G (2001) Prediction of the disposition of midazolam in surgical patients by a physiologically based pharmacokinetic model. *J Pharm Sci* **90**:1226-1241.

Boess F, Kamber M, Romer S, Gasser R, Muller D, Albertini S and Suter L (2003) Gene expression in two hepatic cell lines, cultured primary hepatocytes, and liver slices compared to the in vivo liver gene expression in rats: possible implications for toxicogenomics use of in vitro systems. *Toxicol Sci* **73**:386-402.

Bourdet DL, Pollack GM and Thakker DR (2006) Intestinal absorptive transport of the hydrophilic cation ranitidine: a kinetic modeling approach to elucidate the role of uptake and efflux transporters and paracellular vs. transcellular transport in Caco-2 cells. *Pharm Res* **23**:1178-1187.

Bourdet DL, Pritchard JB and Thakker DR (2005) Differential substrate and inhibitory activities of ranitidine and famotidine toward human organic cation transporter 1 (hOCT1; SLC22A1), hOCT2 (SLC22A2), and hOCT3 (SLC22A3). *J Pharmacol Exp Ther* **315**:1288-1297.

Bouteille B, Oukem O, Bisser S and Dumas M (2003) Treatment perspectives for human African trypanosomiasis. *Fundam Clin Pharmacol* **17**:171-181.

Bow DA, Perry JL, Miller DS, Pritchard JB and Brouwer KLR (2008) Localization of P-gp (Abcb1) and Mrp2 (Abcc2) in freshly isolated rat hepatocytes. *Drug Metab Dispos* **36**:198-202.

Boxenbaum H and DiLea C (1995) First-time-in-human dose selection: allometric thoughts and perspectives. *J Clin Pharmacol* **35**:957-966.

Boykin DW, Kumar A, Hall JE, Bender BC and Tidwell RR (1996) Anti-*Pneumocystis carinii* activity of bis-amidoximes and bis-*O*-alkylamidoxime prodrugs. *Bioorg Med Chem* **6**:3017-3020.

Brandon EF, Raap CD, Meijerman I, Beijnen JH and Schellens JH (2003) An update on in vitro test methods in human hepatic drug biotransformation research: pros and cons. *Toxicol Appl Pharmacol* **189**:233-246.

Brouwer KLR and Thurman RG (1996) Isolated perfused liver. *Pharm Biotechnol* **8**:161-192.

Brown RP, Delp MD, Lindstedt SL, Rhomberg LR and Beliles RP (1997) Physiological parameter values for physiologically based pharmacokinetic models. *Toxicol Ind Health* **13**:407-484.

Burri C, Nkunku S, Merolle A, Smith T, Blum J and Brun R (2000) Efficacy of new, concise schedule for melarsoprol in treatment of sleeping sickness caused by Trypanosoma brucei gambiense: a randomised trial. *Lancet* **355**:1419-1425.

Checchi F and Barrett MP (2008) African sleeping sickness. *Bmj* **336**:679-680.

Chiu WA, Barton HA, DeWoskin RS, Schlosser P, Thompson CM, Sonawane B, Lipscomb JC and Krishnan K (2007) Evaluation of physiologically based pharmacokinetic models for use in risk assessment. *J Appl Toxicol* **27**:218-237.

Chong S, Dando SA, Soucek KM and Morrison RA (1996) In vitro permeability through caco-2 cells is not quantitatively predictive of in vivo absorption for peptide-like drugs absorbed via the dipeptide transporter system. *Pharm Res* **13**:120-123.

Clarke LL (2009) A guide to Ussing chamber studies of mouse intestine. *Am J Physiol Gastrointest Liver Physiol* **296**:G1151-1166.

Cohen H, Chahine C, Hui A and Mukherji R (2004) Bosentan therapy for pulmonary arterial hypertension. *Am J Health Syst Pharm* **61**:1107-1119.

Collett A, Sims E, Walker D, He YL, Ayrton J, Rowland M and Warhurst G (1996) Comparison of HT29-18-C1 and Caco-2 cell lines as models for studying intestinal paracellular drug absorption. *Pharm Res* **13**:216-221.

DNDi (2009) *Human African trypanosomiasis: Target Product Profile (TPP).*

Dorlo TP and Kager PA (2008) Pentamidine dosage: a base/salt confusion. *PLoS Negl Trop Dis* **2**:e225.

Dressman JB and Reppas C (2000) In vitro-in vivo correlations for lipophilic, poorly water-soluble drugs. *Eur J Pharm Sci* **11 Suppl 2**:S73-80.

Dressman JB, Thelen K and Jantratid E (2008) Towards quantitative prediction of oral drug absorption. *Clin Pharmacokinet* **47**:655-667.

Dunn JC, Yarmush ML, Koebe HG and Tompkins RG (1989) Hepatocyte function and extracellular matrix geometry: long-term culture in a sandwich configuration. *Faseb J* **3**:174-177.

Duvvuri M, Feng W, Mathis A and Krise JP (2004) A cell fractionation approach for the quantitative analysis of subcellular drug disposition. *Pharm Res* **21**:26-32.

Evans AM (2000) Influence of dietary components on the gastrointestinal metabolism and transport of drugs. *Ther Drug Monit* **22**:131-136.

Evans MV, Dowd SM, Kenyon EM, Hughes MF and El-Masri HA (2008) A physiologically based pharmacokinetic model for intravenous and ingested dimethylarsinic acid in mice. *Toxicol Sci* **104**:250-260.

Fairlamb AH (2003) Chemotherapy of human African trypanosomiasis: current and future prospects. *Trends Parasitol* **19**:488-494.

Fan J, Liu S, Du Y, Morrison J, Shipman R and Pang KS (2009) Up-regulation of transporters and enzymes by the vitamin D receptor ligands, 1alpha,25-dihydroxyvitamin D3 and vitamin D analogs, in the Caco-2 cell monolayer. *J Pharmacol Exp Ther* **330**:389-402.

Fan J, Maeng HJ and Pang KS (2010) Interplay of transporters and enzymes in the Caco-2 cell monolayer: I. effect of altered apical secretion. *Biopharm Drug Dispos* **31**:215-227.

Fattinger K, Funk C, Pantze M, Weber C, Reichen J, Stieger B and Meier PJ (2001) The endothelin antagonist bosentan inhibits the canalicular bile salt export pump: a potential mechanism for hepatic adverse reactions. *Clin Pharmacol Ther* **69**:223-231.

Fisher JM, Wrighton SA, Watkins PB, Schmiedlin-Ren P, Calamia JC, Shen DD, Kunze KL and Thummel KE (1999) First-pass midazolam metabolism catalyzed by 1alpha,25-dihydroxy vitamin D3-modified Caco-2 cell monolayers. *J Pharmacol Exp Ther* **289**:1134-1142.

Fukuchi Y, Furihata T, Hashizume M, Iikura M and Chiba K (2010) Characterization of ribavirin uptake systems in human hepatocytes. *J Hepatol* **52**:486-492.

Generaux CN (2010) Effects of Parasitic Infection on the Pharmacokinetics and Disposition of Pentamidine Ananalogs. PhD thesis, in *UNC Eshelman School of Pharmacy*, University of North Carolina, Chapel Hill.

Germani M, Crivori P, Rocchetti M, Burton PS, Wilson AG, Smith ME and Poggesi I (2005) Evaluation of a physiologically-based pharmacokinetic approach for simulating the first-time-in-animal study. *Basic Clin Pharmacol Toxicol* **96**:254-256.

Germani M, Crivori P, Rocchetti M, Burton PS, Wilson AG, Smith ME and Poggesi I (2007) Evaluation of a basic physiologically based pharmacokinetic model for simulating the first-time-in-animal study. *Eur J Pharm Sci* **31**:190-201.

Goldsmith RB (2011) Detection and mechanistic comparison of two anti-trypanosomal diamidines in a rat renal model. PhD thesis, in *School of Medicine* University of North Carolina, Chapel Hill.

Gores GJ, Kost LJ and LaRusso NF (1986) The isolated perfused rat liver: conceptual and practical considerations. *Hepatology* **6**:511-517.

Heemskerk S, Wouterse AC, Russel FG and Masereeuw R (2008) Nitric oxide down-regulates the expression of organic cation transporters (OCT) 1 and 2 in rat kidney during endotoxemia. *Eur J Pharmacol* **584**:390-397.

Hewitt NJ, Lechon MJ, Houston JB, Hallifax D, Brown HS, Maurel P, Kenna JG, Gustavsson L, Lohmann C, Skonberg C, Guillouzo A, Tuschl G, Li AP, LeCluyse E, Groothuis GM and Hengstler JG (2007a) Primary hepatocytes: current understanding of the regulation of metabolic enzymes and transporter proteins, and pharmaceutical practice for the use of hepatocytes in metabolism, enzyme induction, transporter, clearance, and hepatotoxicity studies. *Drug Metab Rev* **39**:159-234.

Hewitt NJ, Lecluyse EL and Ferguson SS (2007b) Induction of hepatic cytochrome P450 enzymes: methods, mechanisms, recommendations, and in vitro-in vivo correlations. *Xenobiotica* **37**:1196-1224.

Hirohashi T, Suzuki H, Chu XY, Tamai I, Tsuji A and Sugiyama Y (2000) Function and expression of multidrug resistance-associated protein family in human colon adenocarcinoma cells (Caco-2). *J Pharmacol Exp Ther* **292**:265-270.

Hoen PA, Commandeur JN, Vermeulen NP, Van Berkel TJ and Bijsterbosch MK (2000) Selective induction of cytochrome P450 3A1 by dexamethasone in cultured rat hepatocytes: analysis with a novel reverse transcriptase-polymerase chain reaction assay section sign. *Biochem Pharmacol* **60**:1509-1518.

Hoffmaster KA, Zamek-Gliszczynski MJ, Pollack GM and Brouwer KL (2005) Multiple transport systems mediate the hepatic uptake and biliary excretion of the metabolically stable opioid peptide [D-penicillamine2,5]enkephalin. *Drug Metab Dispos* **33**:287-293.

Ismail MA and Boykin DW (2006) Synthesis of deuterium and ^{15}N-labelled 2,5-*Bis*[5-amidino-2-pyridyl]furan and 2,5-*Bis*[5-(methoxyamidino)-2-pyridyl]furan. *Journal of Labelled Compounds and Radiopharmaceuticals* **49**:985–996.

Ismail MA, Brun R, Easterbrook JD, Tanious FA, Wilson WD and Boykin DW (2003) Synthesis and antiprotozoal activity of aza-analogues of furamidine. *J Med Chem* **46**:4761-4769.

Ito K and Houston JB (2004) Comparison of the use of liver models for predicting drug clearance using in vitro kinetic data from hepatic microsomes and isolated hepatocytes. *Pharm Res* **21**:785-792.

Ito K and Houston JB (2005) Prediction of human drug clearance from in vitro and preclinical data using physiologically based and empirical approaches. *Pharm Res* **22**:103-112.

Jackson JP, Kabirov KK, Kapetanovic IM and Lyubimov A (2009) In vitro assessment of P450 induction potential of novel chemopreventive agents SR13668, 9-cis-UAB30, and pentamethychromanol in primary cultures of human hepatocytes. *Chem Biol Interact* **179**:263-272.

Jamei M, Turner D, Yang J, Neuhoff S, Polak S, Rostami-Hodjegan A and Tucker G (2009) Population-based mechanistic prediction of oral drug absorption. *Aaps J* **11**:225-237.

Jin R, Koop DR, Raucy JL and Lasker JM (1998) Role of human CYP4F2 in hepatic catabolism of the proinflammatory agent leukotriene B4. *Arch Biochem Biophys* **359**:89-98.

Jones HM, Parrott N, Jorga K and Lave T (2006) A novel strategy for physiologically based predictions of human pharmacokinetics. *Clin Pharmacokinet* **45**:511-542.

Keldenich J (2009) Measurement and prediction of oral absorption. *Chem Biodivers* **6**:2000-2013.

Kienhuis AS, Wortelboer HM, Maas WJ, van Herwijnen M, Kleinjans JC, van Delft JH and Stierum RH (2007) A sandwich-cultured rat hepatocyte system with increased metabolic competence evaluated by gene expression profiling. *Toxicol In Vitro* **21**:892-901.

Kobayashi D, Nozawa T, Imai K, Nezu J, Tsuji A and Tamai I (2003) Involvement of human organic anion transporting polypeptide OATP-B (SLC21A9) in pH-dependent transport across intestinal apical membrane. *J Pharmacol Exp Ther* **306**:703-708.

Kousba A and Sultatos LG (2002) Continuous system modeling of equilibrium dialysis for determinations of tissue partitioning of parathion and paraoxon. *Toxicol Lett* **133**:153-159.

Lalonde RL, Kowalski KG, Hutmacher MM, Ewy W, Nichols DJ, Milligan PA, Corrigan BW, Lockwood PA, Marshall SA, Benincosa LJ, Tensfeldt TG, Parivar K, Amantea M, Glue P, Koide H and Miller R (2007) Model-based drug development. *Clin Pharmacol Ther* **82**:21-32.

Lazarou J, Pomeranz BH and Corey PN (1998) Incidence of adverse drug reactions in hospitalized patients: a meta-analysis of prospective studies. *Jama* **279**:1200-1205.

LeCluyse EL (2001) Human hepatocyte culture systems for the in vitro evaluation of cytochrome P450 expression and regulation. *Eur J Pharm Sci* **13**:343-368.

LeCluyse EL, Audus KL and Hochman JH (1994) Formation of extensive canalicular networks by rat hepatocytes cultured in collagen-sandwich configuration. *Am J Physiol* **266**:C1764-1774.

Lee JK, Leslie EM, Zamek-Gliszczynski MJ and Brouwer KLR (2008) Modulation of trabectedin (ET-743) hepatobiliary disposition by multidrug resistance-associated proteins (Mrps) may prevent hepatotoxicity. *Toxicol Appl Pharmacol* **228**:17-23.

Lee JK, Marion TL, Abe K, Lim C, Pollock GM and Brouwer KLR (2010) Hepatobiliary disposition of troglitazone and metabolites in rat and human sandwich-cultured hepatocytes: use of Monte Carlo simulations to assess the impact of changes in biliary excretion on troglitazone sulfate accumulation. *J Pharmacol Exp Ther* **332**:26-34.

Lengyel G, Veres Z, Tugyi R, Vereczkey L, Molnar T, Glavinas H, Krajcsi P and Jemnitz K (2008) Modulation of sinusoidal and canalicular elimination of bilirubin-glucuronides by rifampicin and other cholestatic drugs in a sandwich culture of rat hepatocytes. *Hepatol Res* **38**:300-309.

Lennernas H (2007) Animal data: the contributions of the Ussing Chamber and perfusion systems to predicting human oral drug delivery in vivo. *Adv Drug Deliv Rev* **59**:1103-1120.

Leslie EM, Watkins PB, Kim RB and Brouwer KL (2007) Differential inhibition of rat and human Na+-dependent taurocholate cotransporting polypeptide (NTCP/SLC10A1)by bosentan: a mechanism for species differences in hepatotoxicity. *J Pharmacol Exp Ther* **321**:1170-1178.

Liao M, Raczynski AR, Chen M, Chuang BC, Zhu Q, Shipman R, Morrison J, Lee D, Lee FW, Balani SK and Xia CQ (2010) Inhibition of hepatic organic anion-transporting polypeptide by RNA interference in sandwich-cultured human hepatocytes: an in

vitro model to assess transporter-mediated drug-drug interactions. *Drug Metab Dispos* **38**:1612-1622.

Lin JH (1998) Applications and limitations of interspecies scaling and in vitro extrapolation in pharmacokinetics. *Drug Metab Dispos* **26**:1202-1212.

Lipscomb JC and Poet TS (2008) In vitro measurements of metabolism for application in pharmacokinetic modeling. *Pharmacol Ther* **118**:82-103.

Liu X, LeCluyse EL, Brouwer KR, Gan LS, Lemasters JJ, Stieger B, Meier PJ and Brouwer KLR (1999a) Biliary excretion in primary rat hepatocytes cultured in a collagen-sandwich configuration. *Am J Physiol* **277**:G12-21.

Liu X, LeCluyse EL, Brouwer KR, Lightfoot RM, Lee JI and Brouwer KLR (1999b) Use of Ca2+ modulation to evaluate biliary excretion in sandwich-cultured rat hepatocytes. *J Pharmacol Exp Ther* **289**:1592-1599.

Luttringer O, Theil FP, Poulin P, Schmitt-Hoffmann AH, Guentert TW and Lave T (2003) Physiologically based pharmacokinetic (PBPK) modeling of disposition of epiroprim in humans. *J Pharm Sci* **92**:1990-2007.

Mahmood I (2000) Critique of prospective allometric scaling: does the emperor have clothes? *J Clin Pharmacol* **40**:341-344; discussion 345-346.

Masaki K, Hashimoto M and Imai T (2007) Intestinal first-pass metabolism via carboxylesterase in rat jejunum and ileum. *Drug Metab Dispos* **35**:1089-1095.

Mdachi RE, Thuita JK, Kagira JM, Ngotho JM, Murilla GA, Ndung'u JM, Tidwell RR, Hall JE and Brun R (2009) Efficacy of the novel diamidine compound 2,5-Bis(4-amidinophenyl)- furan-bis-O-Methlylamidoxime (Pafuramidine, DB289) against Trypanosoma brucei rhodesiense infection in vervet monkeys after oral administration. *Antimicrob Agents Chemother* **53**:953-957.

Midgley I, Fitzpatrick K, Taylor LM, Houchen TL, Henderson SJ, Wright SJ, Cybulski ZR, John BA, McBurney A, Boykin DW and Trendler KL (2007) Pharmacokinetics and metabolism of the prodrug DB289 (2,5-bis[4-(N-methoxyamidino)phenyl]furan monomaleate) in rat and monkey and its conversion to the antiprotozoal/antifungal drug DB75 (2,5-bis(4-guanylphenyl)furan dihydrochloride). *Drug Metab Dispos* **35**:955-967.

Miezan TW, Bronner U, Doua F, Cattand P and Rombo L (1994) Long-term exposure of Trypanosoma brucei gambiense to pentamidine in vitro. *Trans R Soc Trop Med Hyg* **88**:332-333.

Ming X, Ju W, Wu H, Tidwell RR, Hall JE and Thakker DR (2009) Transport of dicationic drugs pentamidine and furamidine by human organic cation transporters. *Drug Metab Dispos* **37**:424-430.

Miret S, Abrahamse L and de Groene EM (2004) Comparison of in vitro models for the prediction of compound absorption across the human intestinal mucosa. *J Biomol Screen* **9**:598-606.

Molina-Arcas M, Casado FJ and Pastor-Anglada M (2009) Nucleoside transporter proteins. *Curr Vasc Pharmacol* **7**:426-434.

Muller J, Lips KS, Metzner L, Neubert RH, Koepsell H and Brandsch M (2005) Drug specificity and intestinal membrane localization of human organic cation transporters (OCT). *Biochem Pharmacol* **70**:1851-1860.

Nok AJ (2003) Arsenicals (melarsoprol), pentamidine and suramin in the treatment of human African trypanosomiasis. *Parasitol Res* **90**:71-79.

Nong A, Tan YM, Krolski ME, Wang J, Lunchick C, Conolly RB and Clewell HJ, 3rd (2008) Bayesian calibration of a physiologically based pharmacokinetic/pharmacodynamic model of carbaryl cholinesterase inhibition. *J Toxicol Environ Health A* **71**:1363-1381.

Obach RS (1999) Prediction of human clearance of twenty-nine drugs from hepatic microsomal intrinsic clearance data: An examination of in vitro half-life approach and nonspecific binding to microsomes. *Drug Metab Dispos* **27**:1350-1359.

Paine MF, Criss AB and Watkins PB (2005) Two major grapefruit juice components differ in time to onset of intestinal CYP3A4 inhibition. *J Pharmacol Exp Ther* **312**:1151-1160.

Paine MF, Wang MZ, Generaux CN, Boykin DW, Wilson WD, De Koning HP, Olson CA, Pohlig G, Burri C, Brun R, Murilla GA, Thuita JK, Barrett MP and Tidwell RR (2010) Diamidines for human African trypanosomiasis. *Curr Opin Investig Drugs* **11**:876-883.

Palma R, Vidon N, Houin G, Pfeiffer A, Rongier M, Barre J and Bernier JJ (1986) Influence of bile salts and lipids on intestinal absorption of griseofulvin in man. *Eur J Clin Pharmacol* **31**:319-325.

Pang KS, Lee WF, Cherry WF, Yuen V, Accaputo J, Fayz S, Schwab AJ and Goresky CA (1988) Effects of perfusate flow rate on measured blood volume, disse space, intracellular water space, and drug extraction in the perfused rat liver preparation: characterization by the multiple indicator dilution technique. *J Pharmacokinet Biopharm* **16**:595-632.

Pang KS, Morris ME and Sun H (2008) Formed and preformed metabolites: facts and comparisons. *J Pharm Pharmacol* **60**:1247-1275.

Parrott N, Jones H, Paquereau N and Lave T (2005) Application of full physiological models for pharmaceutical drug candidate selection and extrapolation of pharmacokinetics to man. *Basic Clin Pharmacol Toxicol* **96**:193-199.

Peck CC and Cross JT (2007) "Getting the dose right": facts, a blueprint, and encouragements. *Clin Pharmacol Ther* **82**:12-14.

Penzotti JE, Landrum GA and Putta S (2004) Building predictive ADMET models for early decisions in drug discovery. *Curr Opin Drug Discov Devel* **7**:49-61.

Pepin J and Milord F (1994) The treatment of human African trypanosomiasis. *Adv Parasitol* **33**:1-47.

Pessayre D, Mansouri A, Haouzi D and Fromenty B (1999) Hepatotoxicity due to mitochondrial dysfunction. *Cell Biol Toxicol* **15**:367-373.

Peters WH and Roelofs HM (1989) Time-dependent activity and expression of glutathione S-transferases in the human colon adenocarcinoma cell line Caco-2. *Biochem J* **264**:613-616.

Polli JE, Abrahamsson BS, Yu LX, Amidon GL, Baldoni JM, Cook JA, Fackler P, Hartauer K, Johnston G, Krill SL, Lipper RA, Malick WA, Shah VP, Sun D, Winkle HN, Wu Y and Zhang H (2008) Summary workshop report: bioequivalence, biopharmaceutics classification system, and beyond. *Aaps J* **10**:373-379.

Poulin P and Theil FP (2000) A priori prediction of tissue:plasma partition coefficients of drugs to facilitate the use of physiologically-based pharmacokinetic models in drug discovery. *J Pharm Sci* **89**:16-35.

Poulin P and Theil FP (2002) Prediction of pharmacokinetics prior to in vivo studies. II. Generic physiologically based pharmacokinetic models of drug disposition. *J Pharm Sci* **91**:1358-1370.

Reigner BG and Blesch KS (2002) Estimating the starting dose for entry into humans: principles and practice. *Eur J Clin Pharmacol* **57**:835-845.

Rodgers T and Rowland M (2006) Physiologically based pharmacokinetic modelling 2: predicting the tissue distribution of acids, very weak bases, neutrals and zwitterions. *J Pharm Sci* **95**:1238-1257.

Rowland M (1985) Physiologic pharmacokinetic models and interanimal species scaling. *Pharmacol Ther* **29**:49-68.

Rowland M, Balant L and Peck C (2004) Physiologically based pharmacokinetics in drug development and regulatory science: a workshop report (Georgetown University, Washington, DC, May 29-30, 2002). *AAPS PharmSci* **6**:E6.

Saha P and Kou JH (2002) Effect of bovine serum albumin on drug permeability estimation across Caco-2 monolayers. *Eur J Pharm Biopharm* **54**:319-324.

Sanderson L, Dogruel M, Rodgers J, De Koning HP and Thomas SA (2009) Pentamidine movement across the murine blood-brain and blood-cerebrospinal fluid barriers: effect of trypanosome infection, combination therapy, P-glycoprotein, and multidrug resistance-associated protein. *J Pharmacol Exp Ther* **329**:967-977.

Saulter JY, Kurian JR, Trepanier LA, Tidwell RR, Bridges AS, Boykin DW, Stephens CE, Anbazhagan M and Hall JE (2005) Unusual dehydroxylation of antimicrobial amidoxime prodrugs by cytochrome b5 and NADH cytochrome b5 reductase. *Drug Metab Dispos* **33**:1886-1893.

Schmiedlin-Ren P, Thummel KE, Fisher JM, Paine MF, Lown KS and Watkins PB (1997) Expression of enzymatically active CYP3A4 by Caco-2 cells grown on extracellular matrix-coated permeable supports in the presence of 1alpha,25-dihydroxyvitamin D3. *Mol Pharmacol* **51**:741-754.

Schuetz JD, Connelly MC, Sun D, Paibir SG, Flynn PM, Srinivas RV, Kumar A and Fridland A (1999) MRP4: A previously unidentified factor in resistance to nucleoside-based antiviral drugs. *Nat Med* **5**:1048-1051.

Sinko PJ, Kunta JR, Usansky HH and Perry BA (2004) Differentiation of gut and hepatic first pass metabolism and secretion of saquinavir in ported rabbits. *J Pharmacol Exp Ther* **310**:359-366.

Stewart BH, Chan OH, Lu RH, Reyner EL, Schmid HL, Hamilton HW, Steinbaugh BA and Taylor MD (1995) Comparison of intestinal permeabilities determined in multiple in vitro and in situ models: relationship to absorption in humans. *Pharm Res* **12**:693-699.

Studenberg SD and Brouwer KLR (1993) Hepatic disposition of acetaminophen and metabolites. Pharmacokinetic modeling, protein binding and subcellular distribution. *Biochem Pharmacol* **46**:739-746.

Sun H, Chow EC, Liu S, Du Y and Pang KS (2008) The Caco-2 cell monolayer: usefulness and limitations. *Expert Opin Drug Metab Toxicol* **4**:395-411.

Swift B, Pfeifer ND and Brouwer KLR (2009) Sandwich-cultured hepatocytes: an in vitro model to evaluate hepatobiliary transporter-based drug interactions and hepatotoxicity. *Drug Metab Rev* **42**:446-471.

Turncliff RZ, Hoffmaster KA, Kalvass JC, Pollack GM and Brouwer KLR (2006) Hepatobiliary disposition of a drug/metabolite pair: Comprehensive pharmacokinetic modeling in sandwich-cultured rat hepatocytes. *J Pharmacol Exp Ther* **318**:881-889.

von Kleist M and Huisinga W (2007) Physiologically based pharmacokinetic modelling: a sub-compartmentalized model of tissue distribution. *J Pharmacokinet Pharmacodyn* **34**:789-806.

Wang MZ, Saulter JY, Usuki E, Cheung YL, Hall M, Bridges AS, Loewen G, Parkinson OT, Stephens CE, Allen JL, Zeldin DC, Boykin DW, Tidwell RR, Parkinson A, Paine MF and Hall JE (2006) CYP4F enzymes are the major enzymes in human liver microsomes that catalyze the O-demethylation of the antiparasitic prodrug DB289 [2,5-bis(4-amidinophenyl)furan-bis-O-methylamidoxime]. *Drug Metab Dispos* **34**:1985-1994.

Wang MZ, Wu JQ, Bridges AS, Zeldin DC, Kornbluth S, Tidwell RR, Hall JE and Paine MF (2007) Human enteric microsomal CYP4F enzymes O-demethylate the antiparasitic prodrug pafuramidine. *Drug Metab Dispos* **35**:2067-2075.

Ward ES, Pollack GM and Brouwer KL (2001) Probenecid-associated alterations in valproate glucuronide hepatobiliary disposition: mechanistic assessment using mathematical modeling. *J Pharmacol Exp Ther* **297**:141-147.

Welling PG (1977) Influence of food and diet on gastrointestinal drug absorption: a review. *J Pharmacokinet Biopharm* **5**:291-334.

Welling PG (1996) Effects of food on drug absorption. *Annu Rev Nutr* **16**:383-415.

Welling PG and Tse FL (1982) The influence of food on the absorption of antimicrobial agents. *J Antimicrob Chemother* **9**:7-27.

Wenzler T, Boykin DW, Ismail MA, Hall JE, Tidwell RR and Brun R (2009) New treatment option for second-stage African sleeping sickness: in vitro and in vivo efficacy of aza analogs of DB289. *Antimicrob Agents Chemother* **53**:4185-4192.

Wetherington JD, Pfister M, Banfield C, Stone JA, Krishna R, Allerheiligen S and Grasela DM (2010) Model-based drug development: strengths, weaknesses, opportunities, and threats for broad application of pharmacometrics in drug development. *J Clin Pharmacol* **50**:31S-46S.

WHO (2006) Human African trypanosomiasis (sleeping sickness): epidemiological update. *Wkly Epidemiol Rec* **81**:71-80.

WHO (2009) WHO includes combination of eflornithine and nifurtimox in its Essential List of Medicines for the treatment of human African trypanosomiasis

WHO (2010) *Neglected tropical diseases. Innovative and Intensified Disease Management (IDM)*.

Wijnholds J, Mol CA, van Deemter L, de Haas M, Scheffer GL, Baas F, Beijnen JH, Scheper RJ, Hatse S, De Clercq E, Balzarini J and Borst P (2000) Multidrug-resistance protein 5 is a multispecific organic anion transporter able to transport nucleotide analogs. *Proc Natl Acad Sci U S A* **97**:7476-7481.

Wolf KK, Bridges AS, Lee JK, Polli JW, Brouwer KR and Pollack GM (2008) Hepatobiliary Disposition of Morphine and Generated Morphine 3-Glucuronide in Sandwich-Cultured Rat Hepatocytes, in *15th Annual ISSX North American Regional Meeting*, San Diego, CA.

Wu H, Ming X, Wang MZ, Tidwell R and Hall JE (2007) Comparative Pharmacokinetics of the Antitrypanosomal Diamidines DB75, DB820 and DB829 Following Oral Administration of Their Dimethamidoximes Prodrugs in Mice. *The AAPS Journal. 2007; 9(S2).*

Xiong H, Turner KC, Ward ES, Jansen PL and Brouwer KLR (2000) Altered hepatobiliary disposition of acetaminophen glucuronide in isolated perfused livers from multidrug resistance-associated protein 2-deficient TR(-) rats. *J Pharmacol Exp Ther* **295**:512-518.

Yan GZ, Brouwer KLR, Pollack GM, Wang MZ, Tidwell RR, Hall JE and Paine MF (2011) Mechanisms Underlying Differences in Systemic Exposure of Structurally Similar Active Metabolites: Comparison of Two Preclinical Hepatic Models
J Pharmacol Exp Ther **In press**.

Yasujima T, Ohta KY, Inoue K, Ishimaru M and Yuasa H (2010) Evaluation of 4',6-diamidino-2-phenylindole as a fluorescent probe substrate for rapid assays of the functionality of human multidrug and toxin extrusion proteins. *Drug Metab Dispos* **38**:715-721.

Yee S (1997) In vitro permeability across Caco-2 cells (colonic) can predict in vivo (small intestinal) absorption in man--fact or myth. *Pharm Res* **14**:763-766.

Yue W, Abe K and Brouwer KL (2009) Knocking down breast cancer resistance protein (Bcrp) by adenoviral vector-mediated RNA interference (RNAi) in sandwich-cultured rat hepatocytes: a novel tool to assess the contribution of Bcrp to drug biliary excretion. *Mol Pharm* **6**:134-143.

Zamek-Gliszczynski MJ, Hoffmaster KA, Humphreys JE, Tian X, Nezasa K and Brouwer KLR (2006) Differential involvement of Mrp2 (Abcc2) and Bcrp (Abcg2) in biliary excretion of 4-methylumbelliferyl glucuronide and sulfate in the rat. *J Pharmacol Exp Ther* **319**:459-467.

Zhang L, Sinha V, Forgue ST, Callies S, Ni L, Peck R and Allerheiligen SR (2006) Model-based drug development: the road to quantitative pharmacology. *J Pharmacokinet Pharmacodyn* **33**:369-393.

Zhou L, Lee K, Thakker DR, Boykin DW, Tidwell RR and Hall JE (2002) Enhanced permeability of the antimicrobial agent 2,5-bis(4-amidinophenyl)furan across Caco-2 cell monolayers via its methylamidoidme prodrug. *Pharm Res* **19**:1689-1695.

Zhou L, Thakker DR, Voyksner RD, Anbazhagan M, Boykin DW, Hall JE and Tidwell RR (2004) Metabolites of an orally active antimicrobial prodrug, 2,5-bis(4-amidinophenyl)furan-bis-O-methylamidoxime, identified by liquid chromatography/tandem mass spectrometry. *J Mass Spectrom* **39**:351-360.